2010-12

Conceptual design and software simulation of a wideband leakage cancellation circuit

Ang, Teo Hong

Monterey, California. Naval Postgraduate School

NAVAL POSTGRADUATE SCHOOL

MONTEREY, CALIFORNIA

THESIS

CONCEPTUAL DESIGN AND SOFTWARE SIMULATION OF A WIDEBAND LEAKAGE CANCELLATION CIRCUIT

by

Ang, Teo Hong

December 2010

Thesis Advisor: David C. Jenn
Second Reader: Phillip E. Pace

Approved for public release; distribution is unlimited

THIS PAGE INTENTIONALLY LEFT BLANK

REPORT DOCUMENTATION PAGE			Form Approved OMB No. 0704-0188
Public reporting burden for this collection of information is estimated to average 1 hour per response, including the time for reviewing instruction, searching existing data sources, gathering and maintaining the data needed, and completing and reviewing the collection of information. Send comments regarding this burden estimate or any other aspect of this collection of information, including suggestions for reducing this burden, to Washington headquarters Services, Directorate for Information Operations and Reports, 1215 Jefferson Davis Highway, Suite 1204, Arlington, VA 22202-4302, and to the Office of Management and Budget, Paperwork Reduction Project (0704-0188) Washington DC 20503.			
1. AGENCY USE ONLY ***(Leave blank)***	**2. REPORT DATE** December 2010	**3. REPORT TYPE AND DATES COVERED** Master's Thesis	
4. TITLE AND SUBTITLE Conceptual Design and Software Simulation of a Wideband Leakage Cancellation Circuit		**5. FUNDING NUMBERS**	
6. AUTHOR(S) Ang, Teo Hong			
7. PERFORMING ORGANIZATION NAME(S) AND ADDRESS(ES) Naval Postgraduate School Monterey, CA 93943-5000		**8. PERFORMING ORGANIZATION REPORT NUMBER**	
9. SPONSORING /MONITORING AGENCY NAME(S) AND ADDRESS(ES) N/A		**10. SPONSORING/MONITORING AGENCY REPORT NUMBER**	
11. SUPPLEMENTARY NOTES The views expressed in this thesis are those of the author and do not reflect the official policy or position of the Department of Defense or the U.S. Government.			
12a. DISTRIBUTION / AVAILABILITY STATEMENT Approved for public release; distribution is unlimited		**12b. DISTRIBUTION CODE**	

13. ABSTRACT (maximum 200 words)

The objective of this thesis is to investigate a Wideband Leakage Cancellation Circuit (WLCC) to facilitate potential improvement of range resolution in single antenna Frequency Modulated Continuous Wave (FMCW) radar, as well as other applications.

The research has successfully extended the operating bandwidth of a basic single frequency LCC by the use of a Frequency Demultiplexing and Multiplexing Circuit (FDMC) consisting of a bank of *N* leakage cancelling branches.

The WLCC was designed, tested and evaluated through a low risk and cost-effective approach, using an electronic-design automation software system known as the Advanced Design System (ADS) 2009 developed by Agilent Technologies.

The WLCC was successfully evaluated by benchmarking its performance against that of a single frequency Leakage Cancellation Circuit (LCC), both with ideal and non-ideal component parameter settings. The robustness of the WLCC was also evaluated by a series of simulations with antenna load mismatch conditions.

Future work and development was proposed on the current WLCC design to support ongoing NPS research on the Wirelessly Networked Distributed Digital Phased Array (WNDDPA).

14. SUBJECT TERMS Wideband, Leakage, Cancellation			**15. NUMBER OF PAGES** 127
			16. PRICE CODE
17. SECURITY CLASSIFICATION OF REPORT Unclassified	**18. SECURITY CLASSIFICATION OF THIS PAGE** Unclassified	**19. SECURITY CLASSIFICATION OF ABSTRACT** Unclassified	**20. LIMITATION OF ABSTRACT** UU

NSN 7540-01-280-5500

Standard Form 298 (Rev. 2-89)
Prescribed by ANSI Std. 239-18

THIS PAGE INTENTIONALLY LEFT BLANK

Approved for public release; distribution is unlimited

CONCEPTUAL DESIGN AND SOFTWARE SIMULATION OF A WIDEBAND LEAKAGE CANCELLATION CIRCUIT

ANG, Teo Hong
Major, Republic of Singapore Air Force
BE, University of New South Wales (Australia), 2001

Submitted in partial fulfillment of requirements for the degree of

MASTER OF SCIENCE IN ELECTRICAL ENGINEERING

From the

NAVAL POSTGRADUATE SCHOOL
December 2010

Author: Ang, Teo Hong

Approved by: David C. Jenn
Thesis Advisor

Phillip E. Pace
Second Reader

R. Clark Robertson
Chairman, Department of Electrical and Computer Engineering

THIS PAGE INTENTIONALLY LEFT BLANK

ABSTRACT

The objective of this thesis is to investigate a Wideband Leakage Cancellation Circuit (WLCC) to facilitate potential improvement of range resolution in single antenna Frequency Modulated Continuous Wave (FMCW) radar, as well as other applications.

The research has successfully extended the operating bandwidth of a basic single frequency Leakage Cancellation Circuit (LCC) by the use of a Frequency Demultiplexing and Multiplexing Circuit (FDMC) consisting of a bank of *N* leakage cancelling branches.

The WLCC was designed, tested and evaluated through a low risk and cost-effective approach, using an electronic-design automation software system known as the Advanced Design System (ADS) 2009 developed by Agilent Technologies.

The WLCC was successfully evaluated by benchmarking its performance against that of a single frequency LCC, both with ideal and non-ideal component parameter settings. The robustness of the WLCC was also evaluated by a series of simulations with antenna load mismatch conditions.

Future work and development was proposed on the current WLCC design to support ongoing NPS research on the Wirelessly Networked Distributed Digital Phased Array (WNDDPA).

THIS PAGE INTENTIONALLY LEFT BLANK

TABLE OF CONTENTS

I. INTRODUCTION 1
A. BACKGROUND 1
1. FMCW Radar 1
2. Circulator 4
3. Leakage Cancellation 6
4. Concept of Wideband Leakage Cancellation 8
B. OBJECTIVE 10
C. SCOPE AND ORGANIZATION 10

II. ESSENTIAL BUILDING BLOCKS 11
A. INTRODUCTION 11
B. BASIC SINGLE FREQUENCY LCC 11
C. FREQUENCY DEMULTIPLEXING AND MULTIPLEXING CIRCUIT (FDMC) 23
1. Design Approach 23
2. Bandpass Filters 28
3. FDMC Using Circulators 36
4. FDMC Using Couplers 42
5. Scattering Parameters 47
D. CONCLUSION 58

III. WIDEBAND LEAKAGE CANCELLATION CIRCUIT 59
A. INTRODUCTION 59
B. DESIGN OF WLCC 59
1. WLCC Using Circulators 59
2. WLCC Using Couplers 63
C. EVALUATION OF FINAL WLCC DESIGN 67
1. Evaluation Approach 67
2. Performance Benchmarking Against Single Frequency LCC With Ideal Component Parameter Settings 74
3. Performance Benchmarking Against Single Frequency LCC With Non-Ideal Component Parameter Settings 80
4. Performance Analysis With Mismatched Load 86
D. CONCLUSION 97

IV. SUMMARY AND CONCLUSIONS 99
A. SUMMARY 99
B. RECOMMENDATIONS 100
1. Software Design of Essential Components in FDMC 100
2. Further ADS Software Simulations 100
3. Building a Hardware Prototype 100
4. Combining WLCC With Digital Cancellation 101

LIST OF REFERENCES 103

INITIAL DISTRIBUTION LIST 105

THIS PAGE INTENTIONALLY LEFT BLANK

LIST OF FIGURES

Figure 1. CWAR for HAWK Missile System (From [1]). 1
Figure 2. Block Diagram of Two-Antenna FMCW Radar (From [2]). 2
Figure 3. Frequency-Time Relation in Linear FMCW Radar (From [2]). 3
Figure 4. Difference Frequency between Transmitted and Received Signals (From [2]). 3
Figure 5. SCOUT Mk2 Surface Radar (From [3]). 4
Figure 6. Three-Port Circulator (From [5]). 5
Figure 7. Operation of the LCC (From Figure 13 of [7]). 6
Figure 8. Effects of Phase and Amplitude Imbalance (From Figure 14 of [7]). 7
Figure 9. Cancellation Level vs. LCC Bandwidth. 8
Figure 10. Conceptual Block Diagram of a WLCC (After Figure 59 from []). 9
Figure 11. Conceptual Cancellation Output (After Figure 60 from [7]). 9
Figure 12. ADS Model of the Basic Single Frequency LCC. 12
Figure 13. Amplitude Plot of SOI for l = 18.908 m. 16
Figure 14. Amplitude Plot of SOI for l = 18.828 m. 17
Figure 15. Amplitude Plot of SOI for l = 18.672 m. 17
Figure 16. Phase Plot of Leakage for l = 18.908 m. 18
Figure 17. Phase Plot of Leakage for l = 18.828 m. 18
Figure 18. Phase Plot of Leakage for l = 18.672 m. 19
Figure 19. Phase Plot of Leakage for l = 6.25 m. 19
Figure 20. Phase Plot of Leakage for l = 18.75 m. 20
Figure 21. Phase Plot of Leakage for l = 31.25 m. 20
Figure 22. LCC Frequency-Domain Plots in dB. 21
Figure 23. LCC Frequency-Domain Plots in dBm. 22
Figure 24. LCC Phase Plots for Points 1 to 3. 23
Figure 25. LCC Phase Plots for Point 4. 23
Figure 26. Demultiplexing Operation (Forward Direction). 24
Figure 27. Multiplexing Operation (Reverse Direction). 24
Figure 28. Ideal Transfer Function of a Three-Channel FDMC. 25
Figure 29. ADS Model of FDMC using Circulators. 27
Figure 30. ADS Model of FDMC using Couplers. 28
Figure 31. Parameter Settings for the Elliptic BPF. 29
Figure 32. Output Amplitude Plot for the Elliptic BPF. 30
Figure 33. Output Phase Plot for the Elliptic BPF. 30
Figure 34. Parameter Settings for the Chebyshev BPF. 31
Figure 35. Output Amplitude Plot for the Chebyshev BPF. 31
Figure 36. Output Phase Plot for the Chebyshev BPF. 32
Figure 37. Parameter Settings for the Butterworth BPF. 32
Figure 38. Output Amplitude Plot for the Butterworth BPF. 33
Figure 39. Output Phase Plot for the Butterworth BPF. 33
Figure 40. Parameter Settings for the Gaussian BPF. 34
Figure 41. Output Amplitude Plot for the Gaussian BPF. 34

Figure 42. Output Phase Plot for the Gaussian BPF. 35
Figure 43. Parameter Settings for the Bessel BPF. 35
Figure 44. Output Amplitude Plot for the Bessel BPF. 36
Figure 45. Output Phase Plot for the Bessel BPF 36
Figure 46. Output Amplitude Plot for the FDMC that uses Circulators and Elliptic Filters. 37
Figure 47. Phase Plot for the FDMC that uses Circulators and Elliptic Filters. 38
Figure 48. Output Amplitude Plot for the FDMC that uses Circulators and Chebyshev Filters. 38
Figure 49. Phase Plot for the FDMC that uses Circulators and Chebyshev Filters. 39
Figure 50. Output Amplitude Plot for the FDMC that uses Circulators and Butterworth Filters. 39
Figure 51. Phase Plot for the FDMC that uses Circulators and Butterworth Filters. 40
Figure 52. Output Amplitude Plot for the FDMC that uses Circulators and Gaussian Filters. 40
Figure 53. Phase Plot for the FDMC that uses Circulators and Gaussian Filters 41
Figure 54. Output Amplitude Plot for the FDMC that uses Circulators and Bessel Filters. 41
Figure 55. Phase Plot for the FDMC that uses Circulators and Bessel Filters. 42
Figure 56. Output Amplitude Plot for the FDMC that uses Couplers and Elliptic Filters. 43
Figure 57. Phase Plot for the FDMC that uses Couplers and Elliptic Filters. 43
Figure 58. Output Amplitude Plot for the FDMC that uses Couplers and Chebyshev Filters. 44
Figure 59. Phase Plot for the FDMC that uses Couplers and Chebyshev Filters. 44
Figure 60. Output Amplitude Plot for the FDMC that uses Couplers and Butterworth Filters. 45
Figure 61. Phase Plot for the FDMC that uses Couplers and Butterworth Filters. 45
Figure 62. Output Amplitude Plot for the FDMC that uses Couplers and Gaussian Filters. 46
Figure 63. Phase Plot for the FDMC that uses Couplers and Gaussian Filters. 46
Figure 64. Output Amplitude Plot for the FDMC that uses Couplers and Bessel Filters. 47
Figure 65. Phase Plot for the FDMC that uses Couplers and Bessel Filters. 47
Figure 66. Demultiplexer of FDMC using Circulators. 48
Figure 67. Demultiplexer of FDMC using Couplers. 48
Figure 68. S-Parameter Simulation Model for the Demultiplexer of FDMC using Circulators. 50
Figure 69. S-Parameter Simulation Model for the Demultiplexer of FDMC using Couplers. 51
Figure 70. Phase Plots of S-Parameters for the FDMC Using Circulators. 53
Figure 71. Amplitude Plots of S-Parameters at Port 1 for the FDMC Using Circulators. 53
Figure 72. Amplitude Plots of S-Parameters at Port 2 for the FDMC Using Circulators. 54

Figure 73. Amplitude Plots of S-Parameters at Port 3 for the FDMC Using Circulators. 54
Figure 74. Amplitude Plots of S-Parameters at Port 4 for the FDMC Using Circulators. 55
Figure 75. Phase Plots of S-Parameters for the FDMC Using Couplers. 56
Figure 76. Amplitude Plots of S-Parameters at Port 1 for the FDMC Using Couplers. 56
Figure 77. Amplitude Plots of S-Parameters at Port 2 for the FDMC Using Couplers. 57
Figure 78. Amplitude Plots of S-Parameters at Port 3 for the FDMC Using Couplers. 57
Figure 79. Amplitude Plots of S-Parameters at Port 4 for the FDMC Using Couplers. 58
Figure 80. ADS Model of WLCC with FDMC using Circulators with Ideal Component Parameter Settings. 60
Figure 81. Amplitude Plot of SOI in WLCC. 61
Figure 82. Phase Plot of Leakage in WLCC. 62
Figure 83. Phase Plot of Cancellation in WLCC 62
Figure 84. Phase Plot of SOI in WLCC. 63
Figure 85. ADS Model of WLCC with FDMC using Couplers with Ideal Component Settings. 64
Figure 86. Amplitude Plot of SOI in WLCC. 65
Figure 87. Phase Plot of Leakage in WLCC. 66
Figure 88. Phase Plot of Cancellation in WLCC 66
Figure 89. Phase Plot of SOI in WLCC. 67
Figure 90. Comparison of Amplitude Plots for both WLCC Designs with Ideal Devices. 68
Figure 91. ADS Model of Single Frequency LCC with Ideal Component Parameter Settings. 71
Figure 92. ADS Model of Single Frequency LCC with Non-Ideal Component Parameter Settings. 72
Figure 93. ADS Model of WLCC with Non-Ideal Parameter Settings. 73
Figure 94. Amplitude Plot of SOI for both WLCC and LCC with Ideal Component Parameter Settings in dBm 76
Figure 95. Amplitude Plot of SOI for both WLCC and LCC with Ideal Component Parameter Settings in dB 76
Figure 96. Phase Plot of Leakage in WLCC with Ideal Component Parameter Settings in Degrees. 77
Figure 97. Phase Plot of Leakage in LCC with Ideal Component Parameter Settings in Degrees. 77
Figure 98. Phase Plot of Cancellation in WLCC with Ideal Component Parameter Settings in Degrees. 78
Figure 99. Phase Plot of Cancellation in LCC with Ideal Component Parameter Settings in Degrees. 78
Figure 100. Phase Plot of SOI in WLCC with Ideal Component Parameter Settings in Degrees. 79
Figure 101. Phase Plot of SOI in LCC with Ideal Component Parameter Settings in Degrees. 79

Figure 102. Amplitude Plot of SOI for both WLCC and LCC with Non-Ideal Component Parameter Settings in dBm. 82
Figure 103. Amplitude Plot of SOI for both WLCC and LCC with Non-Ideal Component Parameter Settings in dB. 82
Figure 104. Phase Plot of Leakage in WLCC with Non-Ideal Component Parameter Settings in Degrees. 83
Figure 105. Phase Plot of Leakage in LCC with Non-Ideal Component Parameter Settings in Degrees. 83
Figure 106. Phase Plot of Cancellation in WLCC with Non-Ideal Component Parameter Settings in Degrees. 84
Figure 107. Phase Plot of Cancellation in LCC with Non-Ideal Component Parameter Settings in Degrees. 84
Figure 108. Phase Plot of SOI in WLCC with Non-Ideal Component Parameter Settings in Degrees. 85
Figure 109. Phase Plot of SOI in LCC with Non-Ideal Component Parameter Settings in Degrees. 85
Figure 110. Amplitude Plot of SOI for both WLCC and LCC with Non-Ideal Component Parameter Settings in dBm with 60 Ω Load. 86
Figure 111. Amplitude Plot of SOI for both WLCC and LCC with Non-Ideal Component Parameter Settings in dBm with 70 Ω Load. 87
Figure 112. Amplitude Plot of SOI for both WLCC and LCC with Non-Ideal Component Parameter Settings in dBm with 80 Ω Load. 87
Figure 113. Amplitude Plot of SOI for both WLCC and LCC with Non-Ideal Component Parameter Settings in dBm with 90 Ω Load. 88
Figure 114. Amplitude Plot of SOI for both WLCC and LCC with Non-Ideal Component Parameter Settings in dBm with 100 Ω Load. 88
Figure 115. Amplitude Plot of SOI for both WLCC and LCC with Non-Ideal Component Parameter Settings in dBm with 40 Ω Load. 89
Figure 116. Amplitude Plot of SOI for both WLCC and LCC with Non-Ideal Component Parameter Settings in dBm with 30 Ω Load. 89
Figure 117. Amplitude Plot of SOI for both WLCC and LCC with Non-Ideal Component Parameter Settings in dBm with 20 Ω Load. 90
Figure 118. Amplitude Plot of SOI for both WLCC and LCC with Non-Ideal Component Parameter Settings in dBm with 10 Ω Load. 90
Figure 119. ADS Model of Re-tuned LCC for 100 Ω Antenna Load. 92
Figure 120. ADS Model of Re-tuned LCC for 10 Ω Antenna Load. 93
Figure 121. ADS Model of Re-tuned WLCC for 100 Ω Antenna Load. 94
Figure 122. ADS Model of Re-tuned WLCC for 10 Ω Antenna Load. 95
Figure 123. Amplitude Plot of SOI for both WLCC and LCC with Non-Ideal Component Parameter Settings in dBm with 10 Ω Load. 96

LIST OF TABLES

Table 1. Signal Notation for ADS Model of the Basic Single Frequency LCC. 13
Table 2. Sample LCC Measurements in dB/ Degrees. 14
Table 3. Sample LCC Measurements in dBm.....14
Table 4. Summary of S-Parameters for the FDMC Using Circulator in dB / Degrees. 52
Table 5. Summary of S-Parameters for the FDMC Using Couplers in dB / Degrees. ..55
Table 6. Summary of Measurements for WLCC using FDMC with Circulators with Ideal Component Parameter Settings.....60
Table 7. Summary of Measurements for WLCC using FDMC with Couplers with Ideal Component Parameter Settings.....65
Table 8. Actual Component Parameters (After Table 2 from [] and Table 4 of [11])...69
Table 9. Measurements at WLCC with Ideal Component Parameter Settings in dB / Degrees. 74
Table 10. Measurements at WLCC with Ideal Component Parameter Settings in dBm.....74
Table 11. Measurements at LCC with Ideal Component Parameter Settings in dB / Degrees. 75
Table 12. Measurements at LCC with Ideal Component Parameter Settings in dBm.....75
Table 13. Measurements at WLCC with Non-Ideal Component Parameter Settings in dB / Degrees.....80
Table 14. Measurements at WLCC with Non-Ideal Component Parameter Settings in dBm.....80
Table 15. Measurements at LCC with Non-Ideal Component Parameter Settings in dB / Degrees.....81
Table 16. Measurements at LCC with Non-Ideal Component Parameter Settings in dBm.....81
Table 17. Comparison of Achieved Attenuation Level for both LCC and WLCC. 98
Table 18. Comparison of Achieved Bandwidth for both LCC and WLCC.....98

THIS PAGE INTENTIONALLY LEFT BLANK

EXECUTIVE SUMMARY

The objective of this thesis is to design a Wideband Leakage Cancellation Circuit (WLCC) to facilitate potential improvement of range resolution in single antenna Frequency Modulated Continuous Wave (FMCW) radar, as well as other applications.

This research has successfully extended the operating bandwidth of a basic single frequency Leakage Cancellation Circuit (LCC) by the use of a FDMC consisting of a bank of *N* leakage cancelling branches.

The WLCC was designed, tested and evaluated through a low risk and cost-effective approach, using an electronic-design automation software system known as the Advanced Design System (ADS) 2009 developed by Agilent Technologies. A design process was also developed based on an understanding of various microwave engineering concepts, as well as an understanding of the analysis of components and their impact on circuit responses.

The objective of the thesis and necessary background are provided through a brief introduction of relevant topics, such as FMCW radar, circulator, and the concept of leakage cancellation. The conceptual design of the WLCC is also covered to provide readers with a quick understanding of how the WLCC will be designed and the desired end-state results.

The essential building blocks required for the design of the WLCC are discussed and include an analysis of a single frequency basic LCC, evaluation of different types of Bandpass Filters (BPFs), as well as the design of the Frequency Demultiplexing and Multiplexing Circuit (FDMC), a key component in the WLCC. First, the conventional narrowband LCC with ideal components was simulated in ADS. This served as a baseline for evaluating new approaches for wideband circuits. Several designs of the FDMC were simulated that used circulators, couplers and various types of filter characteristics. In order to make cancellation effective over a wide band, it is necessary to match the phase slopes of the main channel and cancellation branches.

Simulation results supported the use of elliptic filters due to their flat amplitude response in the passband and their very steep roll-off. The phase of elliptic filters is also relatively linear, which is a crucial factor in designing toward a match of the phase in the leakage signal thus allowing cancellation over a wide band of frequencies.

A comparison of FDMC designs was conducted by evaluating a design that uses circulators for the splitting of signal for the processing of a cancellation signal, against another design that uses couplers. It was found that the FDMC design that uses couplers is more suited for use in the design of the WLCC due to its superior phase linearity. An S-parameter simulation was also conducted in ADS to confirm this finding and to provide a general characterization of the FDMC.

The actual design of the WLCC, using both ideal and non-ideal component parameter settings was covered. The results obtained for the WLCC design were also benchmarked against that of a single frequency basic LCC.

The WLCC was successfully evaluated by benchmarking its performance against that of a single frequency LCC. In contrast to the bandwidth-limited single frequency LCC, the WLCC was able to achieve a bandwidth of 55 MHz and 32 MHz, both across a 60 MHz band, with typically cancellation of – 40 dB, with ideal and non-ideal component parameter settings, respectively. The robustness of the WLCC was also evaluated by a series of simulations with antenna load mismatch conditions.

The successful findings of this thesis are summarized, and potential improvement in FMCW radar and new Wirelessly Networked Distributed Digital Phased Array (WNDDPA) applications are offered.

LIST OF ACRONYMS AND ABBREVIATIONS

ADS	Advanced Design System
ATTN	Attenuator
BPFs	Bandpass Filters
COTS	Commercially Off the Shelf
CW	Continuous Wave
CWAR	Continuous Wave Acquisition Radar
DBFC	Digital Beam Former and Controller
FDMC	Frequency Demultiplexing and Multiplexing Circuit
FMCW	Frequency Modulated Continuous Wave
HAWK	Homing All the Way Killer
LCC	Leakage Cancellation Circuit
LPI	Low Probability of Intercept
PRF	Pulse Repetition Frequency
PS	Phase Shifter
SOI	Signal of Interest
S-Parameters	Scattering Parameters
T/R	Transmit/ Receive
TRM	Transmit / Receive Module
VSWR	Voltage Standing Wave Ratio
WLCC	Wideband Leakage Cancellation Circuit
WNDDPA	Wirelessly Networked Distributed Digital Phased Array

THIS PAGE INTENTIONALLY LEFT BLANK

ACKNOWLEDGMENTS

I would like to thank my thesis advisor, Professor David C. Jenn for his guidance, patience and time.

I would also like to thank my wife, Irene, who has supported me behind the scenes and has taken good care of our boys, James and Jovan, while I was away preparing this thesis.

To my elder son, James, thank you for being such a good boy, as well as a good elder brother to Jovan. Thank you, James for taking such a huge amount of load off Daddy and Mommy by being independent and responsible in your daily work.

To my younger son, Jovan, your innocent laughter of joy has never failed to bring down my stress level. Thank you for always bringing laughter in the house and being so loving towards Mommy, James and Daddy.

THIS PAGE INTENTIONALLY LEFT BLANK

I. INTRODUCTION

A. BACKGROUND

1. FMCW Radar

Radar detects targets by transmitting electromagnetic energy followed by observing its return. Pulse radars work by constantly switching between the transmitter to transmit the waveform and the receiver to listen for any returns. Continuous Wave (CW) radars, on the other hand, transmit and receive at all times. Equation Chapter 1 Section 1

Historically, early radars were predominantly CW rather than pulse. A Continuous Wave Acquisition Radar (CWAR) for the Homing All the Way Killer (HAWK) air defense missile system, whose concept dates back to the 1950s, is shown in Figure 1.

Figure 1. CWAR for HAWK Missile System (From [1]).

The CWAR is a good example of CW radar employed operationally by many countries around the world. However, such CW radars have lost their attractiveness over the years due to the development of high-Pulse Repetition Frequency (PRF) pulse doppler radars [2].

A block diagram illustrating the principle of two-antenna FMCW radar is shown in Figure 2. A portion of the transmitter signal acts as the reference signal. This signal is required to produce a beat frequency and is introduced directly into the receiver. The isolation between both antennas must be large in order to reduce the amount of transmit signal arriving at the receiver through coupling. The beat frequency is amplified and limited to remove any amplitude fluctuations. The frequency of the amplitude-limited beat note is measured with a cycle-counting frequency meter calibrated in distance.

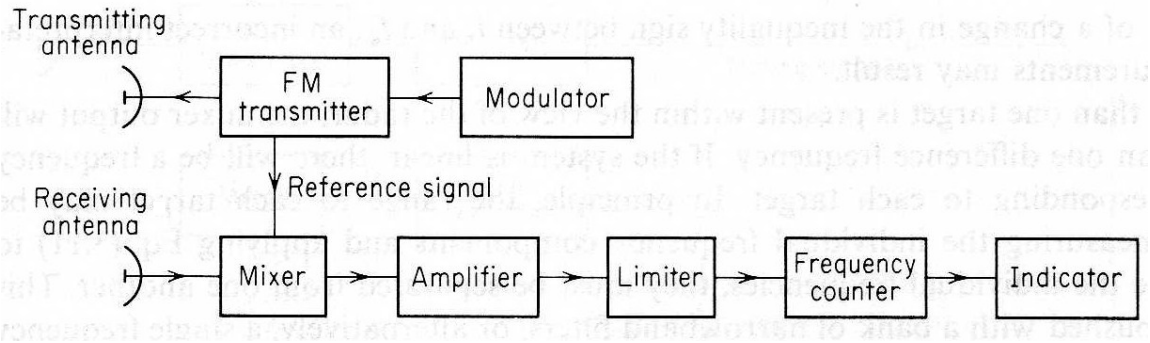

Figure 2. Block Diagram of Two-Antenna FMCW Radar (From [2]).

The determination of range requires a CW waveform to be marked in some manner so that the transit time out to the target and back can be measured. A popular method in CW radar is to linearly frequency modulate the waveform, as shown in Figure 3. The transmitted signal is shown by the solid triangular waveform. The frequency excursion Δf corresponds to the bandwidth of a pulse radar, and the frequency modulation at a rate f_m is the equivalent of the Pulse Repetition Frequency (PRF) of a pulse radar. The dashed curve represents the frequency of the received echo signal from a stationary target. It arrives back at the radar at a time

$$T = \frac{2R}{c} \tag{1}$$

where R is the range to target and c is the speed of light.

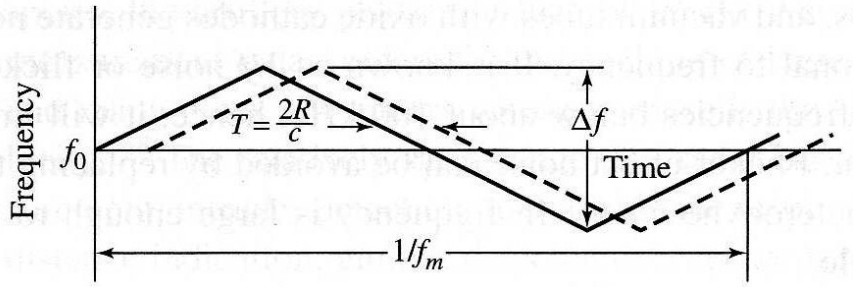

Figure 3. Frequency-Time Relation in Linear FMCW Radar (From [2]).

The time-delayed received signal and the transmitted signal are multiplied in a mixer to produce a difference frequency f_r shown in Figure 4, which can be shown to be

$$\frac{4Rf_m\Delta f}{c} \quad . \tag{2}$$

If there is a Doppler frequency shift f_d from the target, during half the modulation period the difference frequency is

$$f_r + f_d \tag{3}$$

and during the other half of the modulation period it is

$$f_r - f_d \quad . \tag{4}$$

By averaging these two difference frequencies over the period $1 / f_m$ the target range can be obtained.

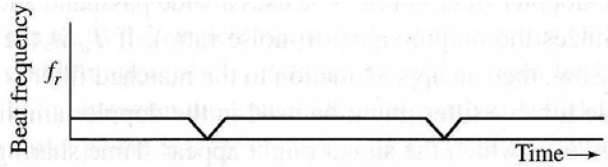

Figure 4. Difference Frequency between Transmitted and Received Signals (From [2]).

The SCOUT Mk2 surface surveillance and tactical navigation radar, shown in Figure 5, is a good example of the current state-of-the-art single antenna FMCW radar that is operating in the real world. It is the improved version of the PILOT radar,

originally developed by the Philips Research Laboratory in 1988. This radar has Low Probability of Intercept (LPI) characteristics, extremely high range resolution, high reliability, low weight, safe maintenance due to the lack of lethal high voltages, low radiation risks and is able to be used stand-alone or integrated with other systems.

Figure 5. SCOUT Mk2 Surface Radar (From [3]).

One of the greatest challenges encountered by designers of single antenna FMCW radars is that of achieving sufficient isolation between the transmitter and receiver. Unlike the case of pulse radars, where this issue can be easily resolved by time gating, the CW version requires simultaneous transmission and reception of signal. The power ratio between the transmitted and the received signal is large, as much as, Watts of transmitted signal versus picowatt or less for the returns. This can lead to a valid target being swamped by the transmitter noise sidebands and desensitization of the receiver due to the power leakage flowing into the receiver [4].

2. Circulator

Systems such as the SCOUT Mk2 surface radar, which use a single antenna, have very stringent Transmit/Receive (T/R) isolation requirements. A ferrite circulator is a three or four port device that can, in principle, offer isolation of the transmitter and receiver. The symbol used to describe a three-port circulator is illustrated in Figure 6. The arrow indicates the direction of "signal circulation" from port to port. Ideally, the input signal to port 1, 2 and 3 should only emerge from port 2, 3 and 1, respectively.

None of the input signal to port 1, 2 and 3 should emerge from port 3, 1 and 2, respectively.

There will always be insertion loss in the forward arrow direction, ranging from 0.5 dB to several dB, and leakage in the reverse arrow direction. Typical values of isolation are 20 to 60 dB. In other words, the leakage signal ranges from 20 to 60 dB below the signal in the forward arrow direction [5].

In a three-port circulator, as shown in Figure 6, the transmitter may be connected to port 1. It radiates out of the antenna connected to port 2. The received echo signal from the antenna is directed to port 3, which connects to the receiver.

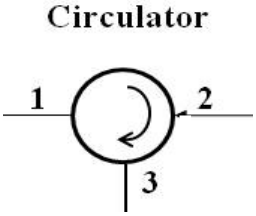

Figure 6. Three-Port Circulator (From [5]).

The limitation in isolation is determined by the reflection of the transmitter signal from the antenna due to impedance mismatch, which is then returned directly to the receiver. For example, if the Voltage Standing Wave Ratio (VSWR) of the antenna was 1.5, about 4 percent of the transmitter power will be reflected by the antenna and returned to the receiver. This corresponds to an isolation of 14 dB. If the VSWR was 2, then the effective isolation is only 10 dB.

Circulators can be made to withstand high peak and average power, but large power capability generally comes with large size and weight. A larger circulator is able to handle 50 kW of average power, while a smaller circulator is rated at 50 W [5]. For example, an S-band differential phase-shift waveguide circulator that weighs 80 pounds has essentially the same insertion loss, isolation and bandwidth of an S-band miniature coaxial Y-junction circulator that weighs 1.5 oz [6].

3. Leakage Cancellation

In order to improve the T/R isolation, a Leakage Cancellation Circuit (LCC), such as the one shown in Figure 7, can be used. The arrows show the major signal flow and multiple reflections are ignored. The power splitters illustrate equal power split, however the coupling ratio can be adjusted so that only the minimum amount of power necessary for cancellation is tapped off [7].

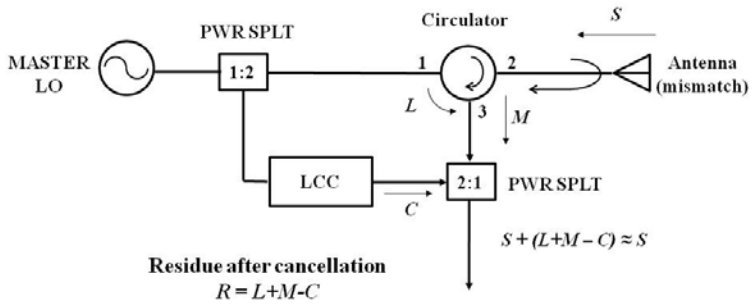

Figure 7. Operation of the LCC (From Figure 13 of [7]).

The cancellation signal level (C) is set to cancel the leakage from the circulator (L). In the ideal case, the cancellation voltage is equal in amplitude but opposite in phase to that of the leakage voltage. Hence, the leakage signal can be eliminated by the cancellation signal. In terms of complex voltages

$$S+\left(L+M-C\right)=S+R\approx S \tag{5}$$

where R is the residue. The other signal components, shown in Figure 7, are the antenna mismatch (M), and desired signal (S). The cancellation improvement (CI, simply referred to as cancellation) in dB is

$$CI=10\log_{10}\left(\frac{R}{L+M}\right)=10\log_{10}\left[1-\frac{C}{L+M}\right]. \tag{6}$$

The minus sign in Equation (5) implies that the cancellation signal should be 180° out of phase with L+M. Generally, this is only true at a single frequency, where the LCC is set to null the leakage and mismatch. A typical LCC is comprised of a phase shifter as well as an attenuator. It is usually difficult to match both the phase and amplitude of the leakage perfectly to achieve $R=0$.

The balance of amplitude and phase between the terms $L+M$ and C is very important. Suppose there are signals from two channels being added. The total voltage is

$$V = V_1 + V_2 = 1 + \alpha e^{i\varphi} \tag{7}$$

where channel 1 is used as a reference (V_1=1) and α and φ are the relative amplitude and phase of channel 2 to the reference. Thus, the amplitude imbalance is simply α and the phase imbalance φ. Let V_1 represent $L+M$ and V_2 the cancellation voltage C. The graph shown in Figure 8 illustrates the effect of phase and amplitude imbalance [8], and it is clear that even a little difference in the phase and amplitude can have a big difference on the cancellation level. To achieve a notch depth of 35 to 40 dB, an amplitude balance of about 0.2 dB and phase balance of about 1° are required.

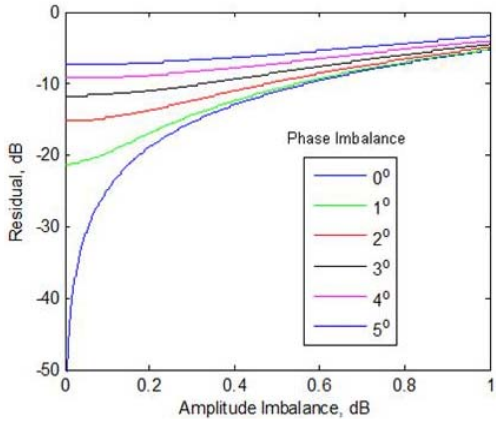

Figure 8. Effects of Phase and Amplitude Imbalance (From Figure 14 of [7]).

There is also a limitation in the amount of bandwidth that a LCC can achieve. In general, the amount of cancellation deteriorates very quickly with the increase of the LCC bandwidth, as shown in Figure 9. Therefore, there is a need for a Wideband LCC (WLCC).

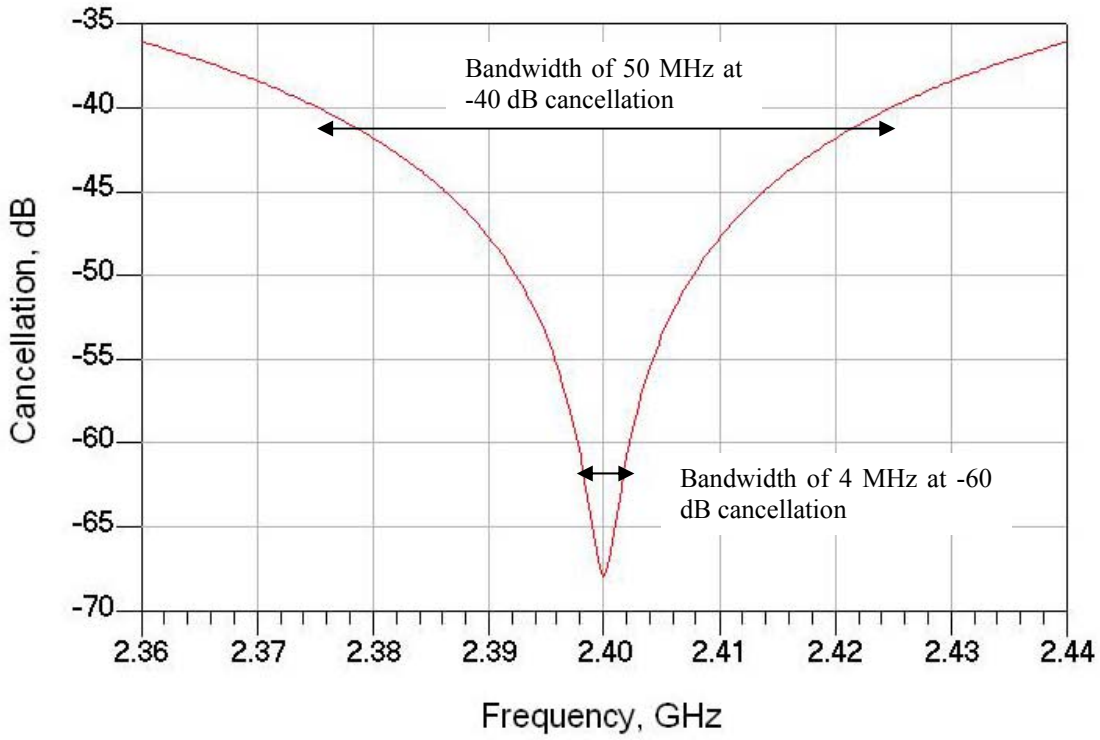

Figure 9. Cancellation Level vs. LCC Bandwidth.

4. Concept of Wideband Leakage Cancellation

Conceptually, the design of a WLCC is comprised of a two port device that consists of a bank of *N* narrowband LCCs. Each LCC forms a specific channel with scalable center frequency and bandwidth. This conceptual design and its cancellation output are shown in Figures 10 and 11, respectively.

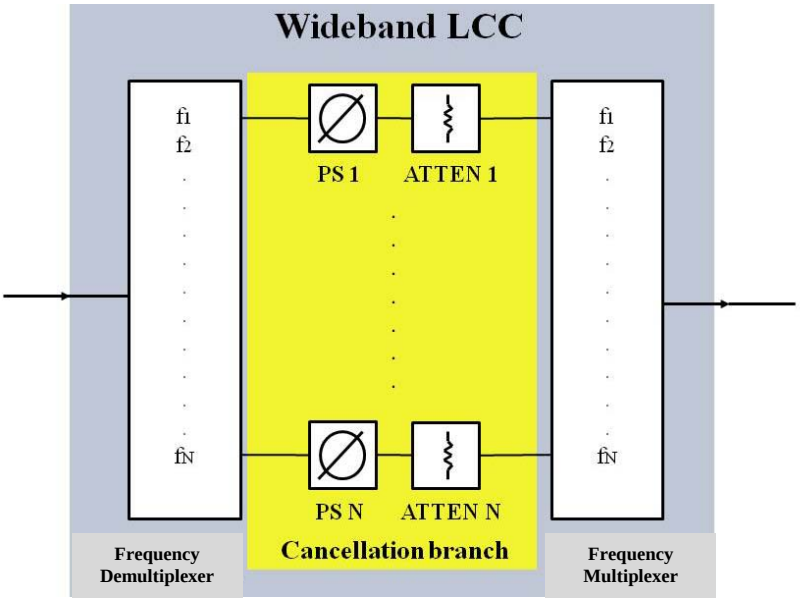

Figure 10. Conceptual Block Diagram of a WLCC (After Figure 59 from [7]).

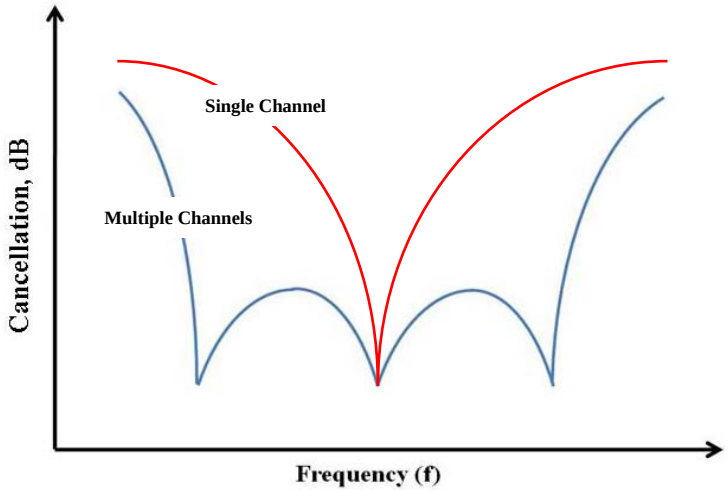

Figure 11. Conceptual Cancellation Output (After Figure 60 from [7]).

The challenge in designing a WLCC lies in the Frequency Demultiplexing and Multiplexing Circuit (FDMC). This circuit is responsible for splitting the input signal into multiple narrowband signals for cancellation by their respective channels, as well as the subsequent step of re-combining these signals into a wideband cancellation signal. The approach in designing the FDMC will be elaborated in Chapter II.

B. OBJECTIVE

The objective of this thesis is to design a WLCC to facilitate potential improvement of range resolution in a single antenna Frequency Modulated Continuous Wave (FMCW) radar, as well as other applications.

The WLCC will be designed, tested and evaluated through a low risk and cost-effective approach, using an electronic-design automation software system known as the Advanced Design System (ADS) 2009 developed by Agilent Technologies.

C. SCOPE AND ORGANIZATION

The overall thesis report consists of four chapters. The objective of the thesis and background, through a brief introduction of relevant topics such as FMCW radar, circulator and leakage cancellation, are covered in Chapter I. The conceptual design of a WLCC is also covered to provide readers a quick understanding of how the proposed WLCC will be designed and the desired end-state results.

The essential building blocks for the WLCC design include the analysis of a single frequency basic LCC, different types of bandpass filters and design of the FDMC are covered in Chapter II.

The actual design of the WLCC, using both ideal and non-ideal component parameters is covered in Chapter III. The results obtained for the WLCC design are benchmarked against that of a single frequency basic LCC.

Finally, the concluding chapter summarizes this thesis and proposes recommendations for future work on the WLCC design.

II. ESSENTIAL BUILDING BLOCKS

The analysis of a basic single frequency LCC model, the types of Bandpass Filters (BPFs) considered and their responses to assess their suitability for use in the WLCC and the design of the FDMC that is a crucial component in the WLCC are documented in this chapter.

A. INTRODUCTION

The simulation software used in this thesis is the Advanced Design System (ADS) 2009, developed by Agilent Technologies and before them, Hewlett-Packard.

ADS is an electronic-design automation software system that provides a complete set of simulation technologies ranging from frequency and time-domain circuit simulation to electromagnetic field simulation.

ADS allows user to fully characterize and optimize designs. The single, integrated design environment provides system and circuit simulators, along with schematic capture, layout, and verification capability. ADS also simplifies design flow by eliminating the stops and starts associated with changing design tools during mid-cycle [9].

B. BASIC SINGLE FREQUENCY LCC

An ADS model of an ideal basic single frequency LCC with component parameters is shown in Figure 12. It consists of an RF power source, two power splitters, two termination loads, a circulator, a phase shifter and an attenuator.

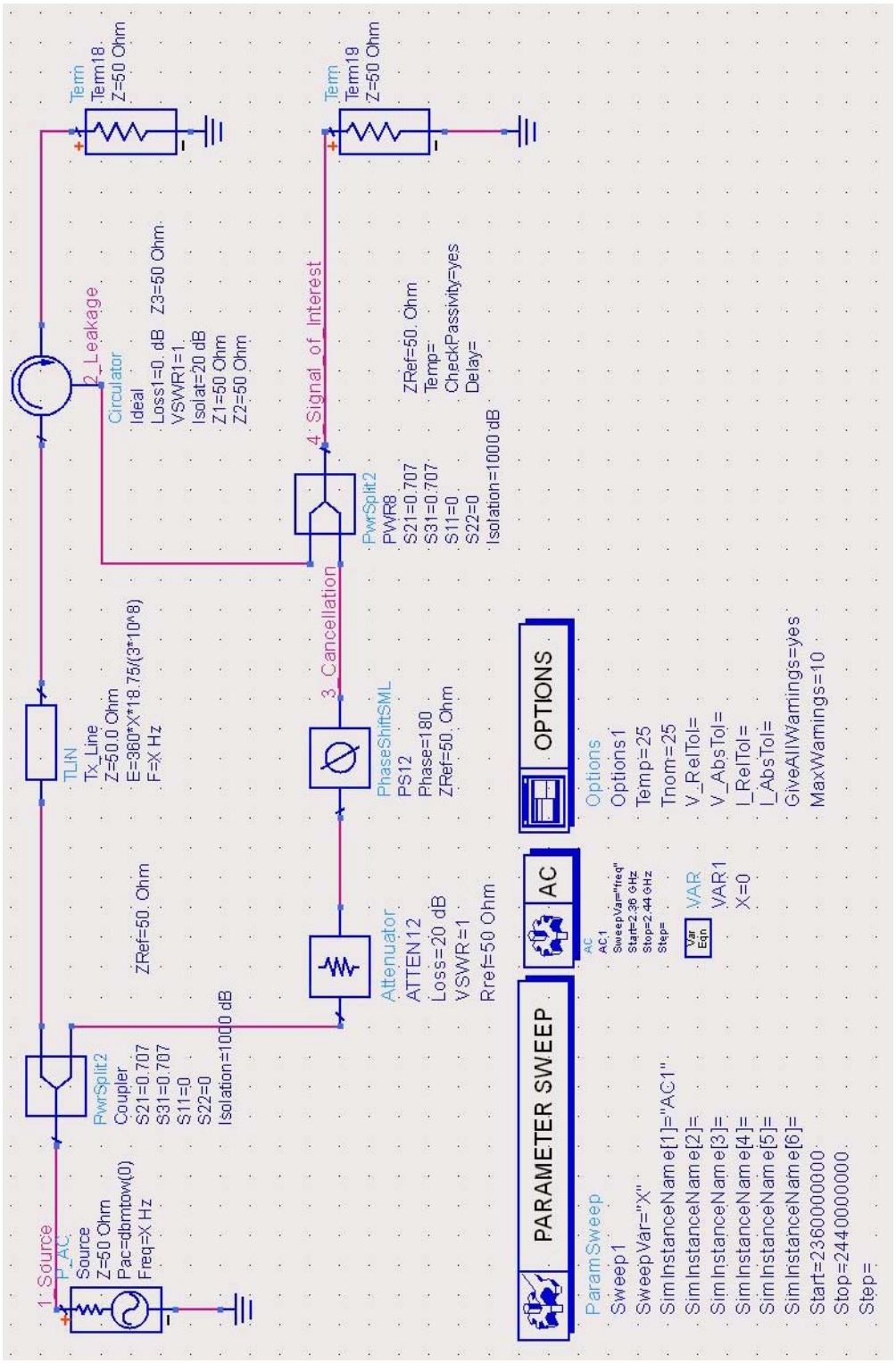

Figure 12. ADS Model of the Basic Single Frequency LCC.

ADS allows users to designate points within the circuit for data collection as illustrated in Table 1.

Table 1. Signal Notation for ADS Model of the Basic Single Frequency LCC.

Name	ADS Label	Circuit Data Point	Variable(s) (Eq 5)
Source	1_Source	1	-
Leakage	2_Leakage	2	L or $L+M$
Cancellation	3_Cancellation	3	C
SOI	4_Signal_of_Interest	4	S

The model was first simulated using ideal component parameters such as 1000 dB of isolation for the power dividers, perfectly matched loads, and zero losses in the circulator.

The power source output was arbitrarily set to 0 dBm for convenience. The circulator isolation was set to 20 dB to allow a realistic amount of leakage in the circuit. The perfectly matched load at port 2 of the circulator ensured that there was no circulating of signal from port 2 to 3, resulting in the signal received at port 3 to be only the leakage signal. This leakage signal was then coupled with a tunable cancellation signal using the second power splitter (PwrSplit2).

The ADS tabulated results can be represented in user-defined units, allowing flexible conversion of data for analysis. Users can also choose to sweep user-defined parameters, such as frequency, to observe response over a range of inputs. The results shown in Tables 2 and 3 are only a truncated version of the entire simulation results. The input frequency was swept from 2.36 GHz to 2.44 GHz in steps of 250 kHz.

The measurements in dB are useful for calculating the amount of attenuation necessary in the LCC branch as the parameters input for the component in ADS are only accepted in dB values. Note that the dB( ) function in ADS returns the decibel measure

of a voltage ratio, while the dBm( ) function returns the decibel measure of a voltage referenced to a 1 milliwatt signal [10]. For example, *y = dB(100)* returns *40*, and *y = dBm(100)* returns *50*.

The measurements of phase angle in degrees allow better understanding of the phase shifts at particular frequencies and provide insight as to why the basic LCC can only achieve a notch at a single frequency.

Table 2. Sample LCC Measurements in dB/ Degrees.

freq	var("1_Source")	var("2_Leakage")	var("3_Cancellation")	var("4_Signal_of_Interest")
2.40000 GHz	-10.00000 / -0.00014	-33.01161 / 0.00029	-33.01161 / 180.00000	-142.04381 / 90.00029
2.40025 GHz	-10.00000 / -3.10474E-16	-33.01161 / -5.62500	-33.01161 / 180.00000	-56.18671 / -92.81250
2.40050 GHz	-10.00000 / 1.21670E-14	-33.01161 / -11.25000	-33.01161 / 180.00000	-50.17658 / -95.62500
2.40075 GHz	-10.00000 / 1.24207E-14	-33.01161 / -16.87500	-33.01161 / 180.00000	-46.67222 / -98.43750
2.40100 GHz	-10.00000 / -4.76799E-15	-33.01161 / -22.50000	-33.01161 / 180.00000	-44.19791 / -101.25000
2.40125 GHz	-10.00000 / 5.16273E-15	-33.01161 / -28.12500	-33.01161 / 180.00000	-42.29121 / -104.06250
2.40150 GHz	-10.00000 / -4.03371E-15	-33.01161 / -33.75000	-33.01161 / 180.00000	-40.74614 / -106.87500
2.40175 GHz	-10.00000 / 3.47480E-15	-33.01161 / -39.37500	-33.01161 / 180.00000	-39.45286 / -109.68750
2.40200 GHz	-10.00000 / -3.17959E-15	-33.01161 / -45.00000	-33.01161 / 180.00000	-38.34583 / -112.50000
2.40225 GHz	-10.00000 / -1.78316E-16	-33.01161 / -50.62500	-33.01161 / 180.00000	-37.38278 / -115.31250
2.40250 GHz	-10.00000 / 2.52676E-15	-33.01161 / -56.25000	-33.01161 / 180.00000	-36.53489 / -118.12500
2.40275 GHz	-10.00000 / -3.84772E-16	-33.01161 / -61.87500	-33.01161 / 180.00000	-35.78163 / -120.93750
2.40300 GHz	-10.00000 / 1.70380E-15	-33.01161 / -67.50000	-33.01161 / 180.00000	-35.10784 / -123.75000

Table 3. Sample LCC Measurements in dBm.

freq	dbm(var("1_Source"))	dbm(var("2_Leakage"))	dbm(var("3_Cancellation"))	dbm(var("4_Signal_of_Interest"))
2.40000 GHz	1.35659E-10	-23.01161	-23.01161	-132.04381
2.40025 GHz	-7.10543E-15	-23.01161	-23.01161	-46.18671
2.40050 GHz	-7.10543E-15	-23.01161	-23.01161	-40.17658
2.40075 GHz	-7.10543E-15	-23.01161	-23.01161	-36.67222
2.40100 GHz	-1.06581E-14	-23.01161	-23.01161	-34.19791
2.40125 GHz	-7.10543E-15	-23.01161	-23.01161	-32.29121
2.40150 GHz	-7.10543E-15	-23.01161	-23.01161	-30.74614
2.40175 GHz	-7.10543E-15	-23.01161	-23.01161	-29.45286
2.40200 GHz	-7.10543E-15	-23.01161	-23.01161	-28.34583
2.40225 GHz	-7.10543E-15	-23.01161	-23.01161	-27.38278
2.40250 GHz	-7.10543E-15	-23.01161	-23.01161	-26.53489
2.40275 GHz	-8.88178E-15	-23.01161	-23.01161	-25.78163
2.40300 GHz	-7.10543E-15	-23.01161	-23.01161	-25.10784

Normally, there is a phase versus frequency difference between the main and cancellation paths due to physical line length variations, and the phases of reflected and transmitted signals through the devices in these paths. For effective wideband cancellation, the phase slope of the main and cancellation branches must be matched. For this purpose, an ideal transmission line (TLIN) of an electrical length *E* was added

between the first coupler and the circulator to balance the frequency slope for the signals propagating through the two branches of the circuit.

The formula for the electrical length of the transmission line is

$$E = \beta \times l \tag{8}$$

where $\beta = \frac{2\pi}{\lambda}$ is the propagation constant, and l is the physical length of the transmission line. Converting to degrees, we see that Equation (8) becomes

$$E = \frac{360 \times f \times l}{c} \tag{9}$$

where the phase velocity is assumed to be $c = 3 \times 10^8$ m/s. The amount of cancellation is affected by this tunable phase that is adjusted through the settings of the attenuator and the phase shifter in the cancellation branch.

The effect of the transmission line inserted in a network tuned to frequencies of 2.38 GHz, 2.39 GHz and 2.41 GHz is shown in Figures 13 to 18. The model in Figure 12 is used and the values of the physical length of transmission line *l* are based on 150 times the wavelength of the frequency of interest, which are 18.908 m, 18.828 m and 18.672 m, respectively. These values are near those required to compensate for phase delays in the multiplexing circuits discussed in Section C.

The effect of the transmission line on the rate of change in the phase angles is illustrated in Figures 19 to 21. In this example, the frequency band of interest is set to 2.36 GHz to 2.44 GHz and the values of the physical length of transmission line *l* are 50 times, 150 times and 250 times the wavelength at 2.4 GHz, which are 6.25 m, 18.75 m and 31.25 m, respectively. Note that for a length of transmission line *l* the phase shift $\Delta\phi$ is related to the frequency shift Δf by

$$\begin{aligned}\Delta\phi &= \phi_2 - \phi_1 \\ &= \frac{2\pi}{c} l(f_2 - f_1) \\ &= \frac{2\pi}{c} l(\Delta f)\end{aligned} \qquad (10)$$

For example, if 6 cycles of 2π shift are required over $(2.44 - 2.36)$ GHz $= 80$ MHz, then the required l is 22.5 m.

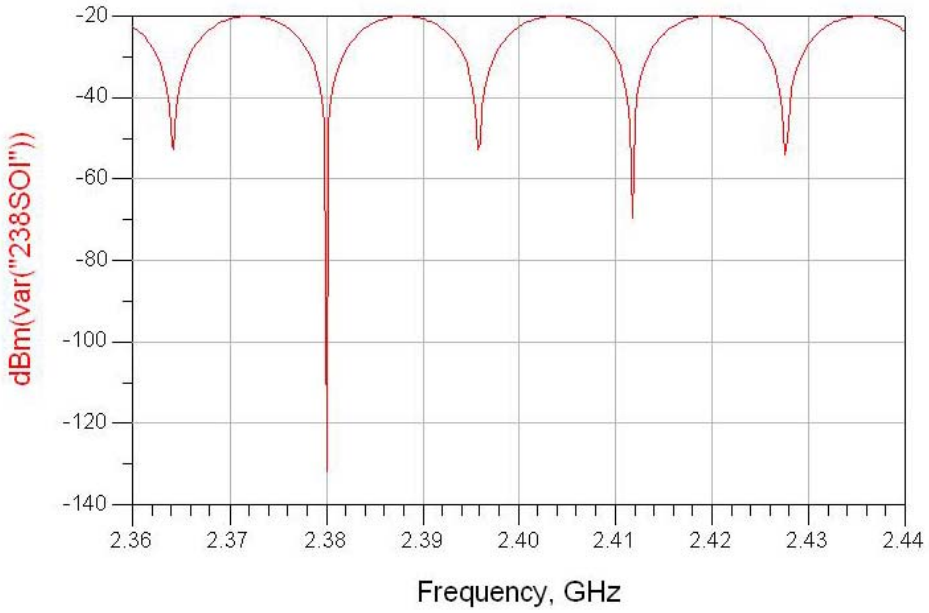

Figure 13. Amplitude Plot of SOI for l = 18.908 m.

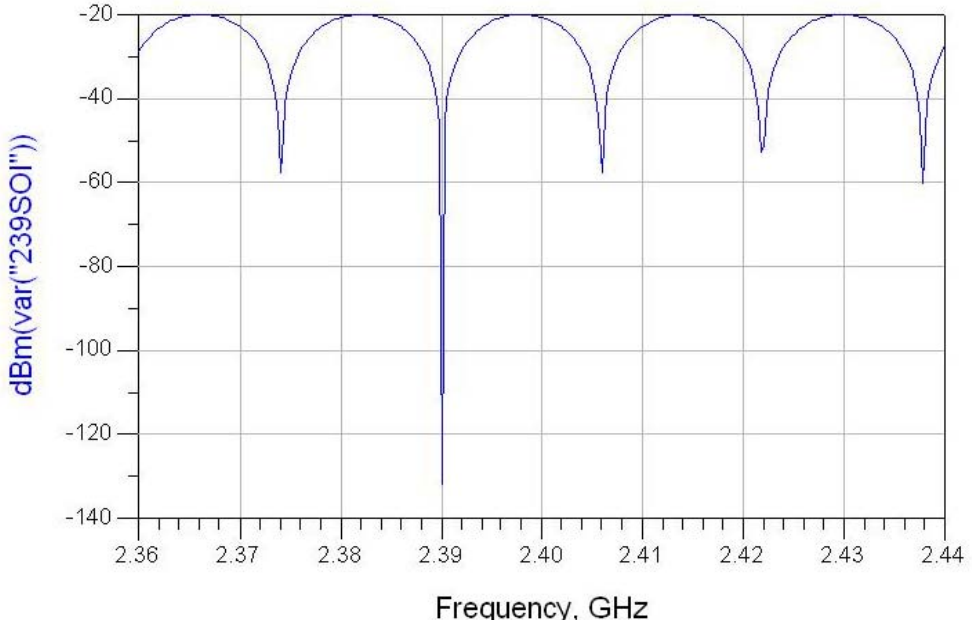

Figure 14. Amplitude Plot of SOI for l = 18.828 m.

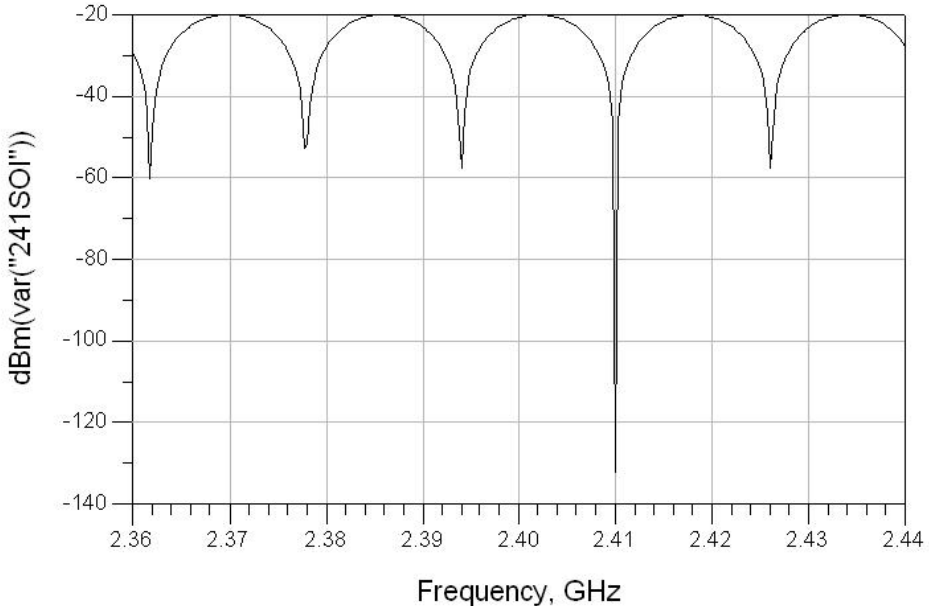

Figure 15. Amplitude Plot of SOI for l = 18.672 m.

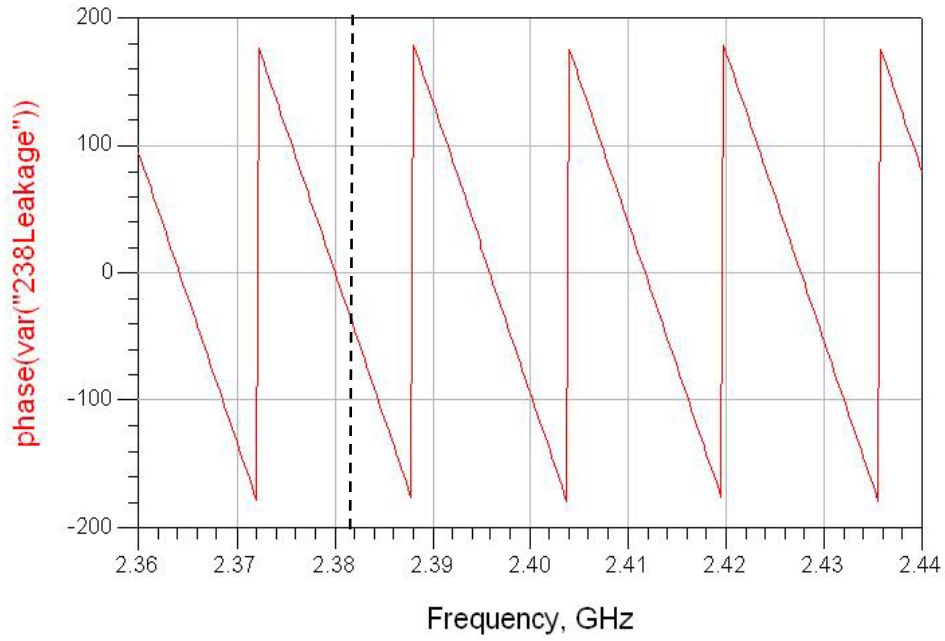

Figure 16. Phase Plot of Leakage for l = 18.908 m.

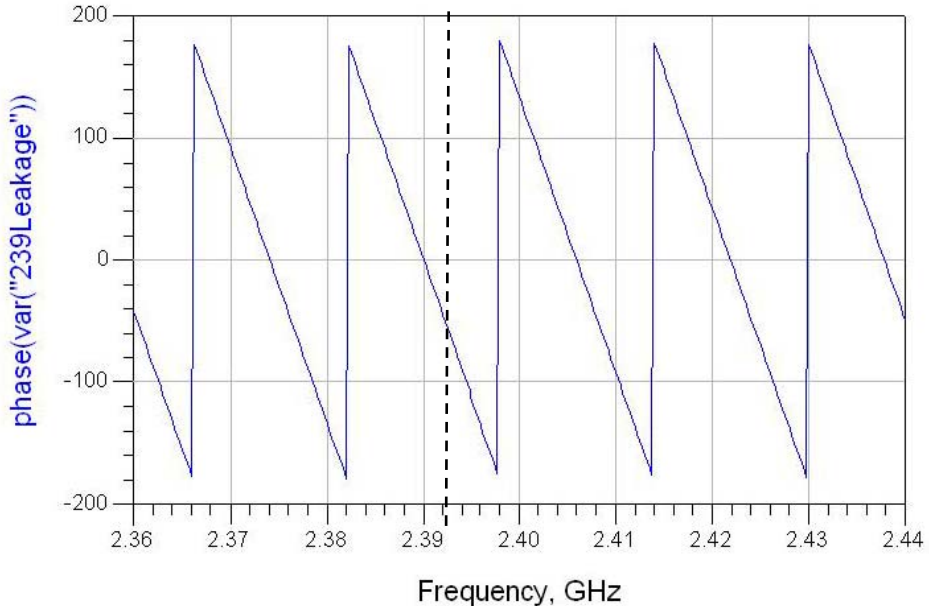

Figure 17. Phase Plot of Leakage for l = 18.828 m.

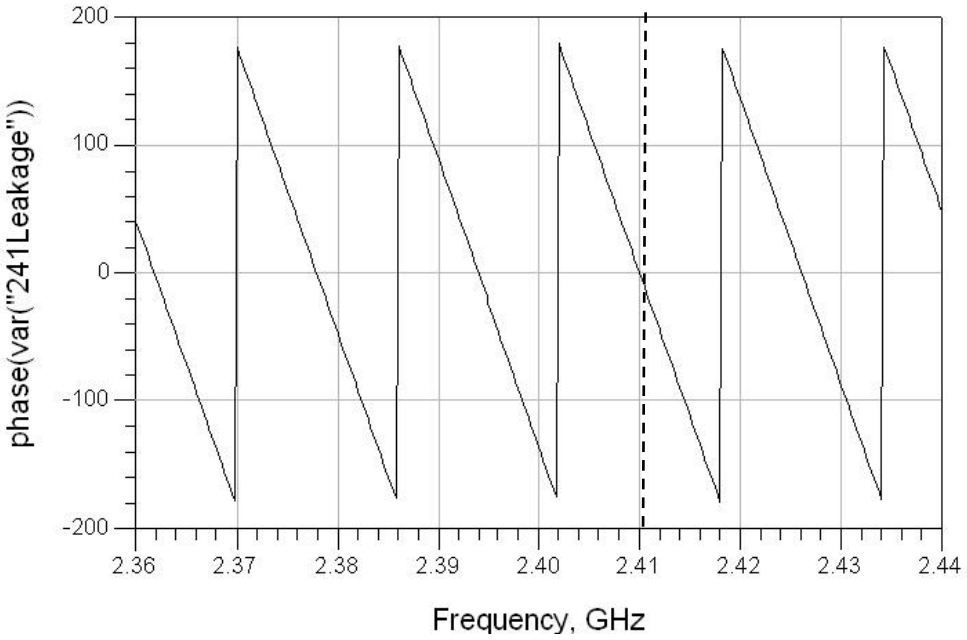

Figure 18. Phase Plot of Leakage for l = 18.672 m.

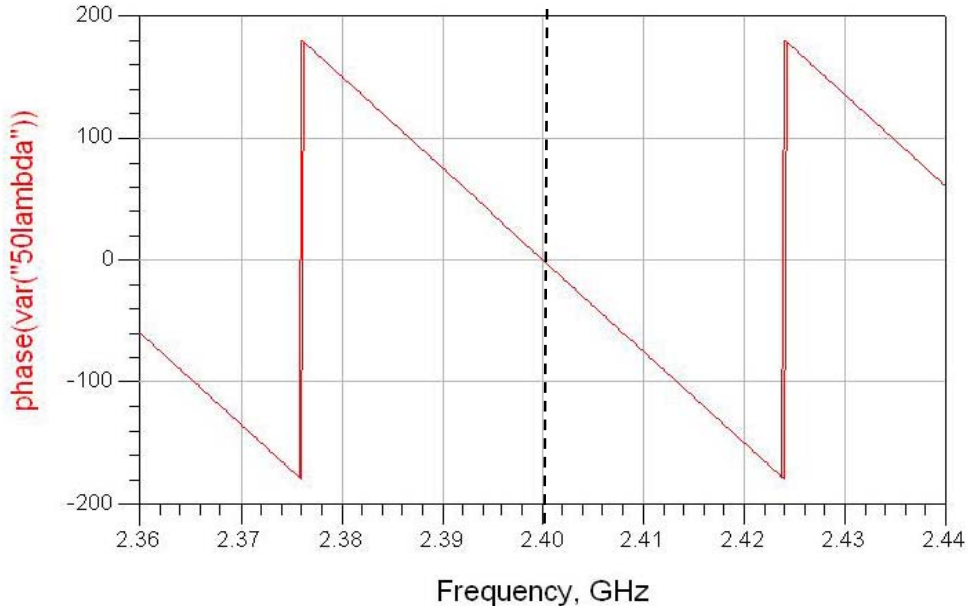

Figure 19. Phase Plot of Leakage for l = 6.25 m.

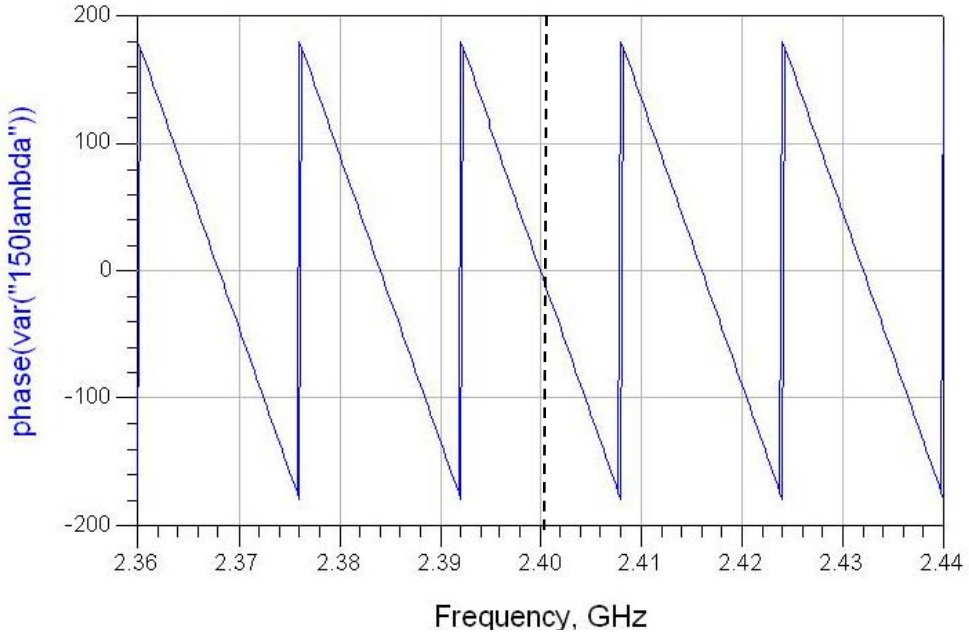

Figure 20. Phase Plot of Leakage for l = 18.75 m.

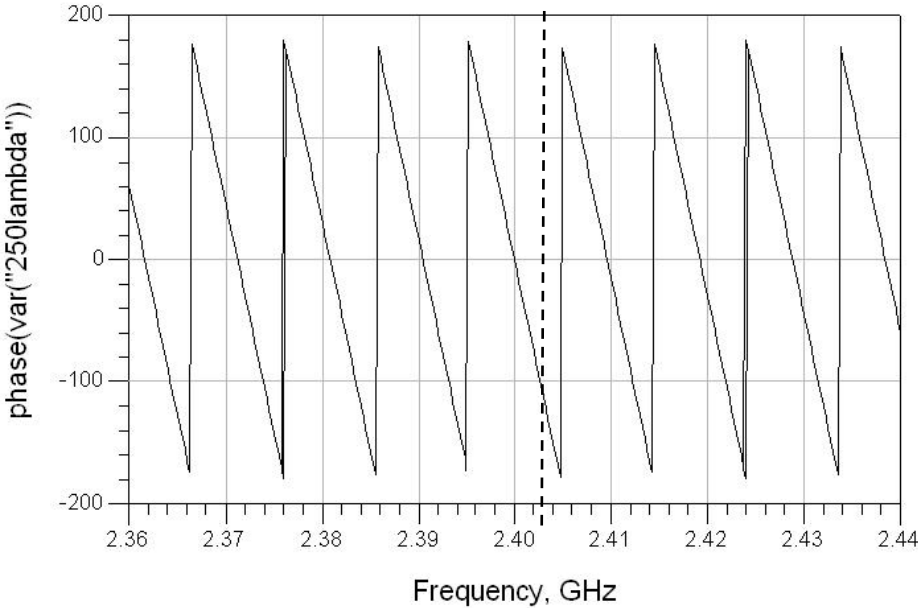

Figure 21. Phase Plot of Leakage for l = 31.25 m.

For the analysis of the single frequency LCC setup shown in Figure 12, the transmission line is customized for $l = 18.75\,\text{m}$. This is to simulate a network tuned to 2.4 GHz frequency, hence, allowing this LCC to function effectively at 2.4 GHz. This is illustrated by the notch at 2.4 GHz in the plot of SOI shown in Figures 22 and 23. The other notches are at frequencies that depend on the electrical length of the transmission line.

For both Figures 24 and 25, the 0 dBm source is plotted in red. Also, both the amplitudes of the leakage and cancellation are equal, hence, overlapping and appear as the light blue plot. The resulting SOI is plotted in black. The notches on the SOI are the result of having a $180\,^{\circ}$ phase difference between the leakage and cancellation signals.

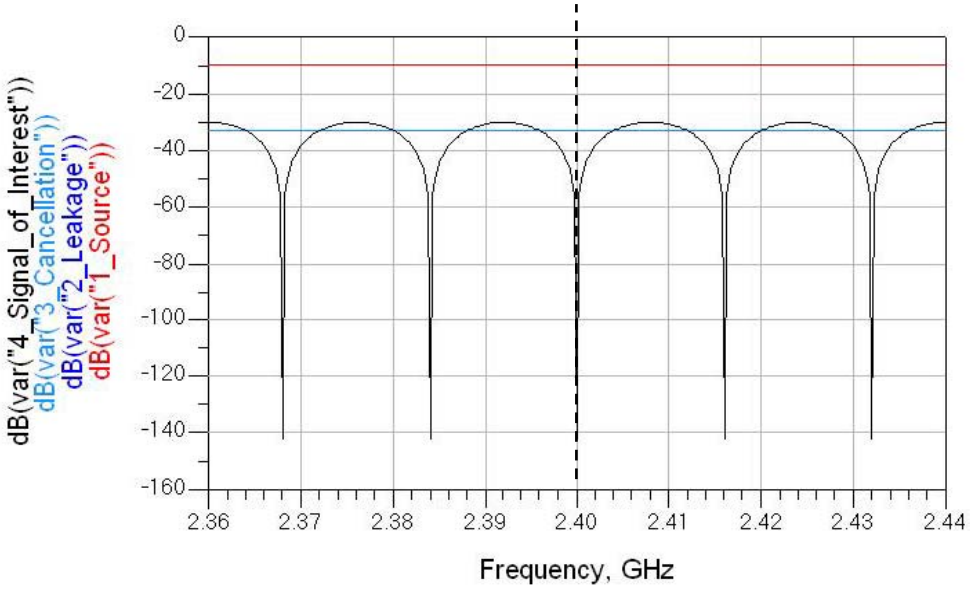

Figure 22. LCC Frequency-Domain Plots in dB.

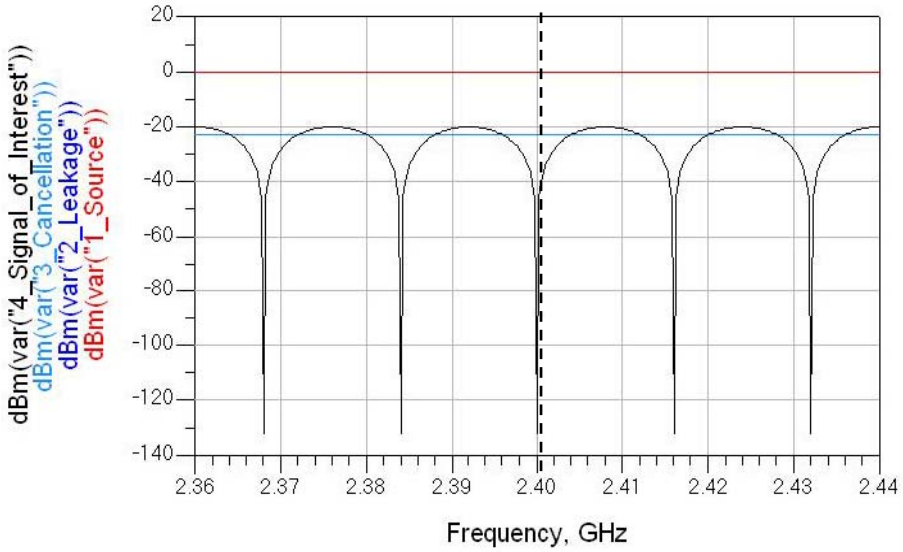

Figure 23. LCC Frequency-Domain Plots in dBm.

The measurement of phase is critical in understanding how the phase of the LCC contributes to its effectiveness. In Figure 24, it can be observed that the frequency where there is a difference of 180° in phase between the leakage and cancellation signals is 2.4 GHz. This condition also occurs at other frequencies where the phase difference is 180°, resulting in the phase response of the SOI shown in Figure 25.

It is observed that the major bandwidth limitation of the basic LCC is its inability to match the phase of the leakage signal across the entire band. The design of the WLCC will reflect this limitation.

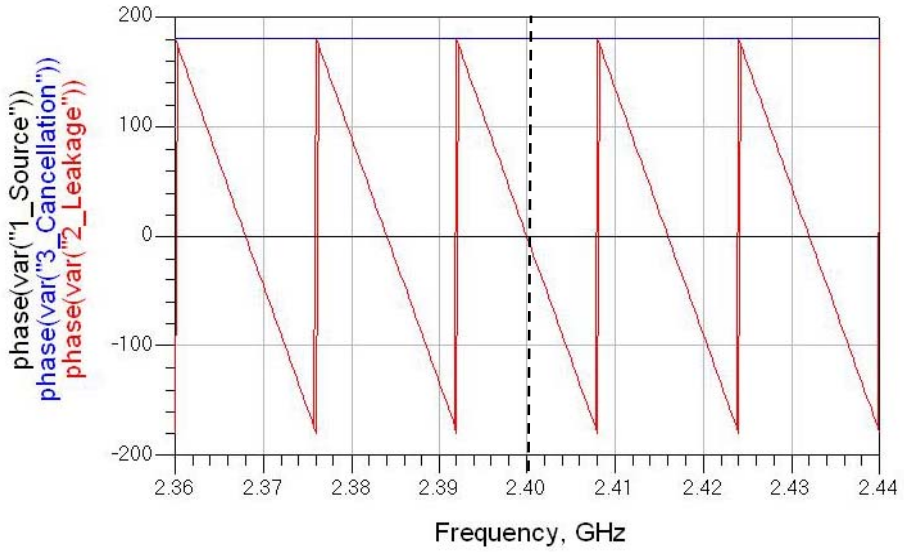

Figure 24. LCC Phase Plots for Points 1 to 3.

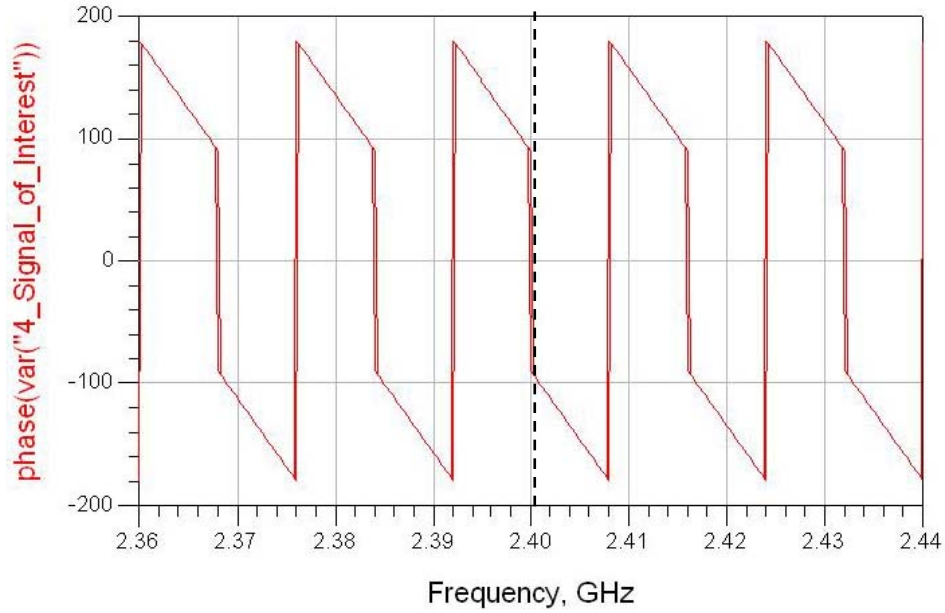

Figure 25. LCC Phase Plots for Point 4.

C. FREQUENCY DEMULTIPLEXING AND MULTIPLEXING CIRCUIT (FDMC)

1. Design Approach

The FDMC is a two-port device that is capable of performing signal demultiplexing in the forward direction and multiplexing in the reverse direction. In the forward direction, an incoming signal consisting of different frequencies is split into its

individual frequency components. This process is known as demultiplexing. In the reverse direction, many signals of different frequencies are combined into a single signal of multiple frequencies. This process is known as multiplexing. Both demultiplexing and multiplexing operations are illustrated in Figures 26 and 27, respectively.

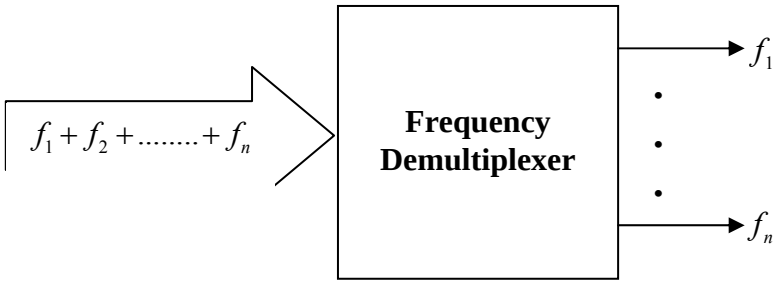

Figure 26. Demultiplexing Operation (Forward Direction).

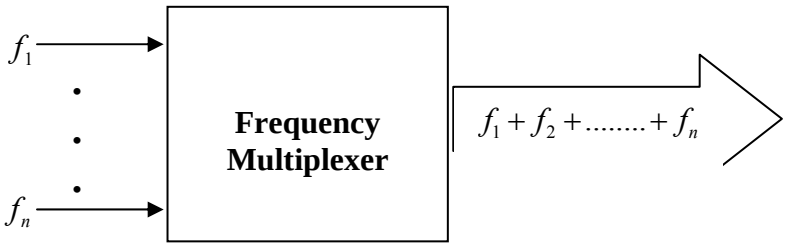

Figure 27. Multiplexing Operation (Reverse Direction).

It was decided that a three-frequency-channel FDMC would be sufficient to demonstrate the concept of a WLCC and, hence, the FDMC was designed assuming a passband of 60 MHz, consisting of three 20 MHz channels with center frequencies of 2.38 GHz, 2.4 GHz and 2.42 GHz. The ideal transfer function of a three-channel FDMC is illustrated in Figure 28.

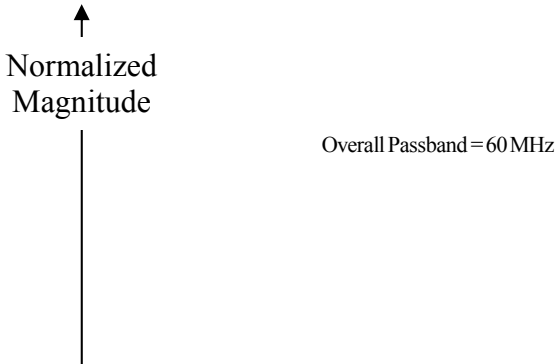

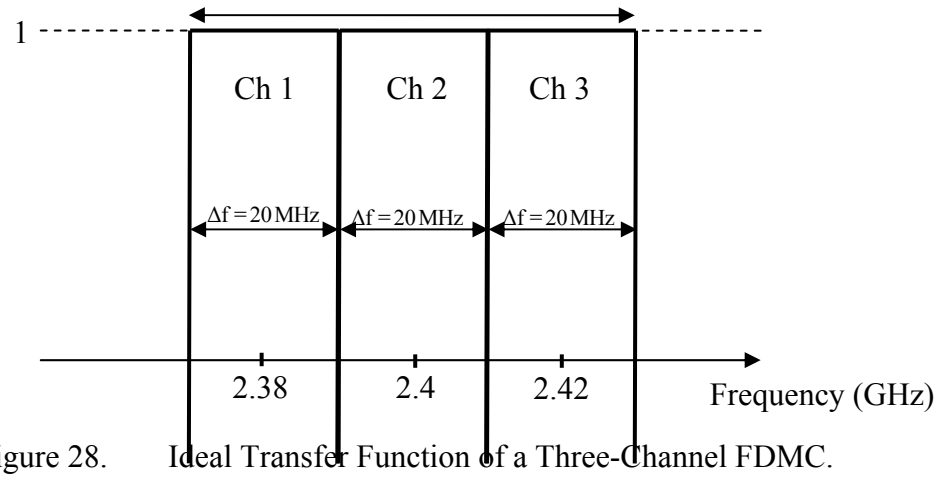

Figure 28. Ideal Transfer Function of a Three-Channel FDMC.

The FDMC was also designed to be a two port device to allow ease of integration into any circuit design, especially in the subsequent building of the WLCC.

The FDMC model was built in ADS using two different methods, both using idealized components. The first method employed circulators to circulate the leakage signal through the bank of channels, as shown in Figure 29. The second method employed couplers to split and combine the leakage signals, as shown in Figure 30.

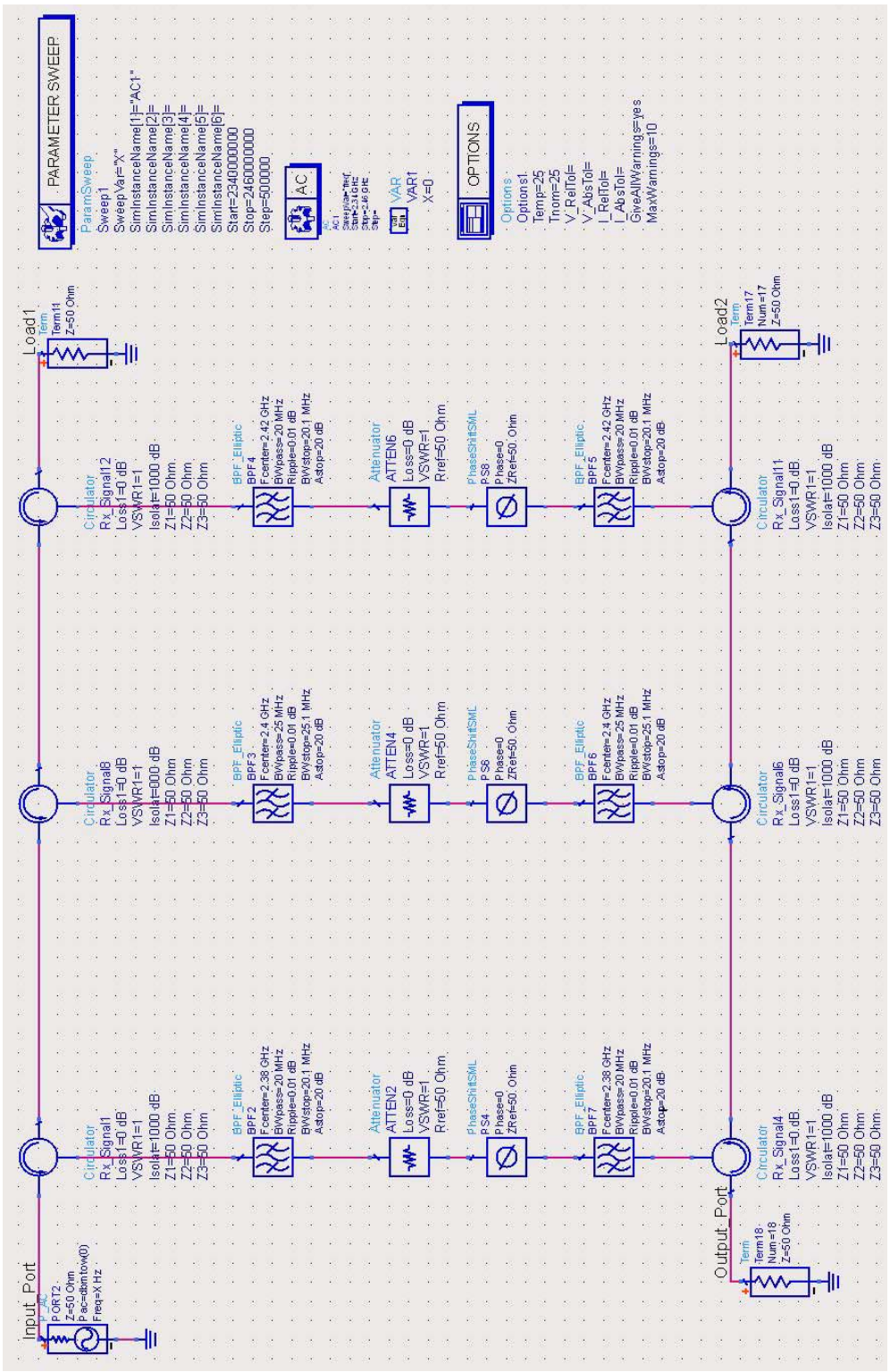
PARAMETER SWEEP
OPTIONS
Input Port
Output Port
Load1
Load2

Figure 29. ADS Model of FDMC using Circulators.

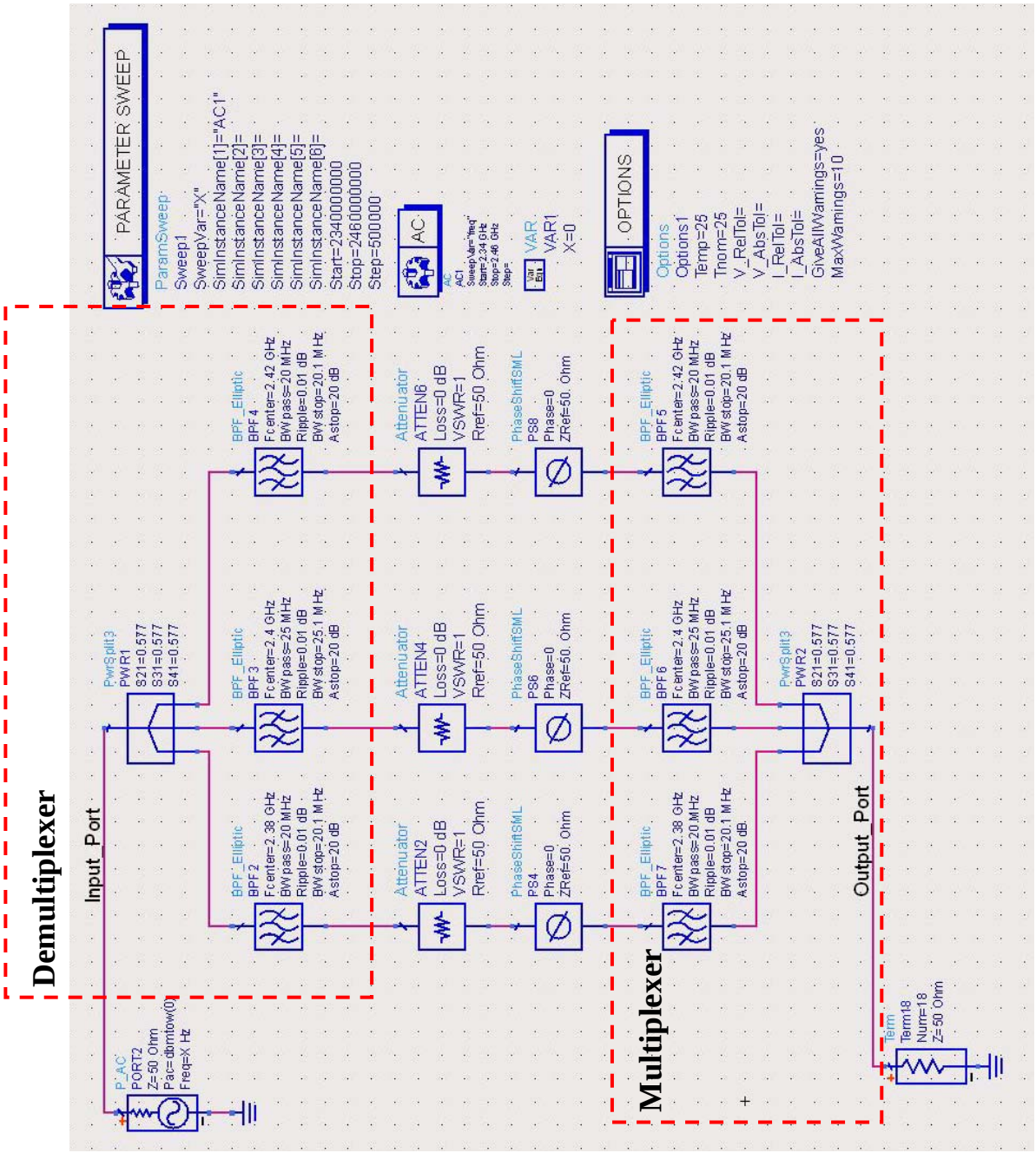

Figure 30. ADS Model of FDMC using Couplers.

2. Bandpass Filters

An *N*-channel WLCC requires the use of BPFs to segregate the coupled signal from the source into the appropriate frequency channels to undergo the process of cancellation. The ideal BPF output response must be flat at the passband and exhibit a

very steep roll-off. These channels of BPF response are subsequently placed side by side in a process known as frequency multiplexing to form a collective wide passband. The wide passband then allows cancellation at *N* number of frequencies.

The Elliptic, Chebyshev, Gaussian, Butterworth and Bessel BPFs were analyzed and it was demonstrated that the elliptic BPF offered the best output response in both amplitude and phase characteristics. The parameter settings and filter responses, both magnitude in dBm as well as phase in degrees, are shown in Figures 31 to 45.

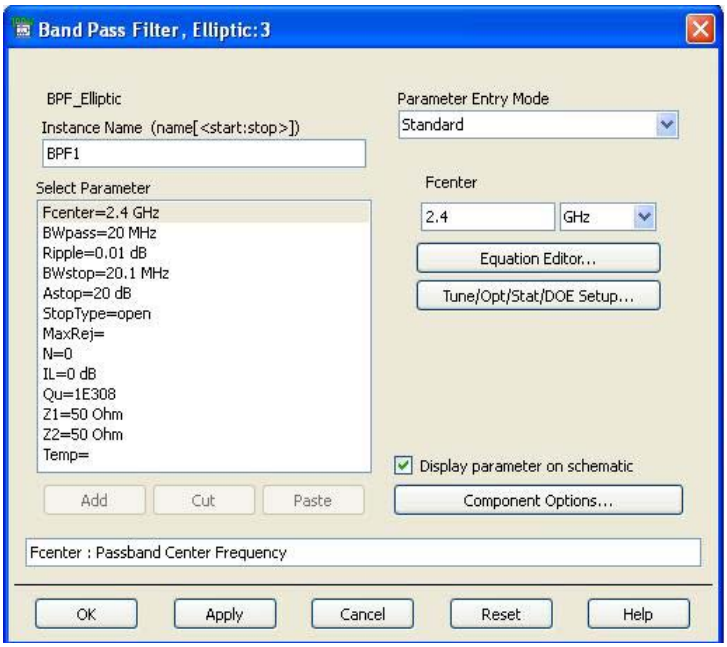

Figure 31. Parameter Settings for the Elliptic BPF.

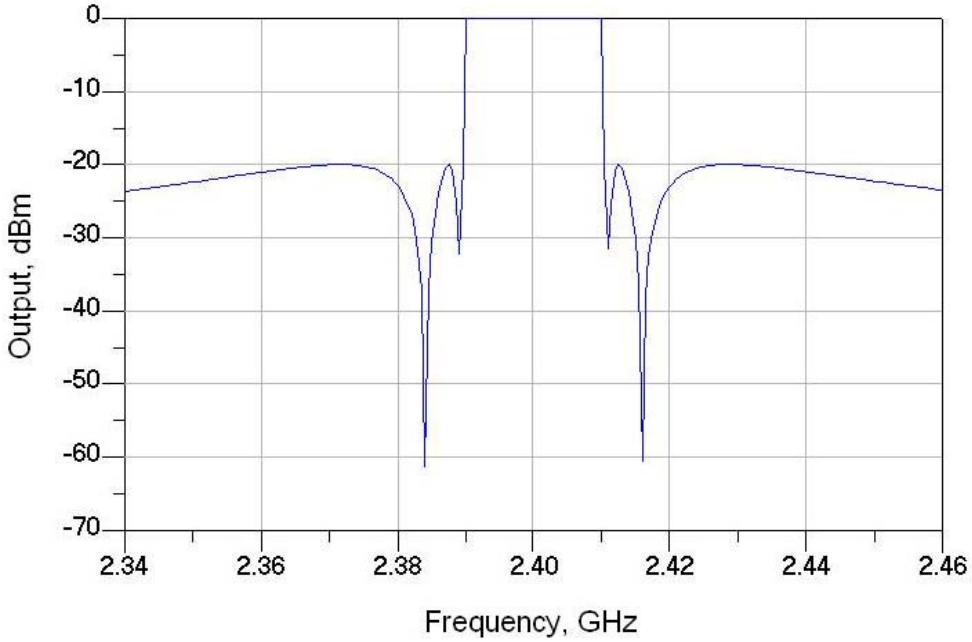

Figure 32. Output Amplitude Plot for the Elliptic BPF.

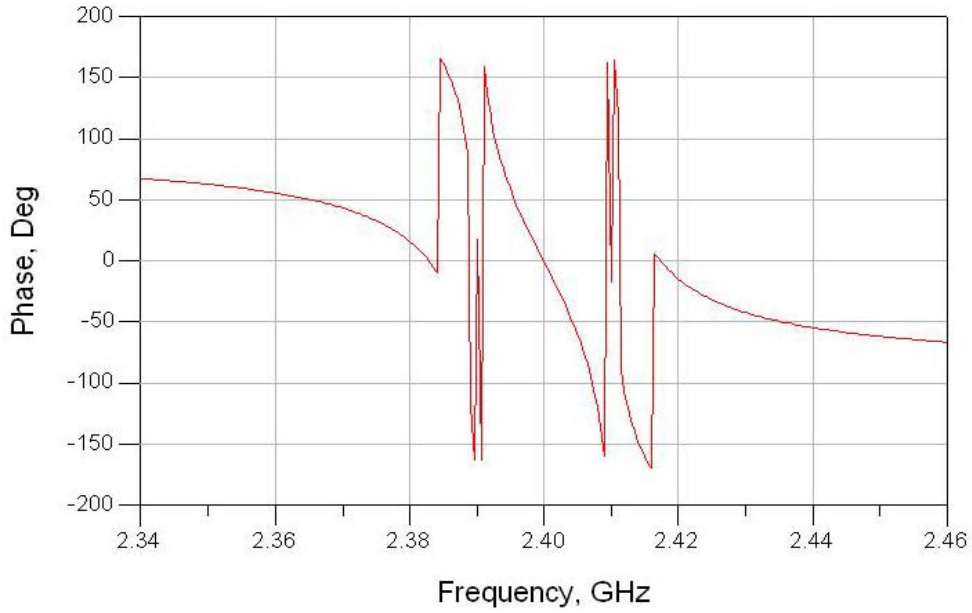

Figure 33. Output Phase Plot for the Elliptic BPF.

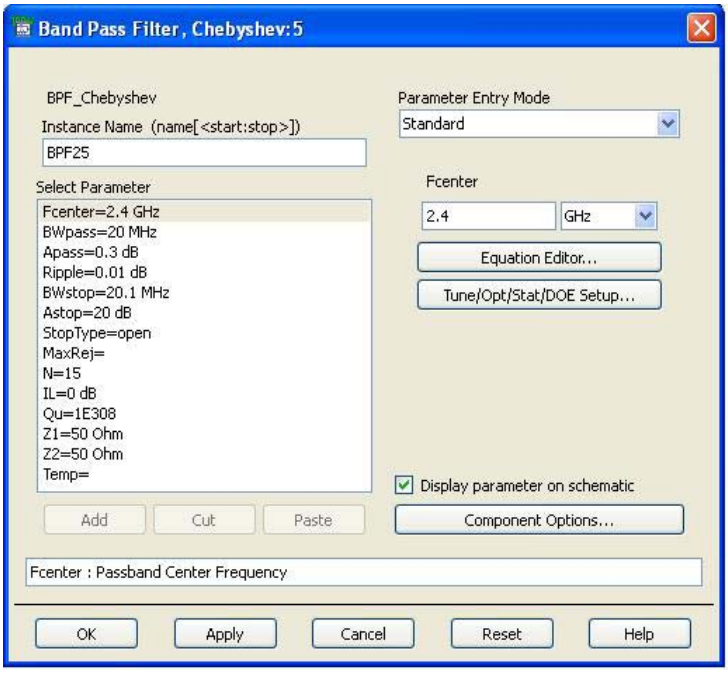

Figure 34. Parameter Settings for the Chebyshev BPF.

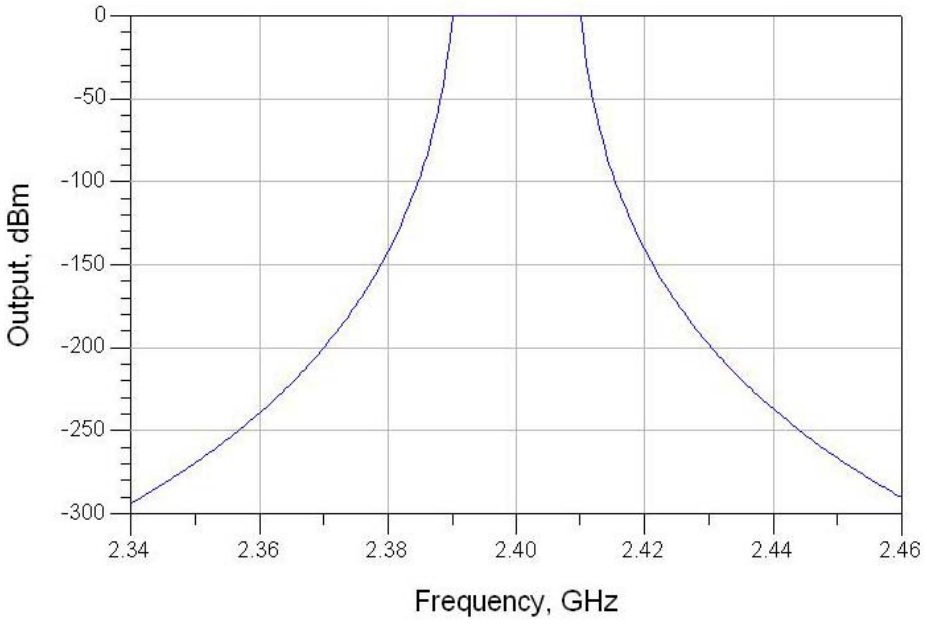

Figure 35. Output Amplitude Plot for the Chebyshev BPF.

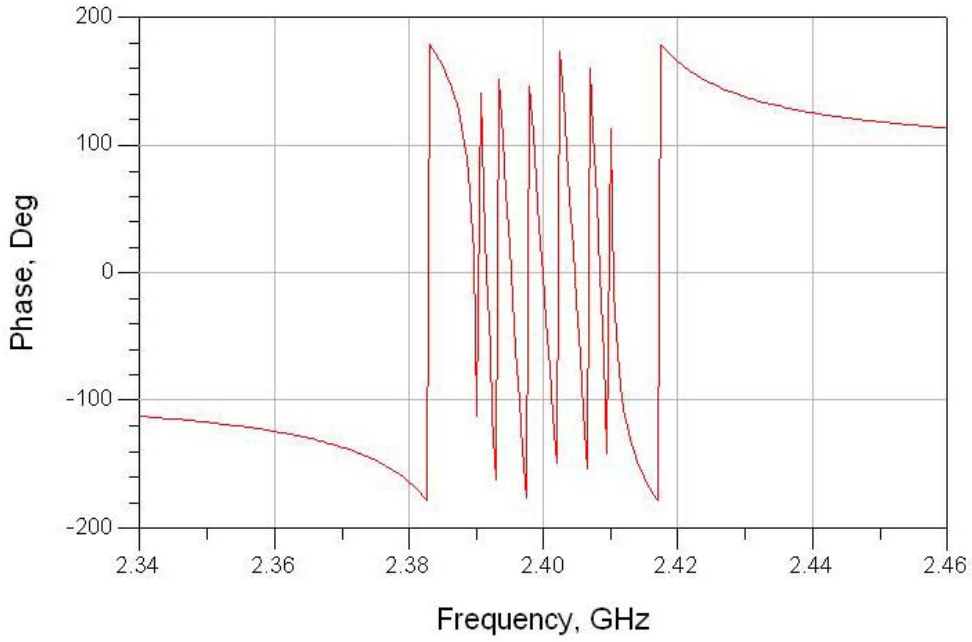

Figure 36. Output Phase Plot for the Chebyshev BPF.

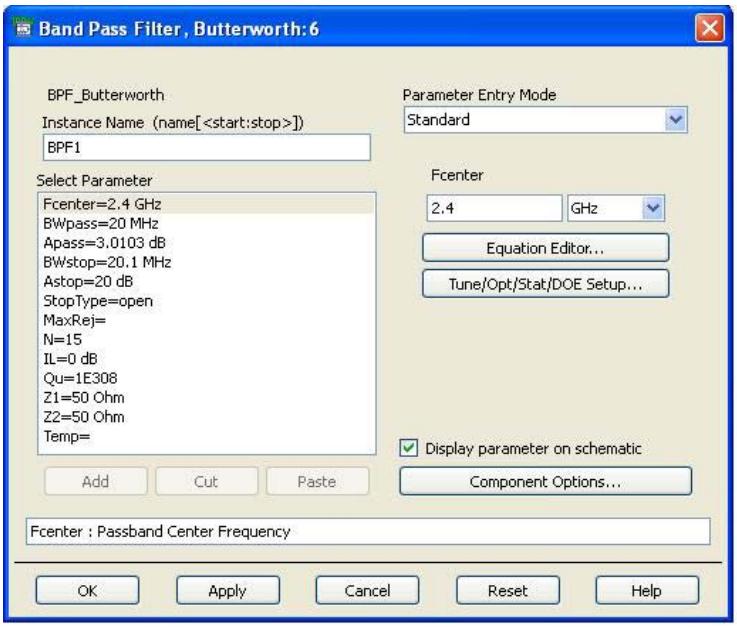

Figure 37. Parameter Settings for the Butterworth BPF.

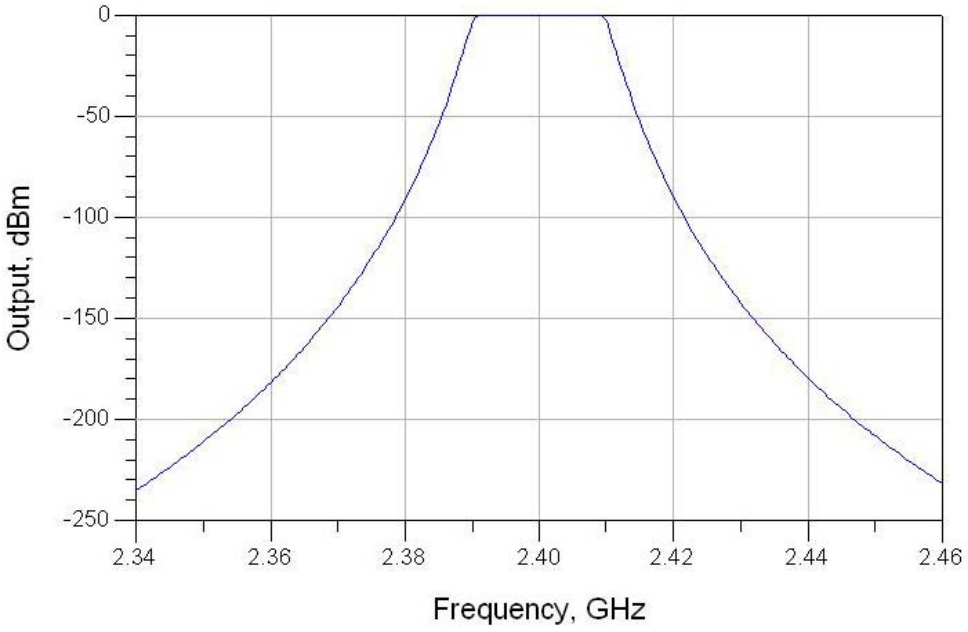

Figure 38. Output Amplitude Plot for the Butterworth BPF.

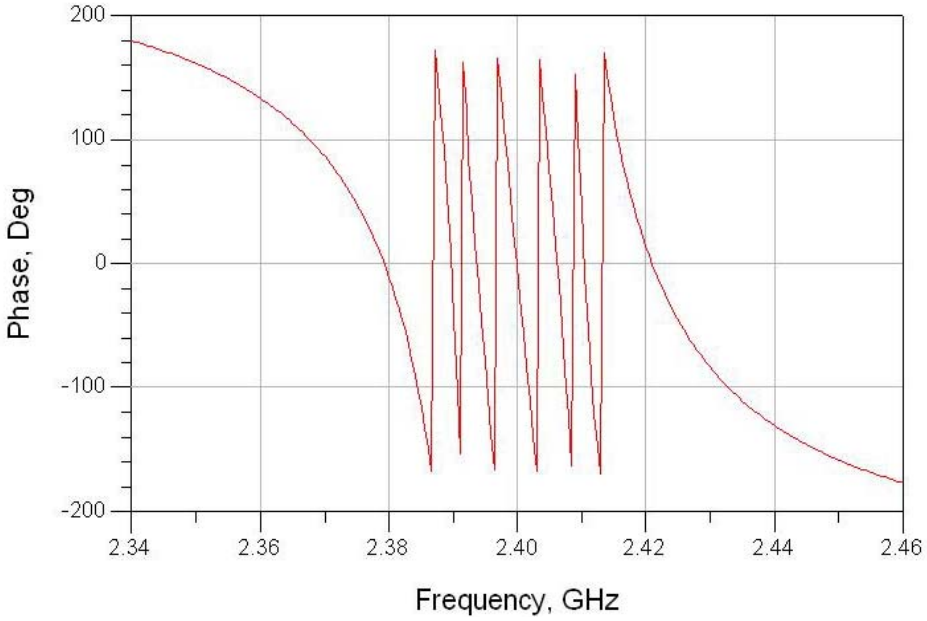

Figure 39. Output Phase Plot for the Butterworth BPF.

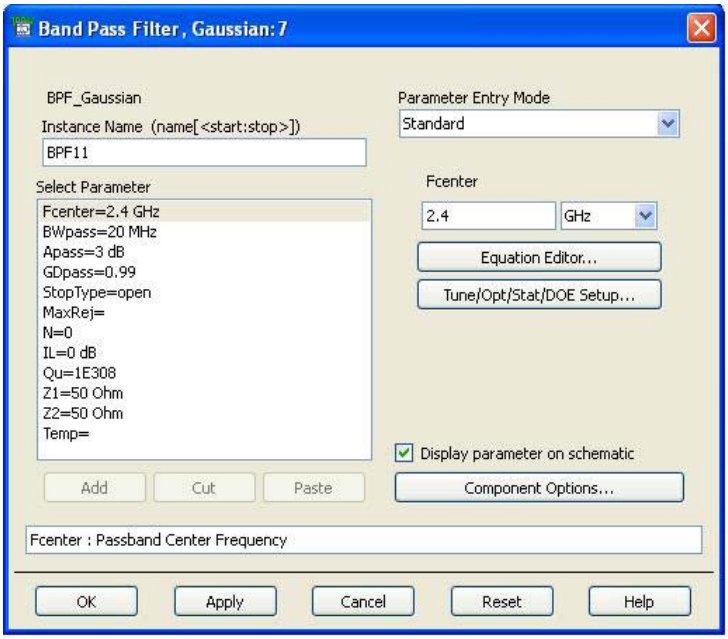

Figure 40. Parameter Settings for the Gaussian BPF.

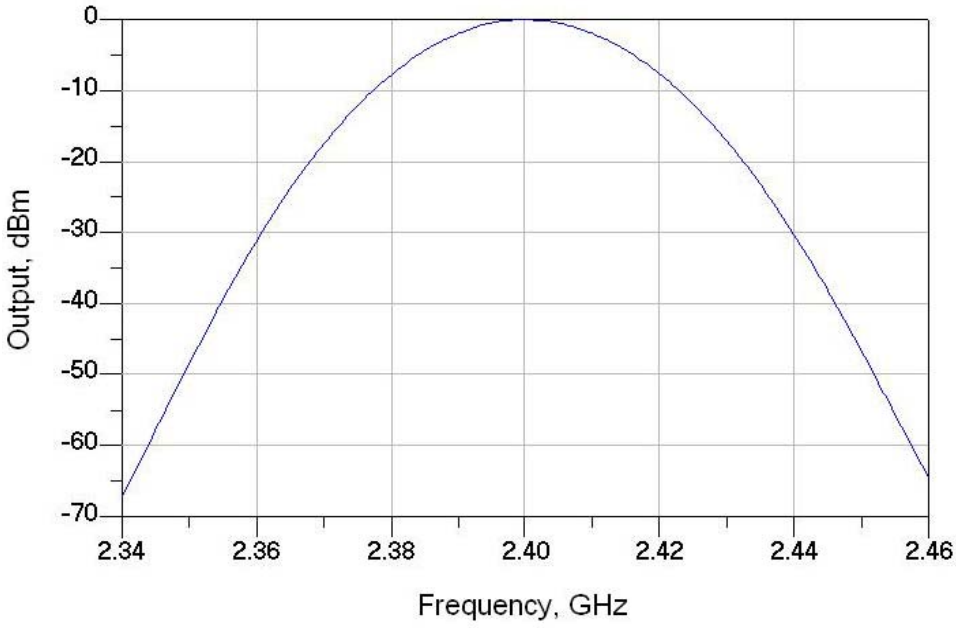

Figure 41. Output Amplitude Plot for the Gaussian BPF.

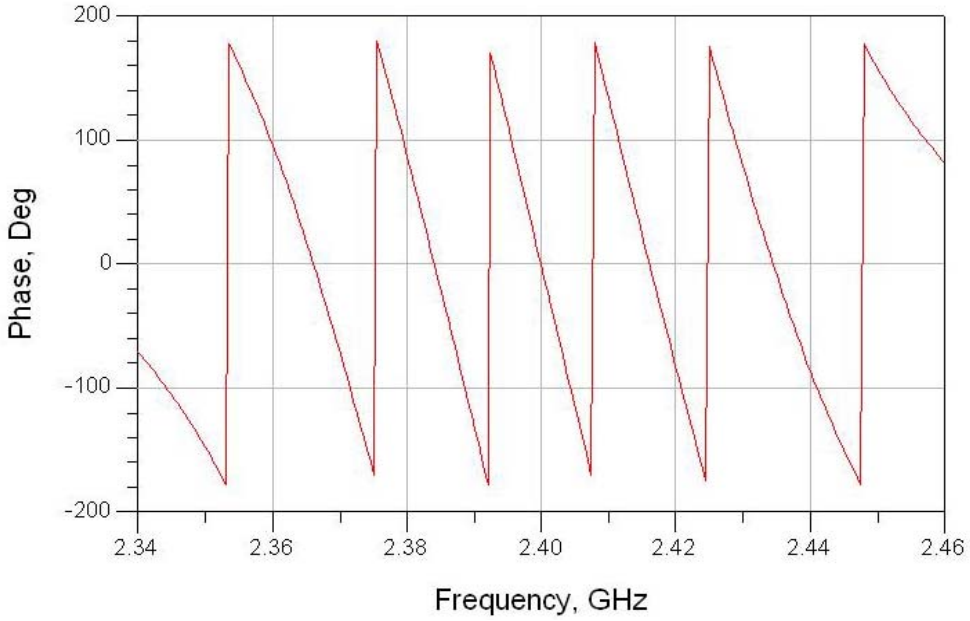

Figure 42. Output Phase Plot for the Gaussian BPF.

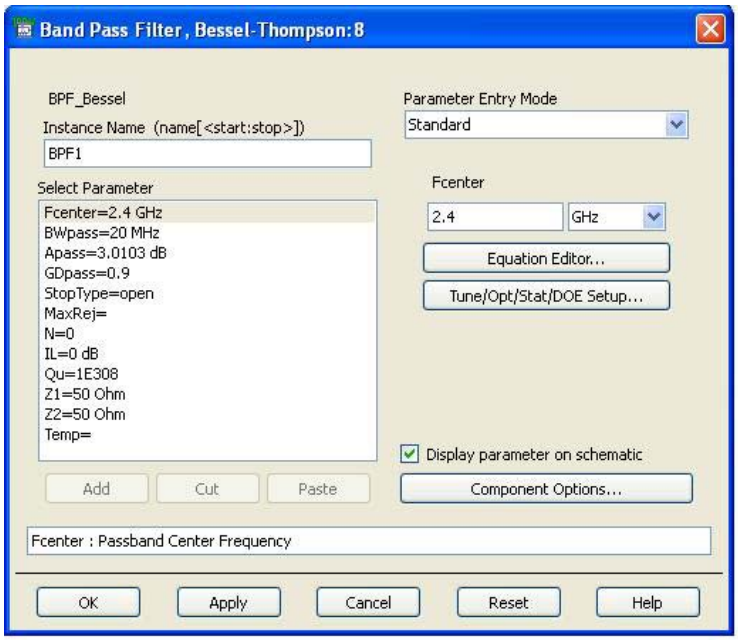

Figure 43. Parameter Settings for the Bessel BPF.

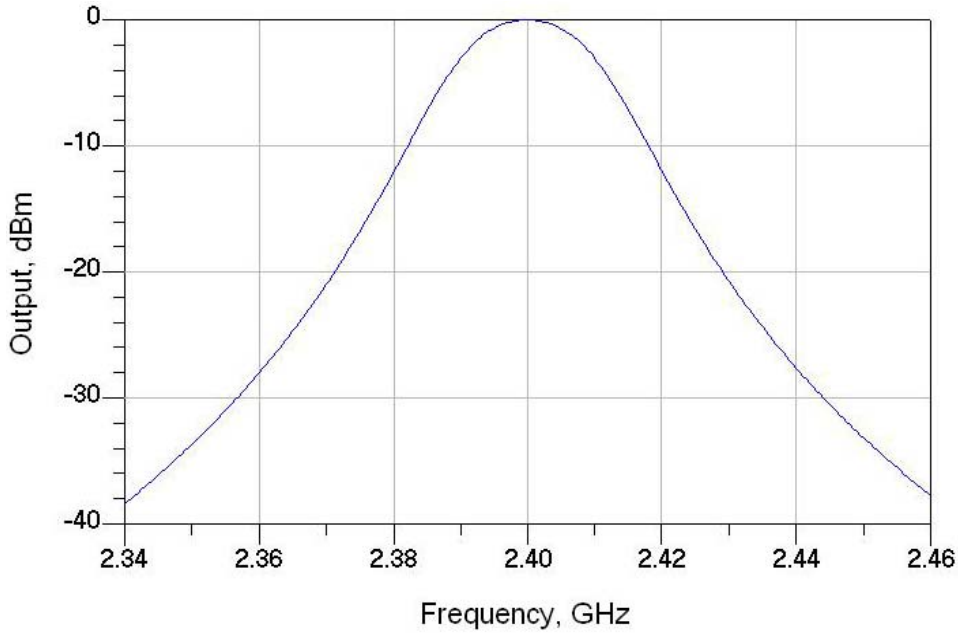

Figure 44. Output Amplitude Plot for the Bessel BPF.

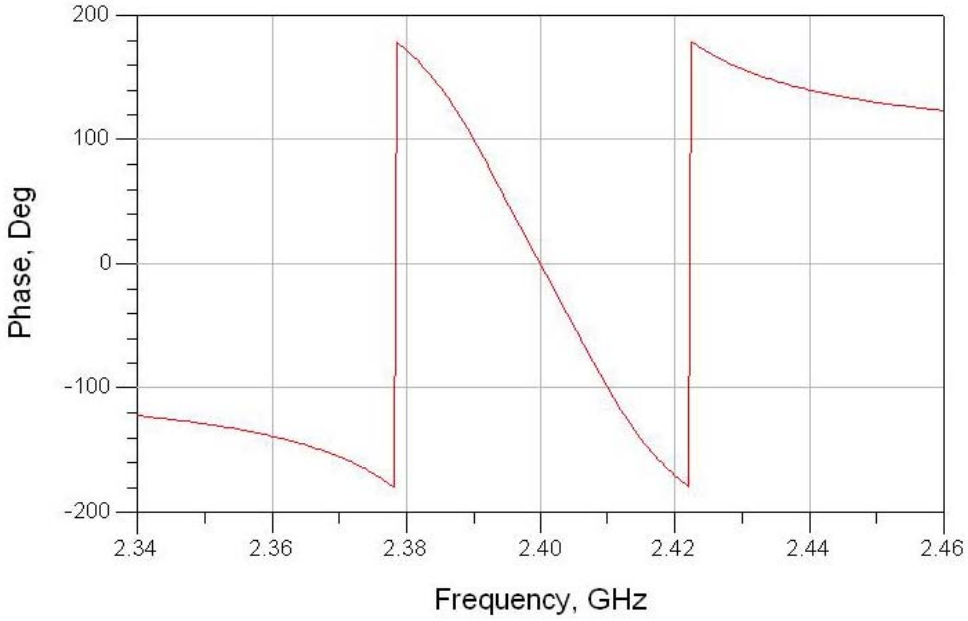

Figure 45. Output Phase Plot for the Bessel BPF.

3. FDMC Using Circulators

All five types of BPFs discussed earlier were tested for their suitability in the FDMC design. The output responses of these BPFs, for both designs of the FDMC, were

captured for analysis. The responses of the FDMC using circulators for various types of BPFs are shown in Figures 46 to 55.

With the exception of the Gaussian and Bessel BPFs, it was observed that the output amplitude level of the FDMC using circulators displayed features suitable for use in the WLCC. In particular, with these BPFs, a flat response across the passband was observed. However, they demonstrated non-linear output phases, an undesirable condition.

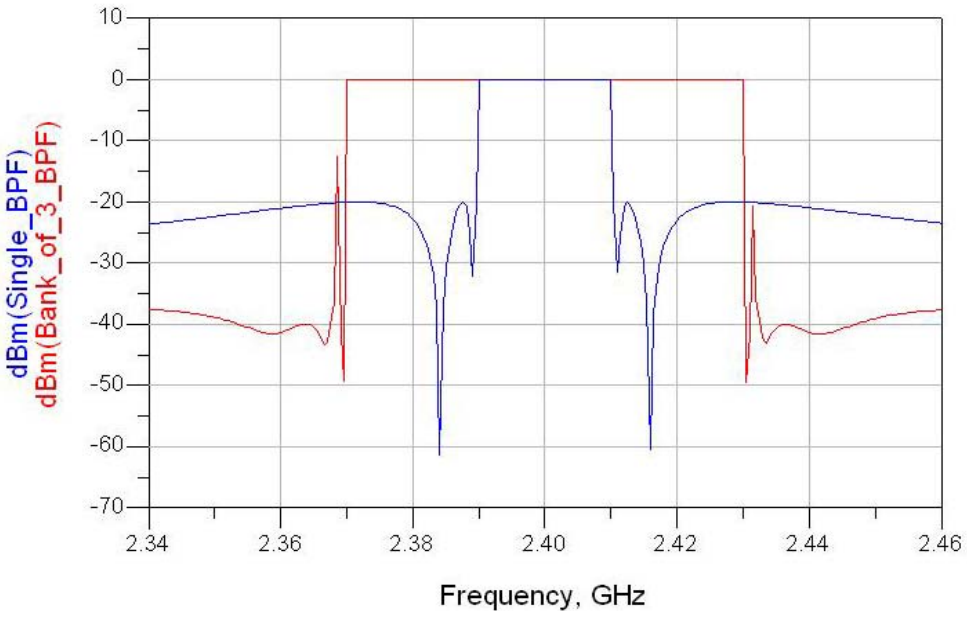

Figure 46. Output Amplitude Plot for the FDMC that uses Circulators and Elliptic Filters.

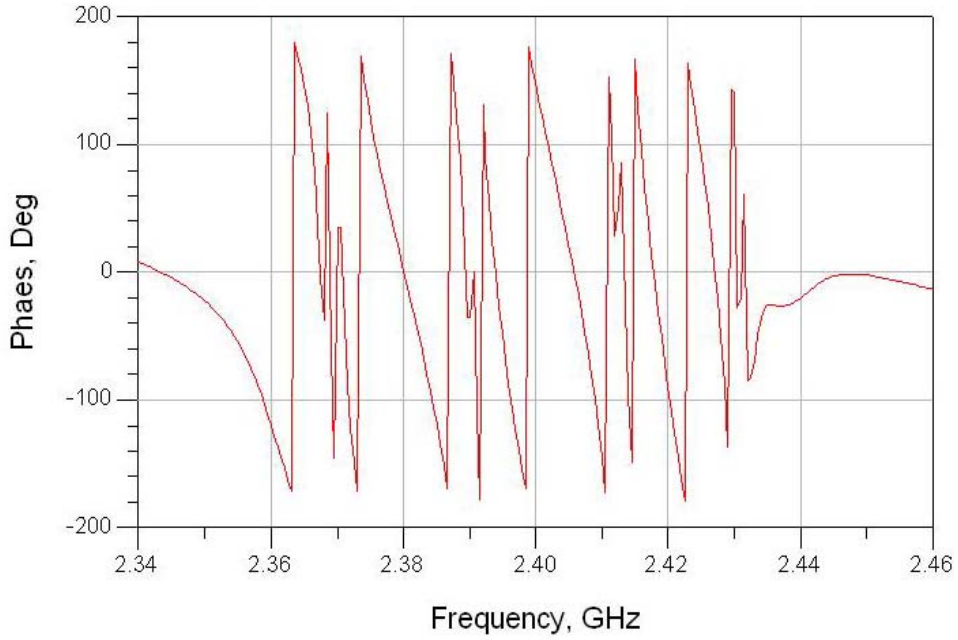

Figure 47. Phase Plot for the FDMC that uses Circulators and Elliptic Filters.

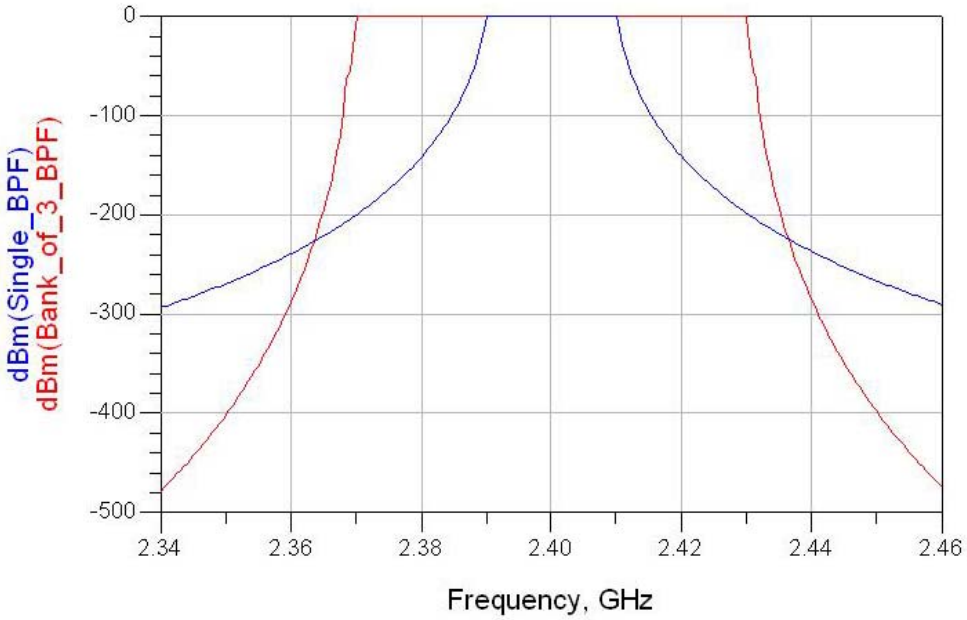

Figure 48. Output Amplitude Plot for the FDMC that uses Circulators and Chebyshev Filters.

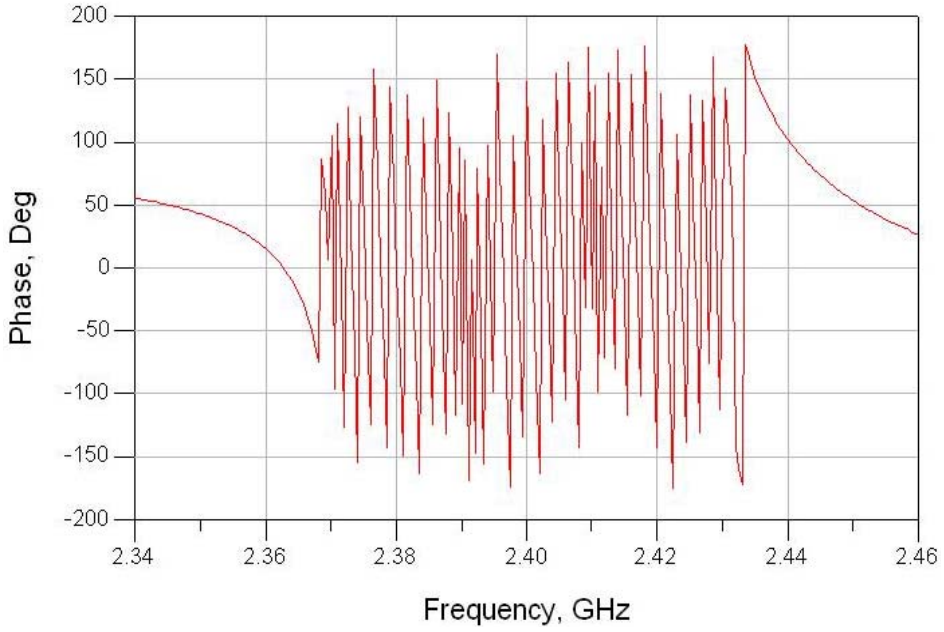

Figure 49. Phase Plot for the FDMC that uses Circulators and Chebyshev Filters.

Figure 50. Output Amplitude Plot for the FDMC that uses Circulators and Butterworth Filters.

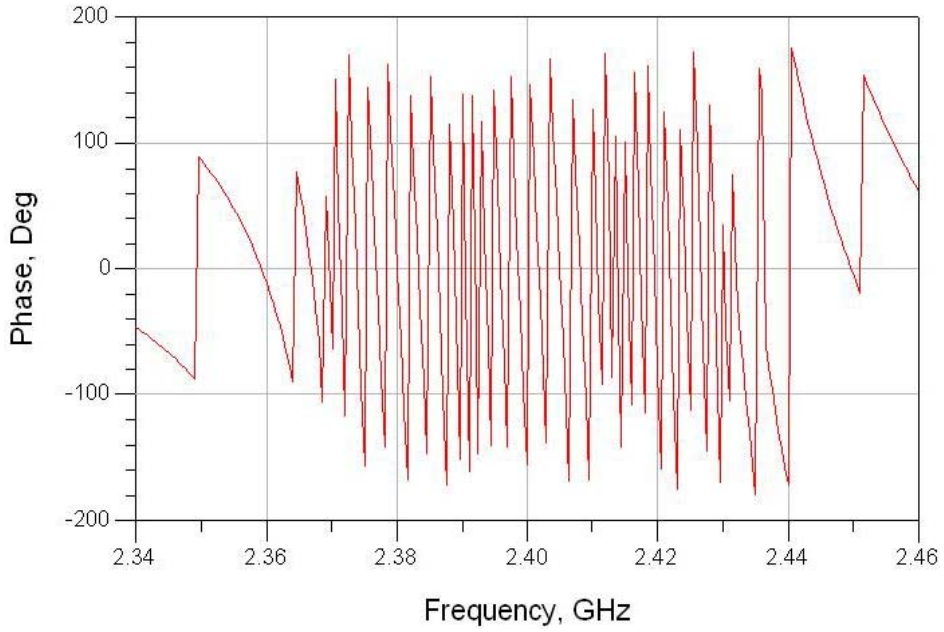

Figure 51. Phase Plot for the FDMC that uses Circulators and Butterworth Filters.

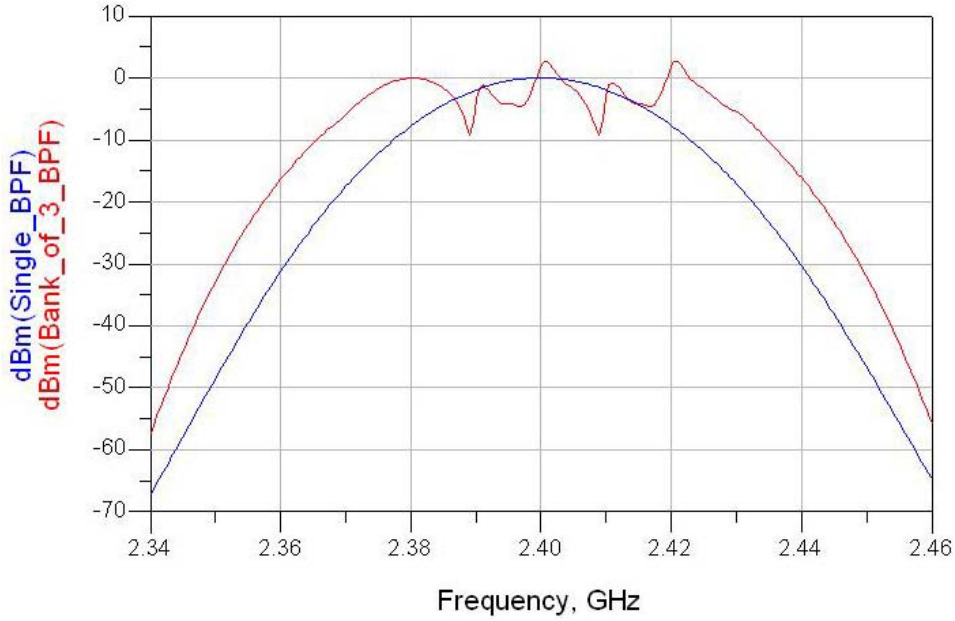

Figure 52. Output Amplitude Plot for the FDMC that uses Circulators and Gaussian Filters.

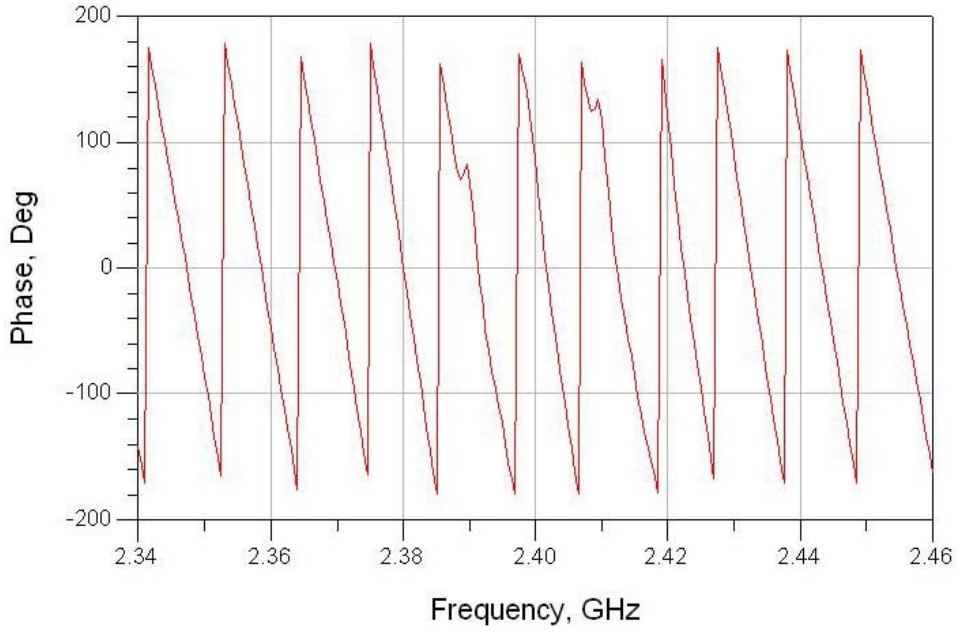

Figure 53. Phase Plot for the FDMC that uses Circulators and Gaussian Filters.

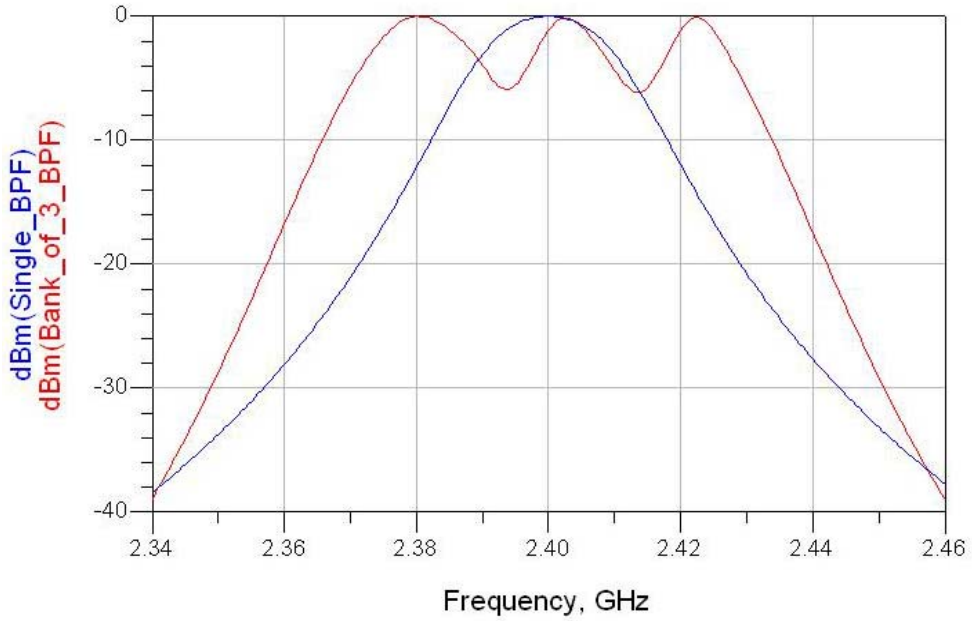

Figure 54. Output Amplitude Plot for the FDMC that uses Circulators and Bessel Filters.

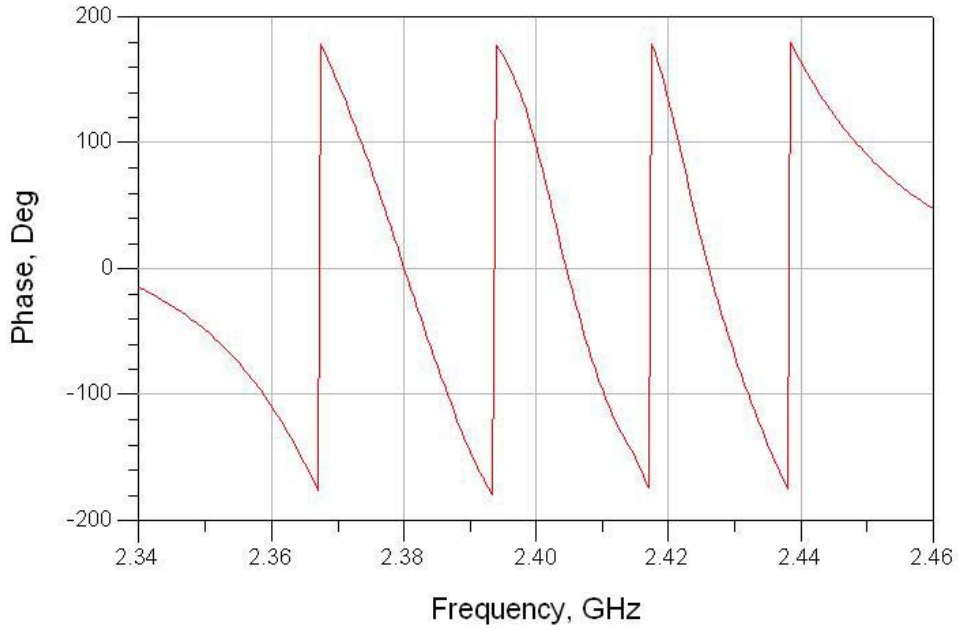

Figure 55. Phase Plot for the FDMC that uses Circulators and Bessel Filters.

4. FDMC Using Couplers

The responses of the FDMC using couplers for various types of BPFs are shown in Figures 56 to 65. In comparison to the previous design of FDMC using circulators, it was observed that there was approximately 10 dB of attenuation of the inband output signal level due to the signal splitting. Some overshoot in the frequency passband at the overlapping of different channels was also observed.

The advantage of this design is that the phases of the output response are much more linear compared to the previous design.

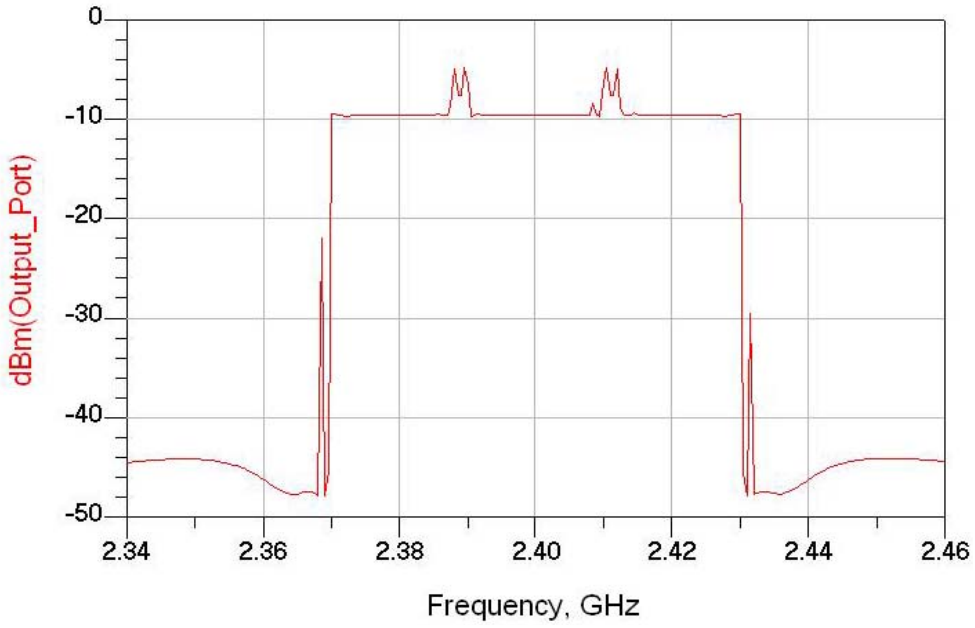

Figure 56. Output Amplitude Plot for the FDMC that uses Couplers and Elliptic Filters.

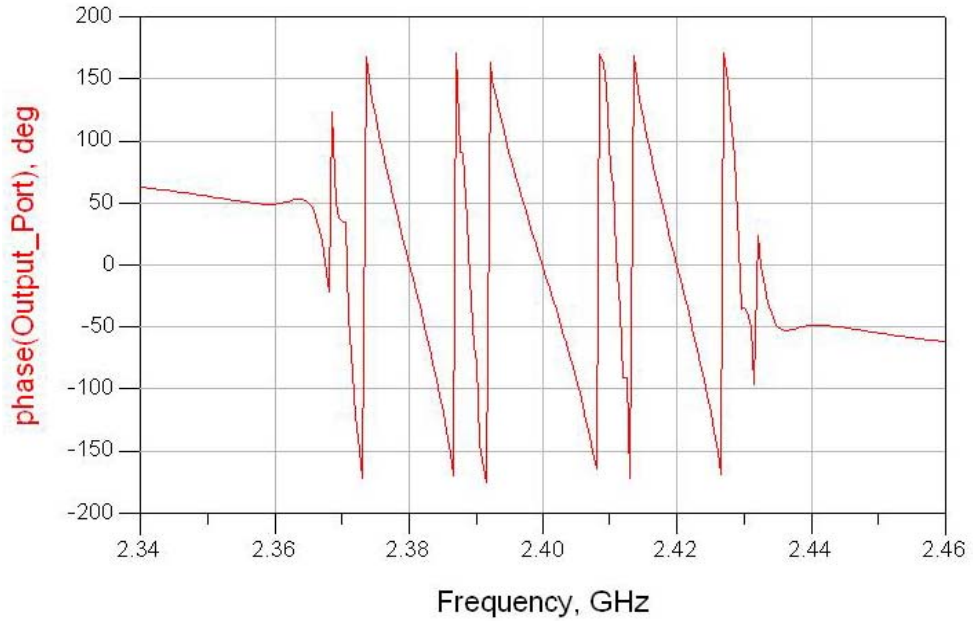

Figure 57. Phase Plot for the FDMC that uses Couplers and Elliptic Filters.

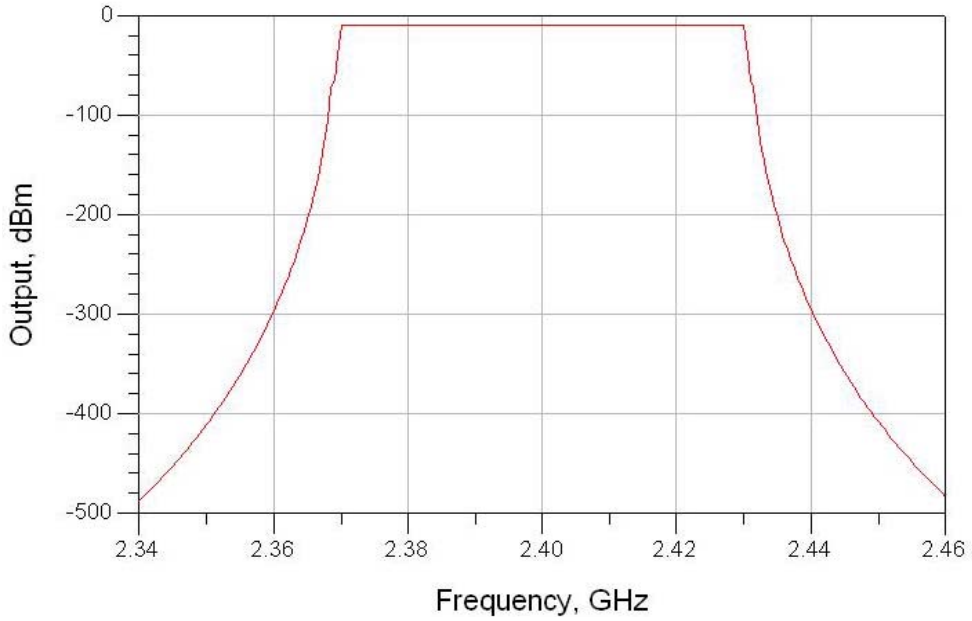

Figure 58. Output Amplitude Plot for the FDMC that uses Couplers and Chebyshev Filters.

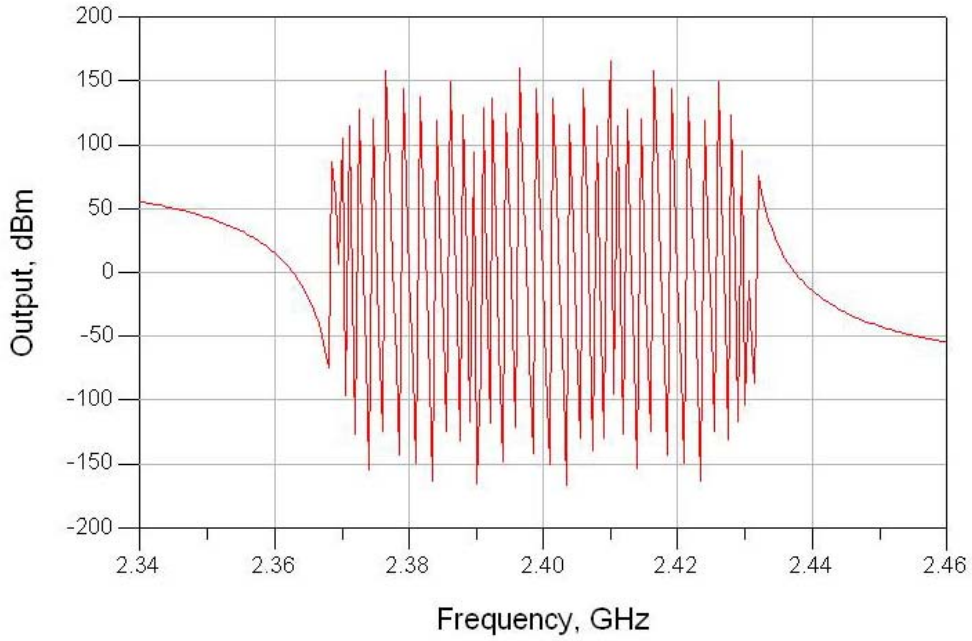

Figure 59. Phase Plot for the FDMC that uses Couplers and Chebyshev Filters.

Figure 60. Output Amplitude Plot for the FDMC that uses Couplers and Butterworth Filters.

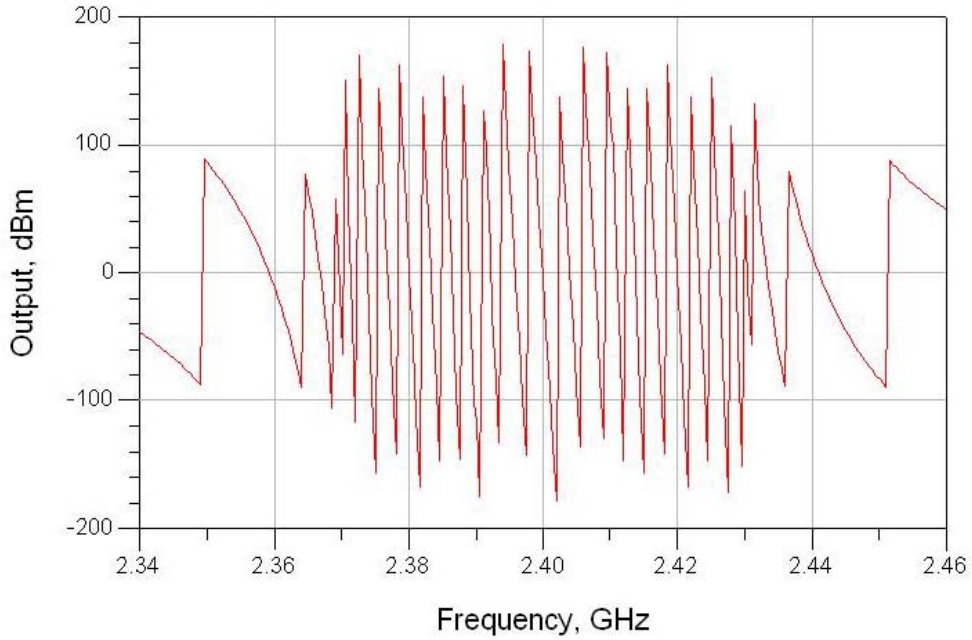

Figure 61. Phase Plot for the FDMC that uses Couplers and Butterworth Filters.

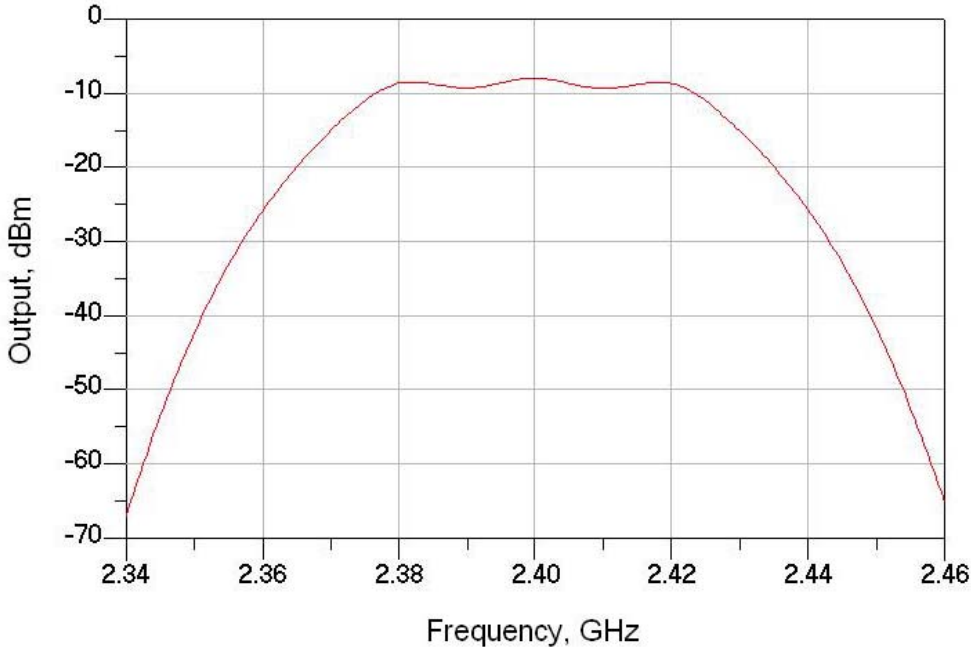

Figure 62. Output Amplitude Plot for the FDMC that uses Couplers and Gaussian Filters.

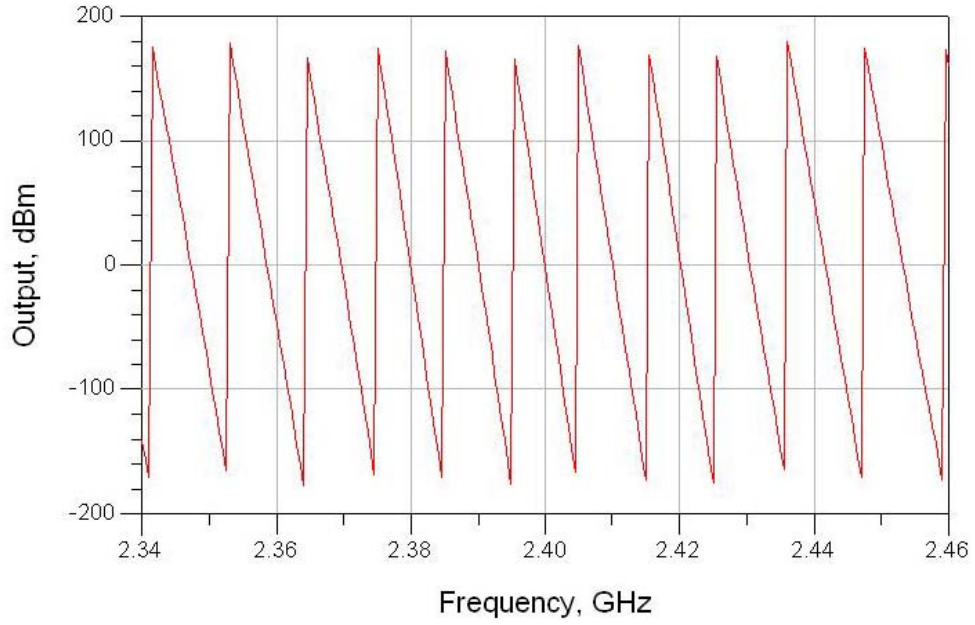

Figure 63. Phase Plot for the FDMC that uses Couplers and Gaussian Filters.

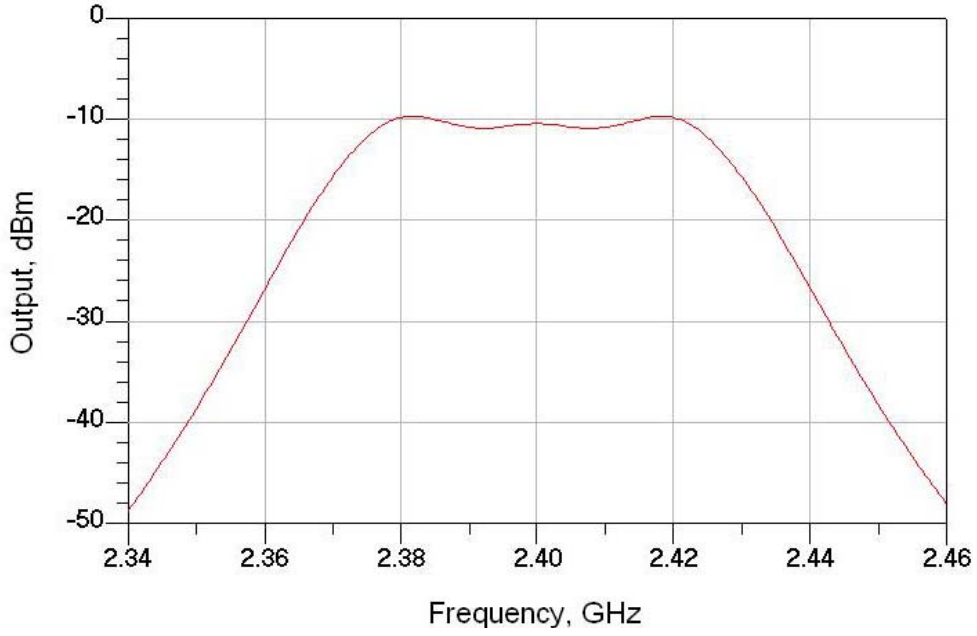

Figure 64. Output Amplitude Plot for the FDMC that uses Couplers and Bessel Filters.

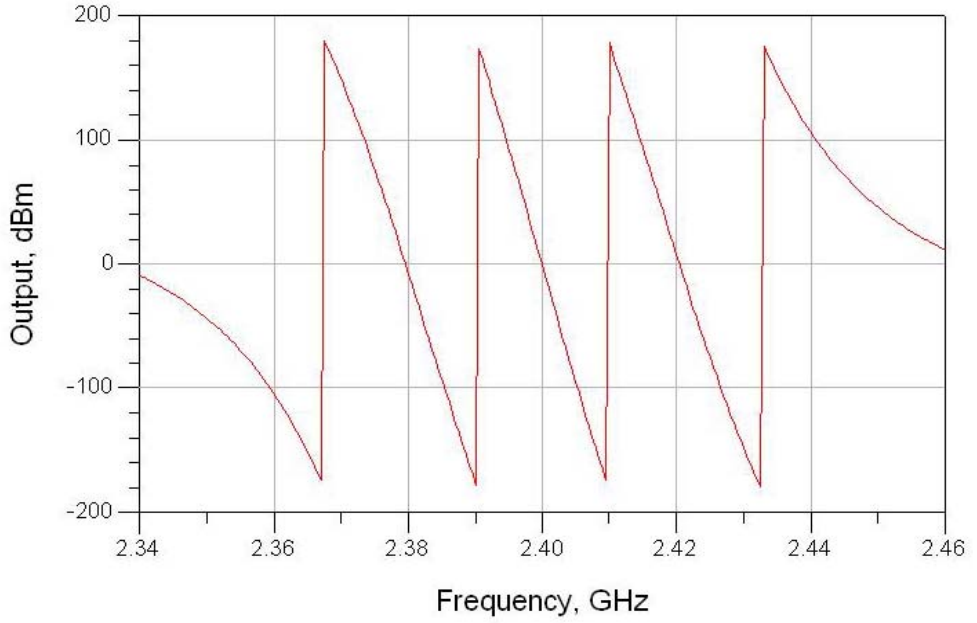

Figure 65. Phase Plot for the FDMC that uses Couplers and Bessel Filters.

5. Scattering Parameters

Measurement of the scattering parameters, or S-parameters, at the ports of the FDMC for both designs as shown in Figures 66 and 67 was conducted through the use of S-parameters simulation in the ADS.

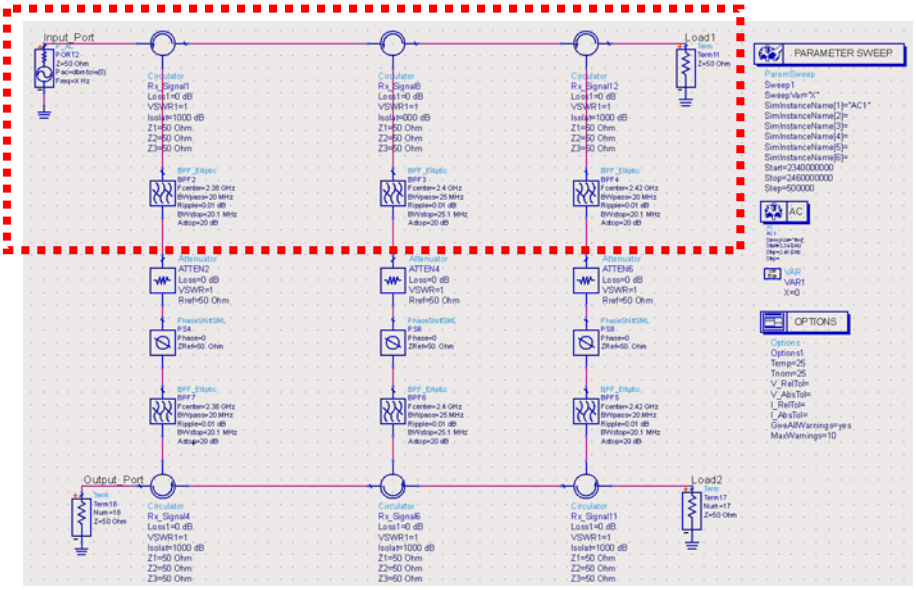

Figure 66. Demultiplexer of FDMC using Circulators.

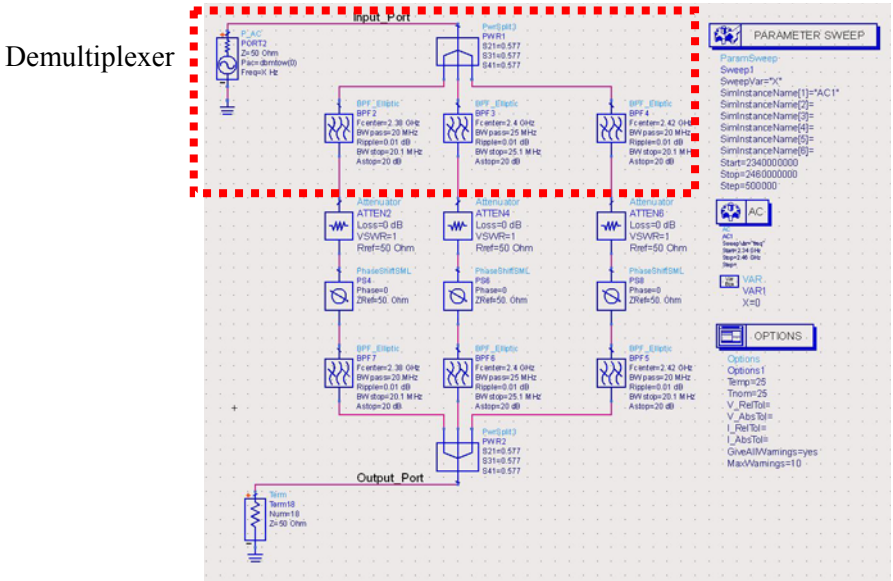

Figure 67. Demultiplexer of FDMC using Couplers.

As highlighted in the previous section, elliptic filters were used in both designs due to the resultant output response. The S-parameter simulation models for both designs

are shown in Figures 68 and 69. The simulation results are displayed in Tables 4 and 5 and in Figures 70 to 79. A large range on the vertical (amplitude) scale is used so that most curves are visible.

For the FDMC using circulators design, it was observed that the phase of the S-parameters was very non-linear. Additionally, analysis of the amplitude response, revealed the low loss nature of this design. Both findings confirm the earlier analysis of Section D.2 of this chapter. For the FDMC using couplers design, the phase of the S-parameters was more linear. However, the amplitude response revealed greater attenuation. Both findings confirm the earlier analysis of Section D.3 of this chapter. The measurement of the S-parameters supports the initial deduction that the FDMC using couplers is more suited for the WLCC design.

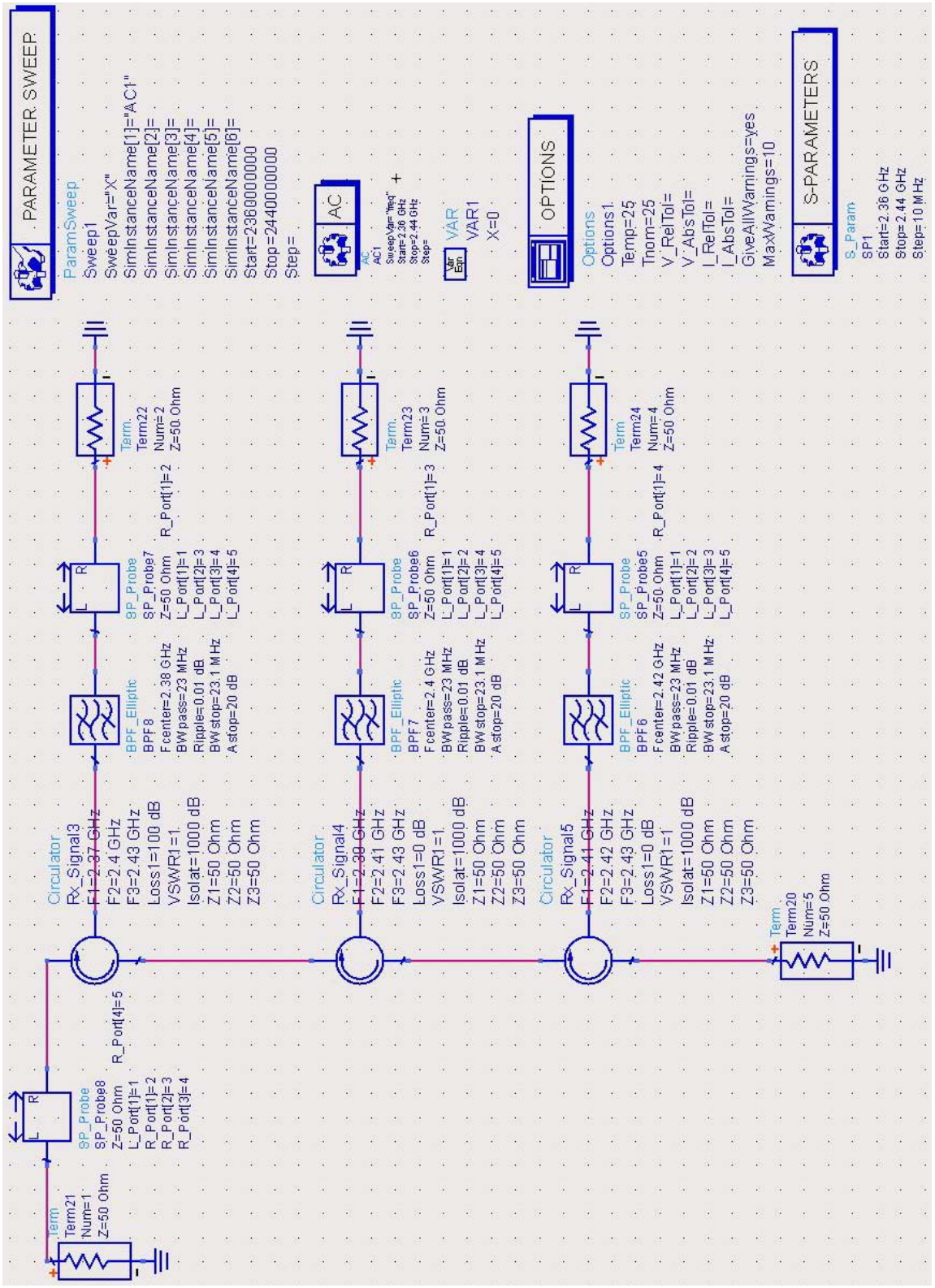

Figure 68. S-Parameter Simulation Model for the Demultiplexer of FDMC using Circulators.

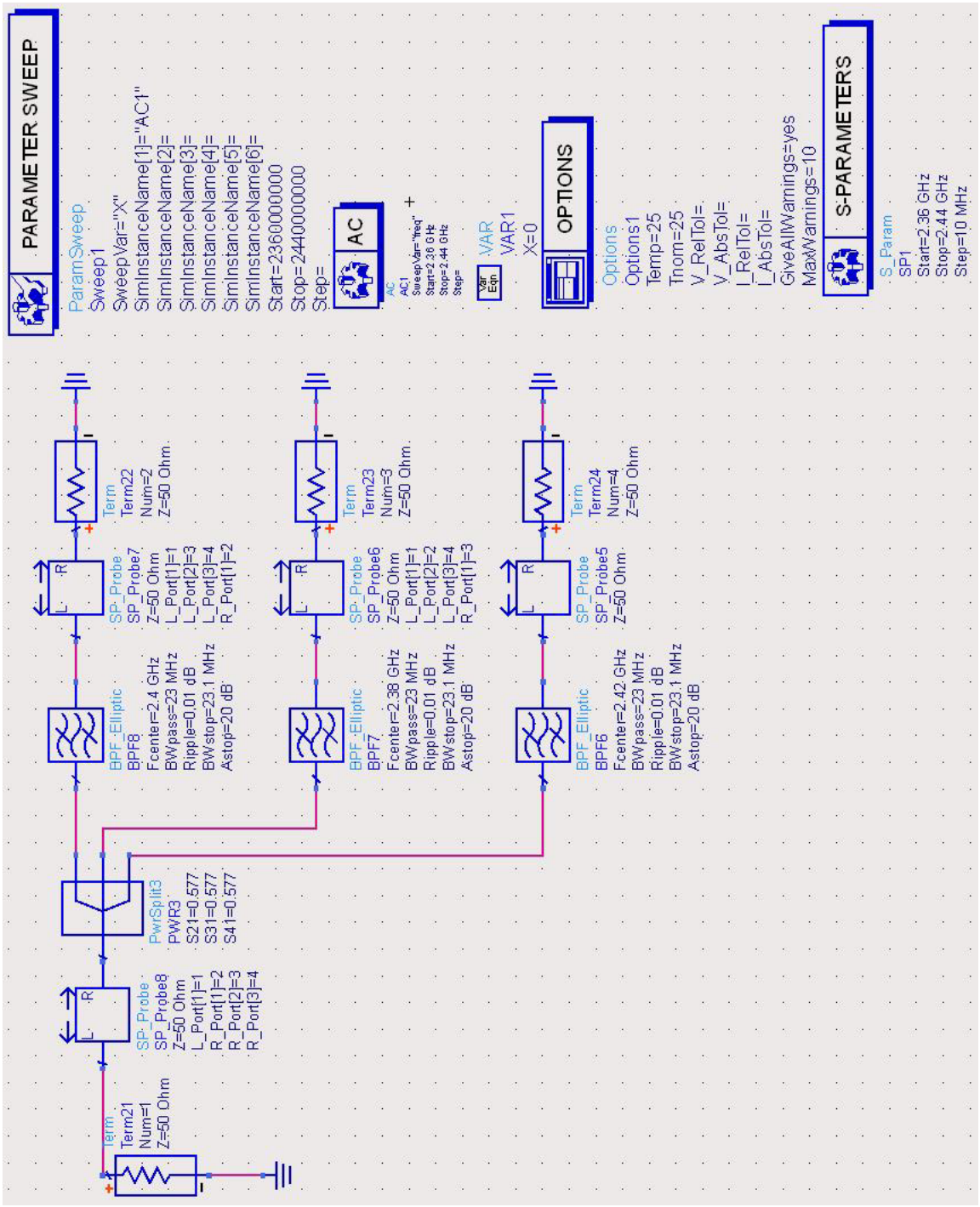

Figure 69. S-Parameter Simulation Model for the Demultiplexer of FDMC using Couplers.

Table 4. Summary of S-Parameters for the FDMC Using Circulator in dB / Degrees.

freq	SP.S	freq	SP.S	freq	SP.S	freq	SP.S
SP.S(1,1)		SP.S(2,1)		SP.S(3,1)		SP.S(4,1)	
2.360 GHz	-614.101 / -90.000	2.360 GHz	-129.347 / 1.243	2.360 GHz	-220.435 / -38.601	2.360 GHz	-222.756 / -64.768
2.370 GHz	-644.204 / 90.000	2.370 GHz	-100.003 / 144.120	2.370 GHz	-251.243 / -31.525	2.370 GHz	-252.743 / -123.113
2.380 GHz	<-infinity> / 0.000	2.380 GHz	-1.061E-6 / -0.264	2.380 GHz	-35.488 / 90.977	2.380 GHz	-86.575 / 51.130
2.390 GHz	<-infinity> / 0.000	2.390 GHz	-0.003 / -144.640	2.390 GHz	-31.434 / -89.477	2.390 GHz	-82.681 / 34.875
2.400 GHz	<-infinity> / 0.000	2.400 GHz	-23.863 / -0.580	2.400 GHz	-0.025 / 88.969	2.400 GHz	-35.589 / -179.793
2.410 GHz	<-infinity> / 0.000	2.410 GHz	-20.103 / -34.724	2.410 GHz	-0.067 / -89.463	2.410 GHz	-31.497 / -34.296
2.420 GHz	-313.032 / -90.000	2.420 GHz	-20.353 / -43.318	2.420 GHz	-29.322 / 40.028	2.420 GHz	-0.087 / 123.579
2.430 GHz	<-infinity> / 0.000	2.430 GHz	-21.391 / -57.662	2.430 GHz	-20.156 / -2.444	2.430 GHz	-0.113 / -57.182
2.440 GHz	<-infinity> / 0.000	2.440 GHz	-122.508 / -63.111	2.440 GHz	-320.399 / -22.478	2.440 GHz	-523.965 / 66.866
SP.S(1,2)		SP.S(2,2)		SP.S(3,2)		SP.S(4,2)	
2.360 GHz	-543.695 / 18.435	2.360 GHz	-0.026 / -88.570	2.360 GHz	-149.756 / 51.211	2.360 GHz	-152.077 / 25.044
2.370 GHz	-512.927 / -21.516	2.370 GHz	-31.174 / -126.838	2.370 GHz	-120.078 / 179.434	2.370 GHz	-121.571 / 147.906
2.380 GHz	-321.115 / 80.447	2.380 GHz	-66.140 / 89.737	2.380 GHz	-29.349 / 0.976	2.380 GHz	-20.435 / -38.871
2.390 GHz	-330.870 / -14.036	2.390 GHz	-31.431 / 126.400	2.390 GHz	-0.006 / -0.518	2.390 GHz	-51.253 / 123.834
2.400 GHz	-349.195 / 180.000	2.400 GHz	-0.025 / 89.231	2.400 GHz	-23.863 / -0.841	2.400 GHz	-125.426 / 90.397
2.410 GHz	<-infinity> / 0.000	2.410 GHz	-0.064 / 55.175	2.410 GHz	-20.106 / -179.362	2.410 GHz	-51.536 / -124.137
2.420 GHz	-334.143 / 135.000	2.420 GHz	-0.061 / 40.611	2.420 GHz	-50.214 / -43.900	2.420 GHz	-20.379 / 39.651
2.430 GHz	<-infinity> / 0.000	2.430 GHz	-0.053 / 32.282	2.430 GHz	-41.495 / -92.389	2.430 GHz	-21.458 / -147.126
2.440 GHz	-535.833 / 180.000	2.440 GHz	-0.045 / 26.843	2.440 GHz	-242.862 / -112.432	2.440 GHz	-452.428 / -23.088
SP.S(1,3)		SP.S(2,3)		SP.S(3,3)		SP.S(4,3)	
2.360 GHz	-443.174 / -90.000	2.360 GHz	-1.373E3 / -88.757	2.360 GHz	-0.061 / -39.962	2.360 GHz	-43.079 / 113.731
2.370 GHz	-437.154 / 1.266E-55	2.370 GHz	-1.337E3 / 144.120	2.370 GHz	-0.064 / -54.527	2.370 GHz	-41.579 / 93.686
2.380 GHz	-342.205 / 116.565	2.380 GHz	-1.342E3 / 116.301	2.380 GHz	-0.026 / -88.573	2.380 GHz	-43.757 / 51.205
2.390 GHz	-310.061 / -45.000	2.390 GHz	-1.310E3 / 170.360	2.390 GHz	-31.176 / -126.896	2.390 GHz	-20.078 / 179.493
2.400 GHz	<-infinity> / 0.000	2.400 GHz	<-infinity> / 0.000	2.400 GHz	-66.212 / 89.739	2.400 GHz	-23.351 / 0.976
2.410 GHz	-312.102 / -116.565	2.410 GHz	-1.332E3 / -151.289	2.410 GHz	-31.430 / 126.402	2.410 GHz	-0.006 / -0.513
2.420 GHz	-349.195 / 180.000	2.420 GHz	-1.370E3 / 130.682	2.420 GHz	-0.025 / 89.228	2.420 GHz	-23.861 / -0.842
2.430 GHz	-336.184 / -153.435	2.430 GHz	-1.358E3 / 148.903	2.430 GHz	-0.064 / 55.172	2.430 GHz	-20.106 / -179.363
2.440 GHz	-627.875 / -2.574E-54	2.440 GHz	-1.550E3 / -63.111	2.440 GHz	-0.061 / 40.608	2.440 GHz	-250.212 / -43.906
SP.S(1,4)		SP.S(2,4)		SP.S(3,4)		SP.S(4,4)	
2.360 GHz	-1.123E3 / 63.763	2.360 GHz	-2.052E3 / 65.006	2.360 GHz	-1.354E3 / 160.500	2.360 GHz	-0.045 / -26.132
2.370 GHz	-1.122E3 / 58.312	2.370 GHz	-2.022E3 / -157.567	2.370 GHz	-1.351E3 / -60.645	2.370 GHz	-0.052 / -31.634
2.380 GHz	-1.020E3 / 43.966	2.380 GHz	-2.020E3 / 43.702	2.380 GHz	-1.365E3 / -44.386	2.380 GHz	-0.061 / -39.964
2.390 GHz	-1.020E3 / 35.371	2.390 GHz	-2.020E3 / -109.270	2.390 GHz	<-infinity> / 0.000	2.390 GHz	-0.064 / -54.529
2.400 GHz	-1.029E3 / 1.237	2.400 GHz	-2.059E3 / 0.657	2.400 GHz	-1.343E3 / -0.233	2.400 GHz	-0.026 / -88.575
2.410 GHz	-1.000E3 / 144.125	2.410 GHz	-2.020E3 / 109.401	2.410 GHz	-1.313E3 / -143.421	2.410 GHz	-31.177 / -126.884
2.420 GHz	-1.000E3 / -0.259	2.420 GHz	-2.020E3 / -43.577	2.420 GHz	-1.358E3 / 134.719	2.420 GHz	-66.284 / 89.741
2.430 GHz	-1.000E3 / -144.636	2.430 GHz	-2.021E3 / 157.702	2.430 GHz	-1.338E3 / -152.714	2.430 GHz	-31.429 / 126.404
2.440 GHz	-1.230E3 / -0.585	2.440 GHz	-2.152E3 / -63.696	2.440 GHz	-1.576E3 / 19.830	2.440 GHz	-0.025 / 89.225

The graphical plots of the measurements in Table 4 are shown in Figures 70 to 74. Measurements with infinity as well as very small values resulted in discontinuity of the plots in Figures 71, 72 and 73. The hash marks on the horizontal axis signify that curves are below the axis minimum value.

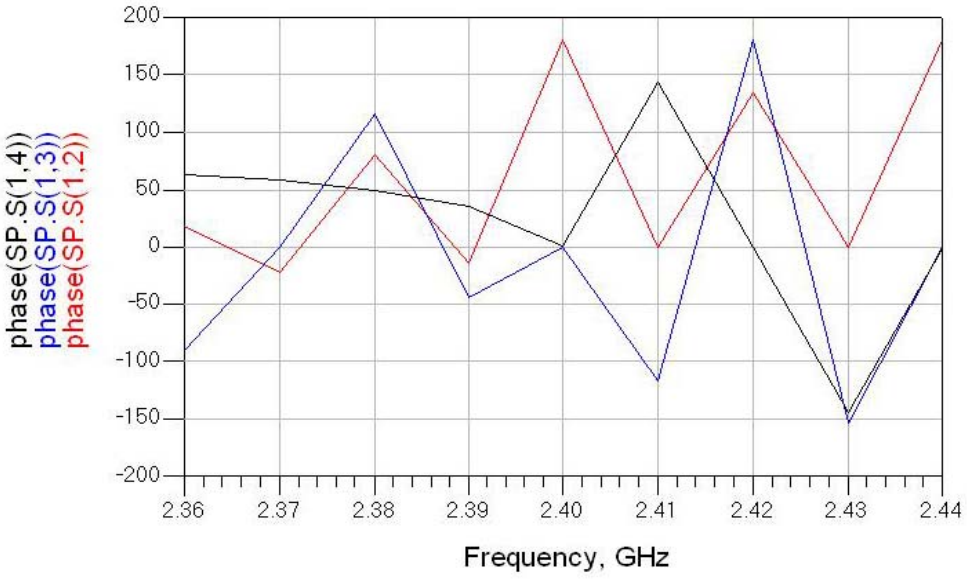

Figure 70. Phase Plots of S-Parameters for the FDMC Using Circulators.

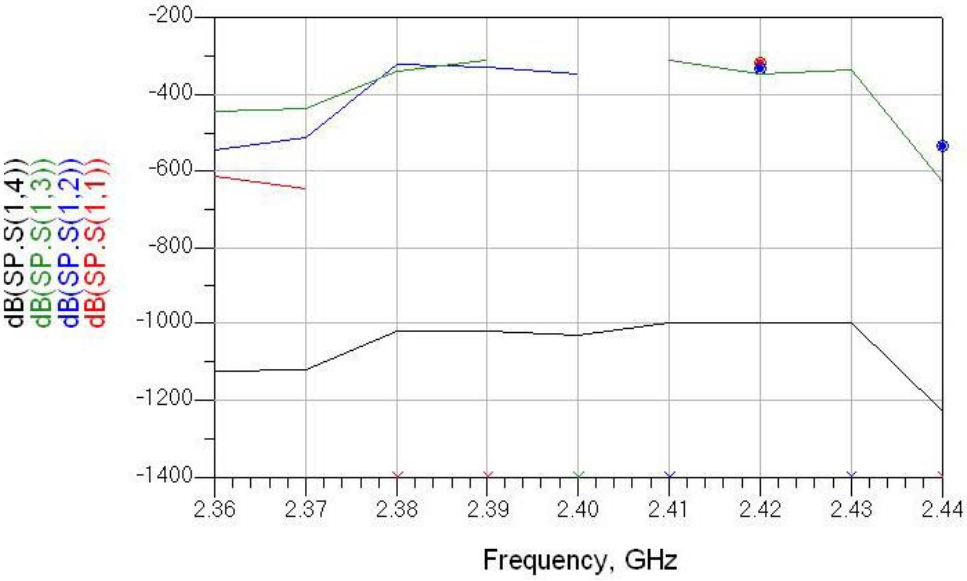

Figure 71. Amplitude Plots of S-Parameters at Port 1 for the FDMC Using Circulators.

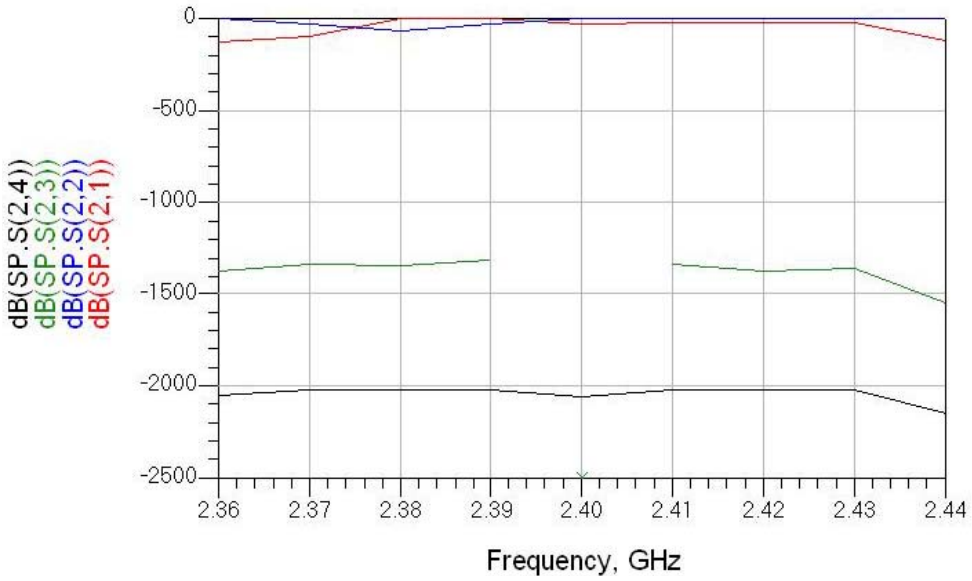

Figure 72. Amplitude Plots of S-Parameters at Port 2 for the FDMC Using Circulators.

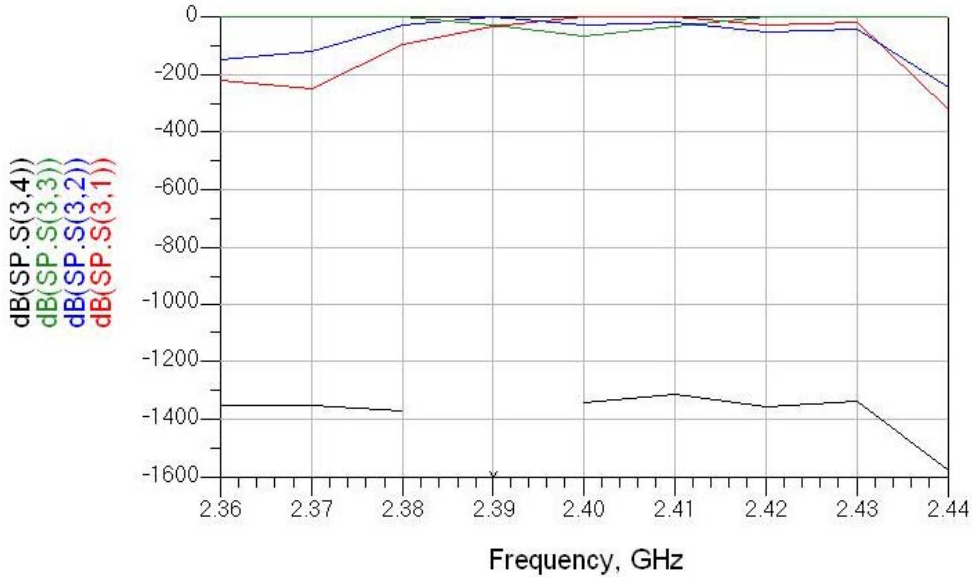

Figure 73. Amplitude Plots of S-Parameters at Port 3 for the FDMC Using Circulators.

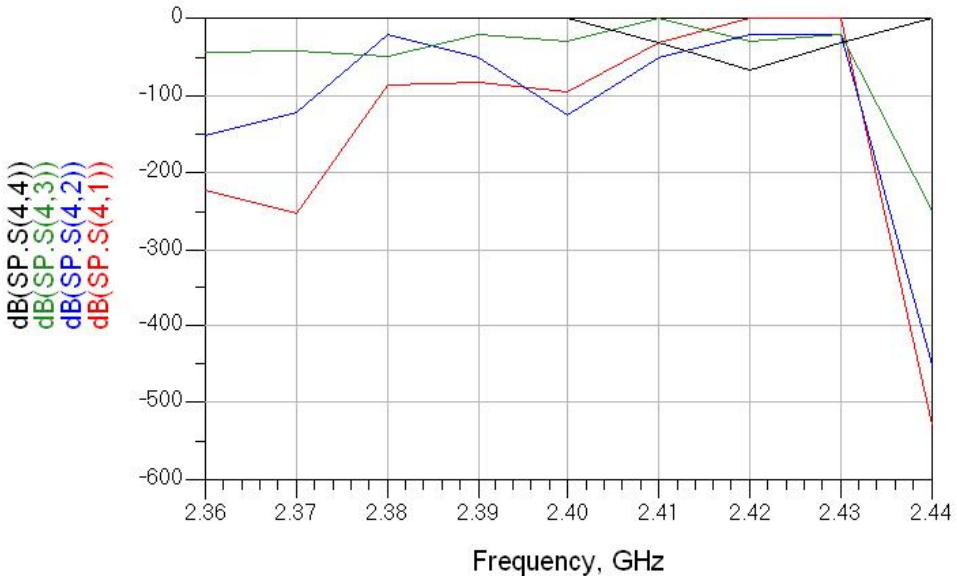

Figure 74. Amplitude Plots of S-Parameters at Port 4 for the FDMC Using Circulators.

Table 5. Summary of S-Parameters for the FDMC Using Couplers in dB / Degrees.

freq	SP.S
SP.S(1,1)	
2.360 GHz	-1.029 / -51.007
2.370 GHz	-3.751 / -43.879
2.380 GHz	-4.384 / -64.313
2.390 GHz	-9.777 / -56.102
2.400 GHz	-37.314 / 1.158
2.410 GHz	-9.781 / 56.727
2.420 GHz	-4.380 / 64.979
2.430 GHz	-3.749 / 44.501
2.440 GHz	-1.030 / 51.660
SP.S(1,2)	
2.360 GHz	-25.186 / 43.968
2.370 GHz	-24.851 / 35.373
2.380 GHz	-34.125 / 1.240
2.390 GHz	-4.780 / 144.123
2.400 GHz	-4.776 / -0.261
2.410 GHz	-4.780 / -144.638
2.420 GHz	-34.637 / -0.582
2.430 GHz	-24.880 / -34.727
2.440 GHz	-25.130 / -43.321
SP.S(1,3)	
2.360 GHz	-34.123 / 1.243
2.370 GHz	-4.780 / 144.120
2.380 GHz	-4.776 / -0.264
2.390 GHz	-4.780 / -144.640
2.400 GHz	-34.640 / -0.580
2.410 GHz	-24.880 / -34.724
2.420 GHz	-25.130 / -43.318
2.430 GHz	-26.168 / -57.662
2.440 GHz	-27.284 / -63.111
SP.S(1,4)	
2.360 GHz	-27.446 / 63.763
2.370 GHz	-26.281 / 58.312
2.380 GHz	-25.185 / 43.966
2.390 GHz	-24.851 / 35.371
2.400 GHz	-34.127 / 1.237
2.410 GHz	-4.780 / 144.125
2.420 GHz	-4.776 / -0.259
2.430 GHz	-4.780 / -144.636
2.440 GHz	-34.635 / -0.585

freq	SP.S
SP.S(2,1)	
2.360 GHz	-25.186 / 43.968
2.370 GHz	-24.851 / 35.373
2.380 GHz	-34.125 / 1.240
2.390 GHz	-4.780 / 144.123
2.400 GHz	-4.776 / -0.261
2.410 GHz	-4.780 / -144.638
2.420 GHz	-34.637 / -0.582
2.430 GHz	-24.880 / -34.727
2.440 GHz	-25.130 / -43.321
SP.S(2,2)	
2.360 GHz	-0.061 / -33.962
2.370 GHz	-0.064 / -54.527
2.380 GHz	-0.026 / -88.573
2.390 GHz	-31.176 / -126.886
2.400 GHz	-66.212 / 89.739
2.410 GHz	-31.430 / 126.402
2.420 GHz	-0.025 / 89.228
2.430 GHz	-0.064 / 55.172
2.440 GHz	-0.061 / 40.608
SP.S(2,3)	
2.360 GHz	<-infinity> / 0.000
2.370 GHz	<-infinity> / 0.000
2.380 GHz	<-infinity> / 0.000
2.390 GHz	<-infinity> / 0.000
2.400 GHz	<-infinity> / 0.000
2.410 GHz	<-infinity> / 0.000
2.420 GHz	<-infinity> / 0.000
2.430 GHz	<-infinity> / 0.000
2.440 GHz	<-infinity> / 0.000
SP.S(2,4)	
2.360 GHz	<-infinity> / 0.000
2.370 GHz	<-infinity> / 0.000
2.380 GHz	<-infinity> / 0.000
2.390 GHz	<-infinity> / 0.000
2.400 GHz	<-infinity> / 0.000
2.410 GHz	<-infinity> / 0.000
2.420 GHz	<-infinity> / 0.000
2.430 GHz	<-infinity> / 0.000
2.440 GHz	<-infinity> / 0.000

freq	SP.S
SP.S(3,1)	
2.360 GHz	-34.123 / 1.243
2.370 GHz	-4.780 / 144.120
2.380 GHz	-4.776 / -0.264
2.390 GHz	-4.780 / -144.640
2.400 GHz	-34.640 / -0.580
2.410 GHz	-24.880 / -34.724
2.420 GHz	-25.130 / -43.318
2.430 GHz	-26.168 / -57.662
2.440 GHz	-27.284 / -63.111
SP.S(3,2)	
2.360 GHz	<-infinity> / 0.000
2.370 GHz	<-infinity> / 0.000
2.380 GHz	<-infinity> / 0.000
2.390 GHz	<-infinity> / 0.000
2.400 GHz	<-infinity> / 0.000
2.410 GHz	<-infinity> / 0.000
2.420 GHz	<-infinity> / 0.000
2.430 GHz	<-infinity> / 0.000
2.440 GHz	<-infinity> / 0.000
SP.S(3,3)	
2.360 GHz	-0.026 / -88.570
2.370 GHz	-31.174 / -126.898
2.380 GHz	-66.140 / 89.737
2.390 GHz	-31.431 / 126.400
2.400 GHz	-0.025 / 89.231
2.410 GHz	-0.064 / 55.175
2.420 GHz	-0.061 / 40.611
2.430 GHz	-0.053 / 32.282
2.440 GHz	-0.045 / 26.843
SP.S(3,4)	
2.360 GHz	<-infinity> / 0.000
2.370 GHz	<-infinity> / 0.000
2.380 GHz	<-infinity> / 0.000
2.390 GHz	<-infinity> / 0.000
2.400 GHz	<-infinity> / 0.000
2.410 GHz	<-infinity> / 0.000
2.420 GHz	<-infinity> / 0.000
2.430 GHz	<-infinity> / 0.000
2.440 GHz	<-infinity> / 0.000

freq	SP.S
SP.S(4,1)	
2.360 GHz	-27.446 / 63.763
2.370 GHz	-26.281 / 58.312
2.380 GHz	-25.185 / 43.966
2.390 GHz	-24.851 / 35.371
2.400 GHz	-34.127 / 1.237
2.410 GHz	-4.780 / 144.125
2.420 GHz	-4.776 / -0.259
2.430 GHz	-4.780 / -144.636
2.440 GHz	-34.635 / -0.585
SP.S(4,2)	
2.360 GHz	<-infinity> / 0.000
2.370 GHz	<-infinity> / 0.000
2.380 GHz	<-infinity> / 0.000
2.390 GHz	<-infinity> / 0.000
2.400 GHz	<-infinity> / 0.000
2.410 GHz	<-infinity> / 0.000
2.420 GHz	<-infinity> / 0.000
2.430 GHz	<-infinity> / 0.000
2.440 GHz	<-infinity> / 0.000
SP.S(4,3)	
2.360 GHz	<-infinity> / 0.000
2.370 GHz	<-infinity> / 0.000
2.380 GHz	<-infinity> / 0.000
2.390 GHz	<-infinity> / 0.000
2.400 GHz	<-infinity> / 0.000
2.410 GHz	<-infinity> / 0.000
2.420 GHz	<-infinity> / 0.000
2.430 GHz	<-infinity> / 0.000
2.440 GHz	<-infinity> / 0.000
SP.S(4,4)	
2.360 GHz	-0.045 / -26.132
2.370 GHz	-0.052 / -31.634
2.380 GHz	-0.061 / -33.964
2.390 GHz	-0.064 / -54.529
2.400 GHz	-0.026 / -88.575
2.410 GHz	-31.177 / -126.894
2.420 GHz	-66.264 / 89.741
2.430 GHz	-31.429 / 126.404
2.440 GHz	-0.025 / 89.225

The graphical plots of the measurements in Table 5 are shown in Figures 75 to 79. Measurements with infinity as well as very small values were off scale and not shown as evident by the hash marks in Figures 77, 78 and 79.

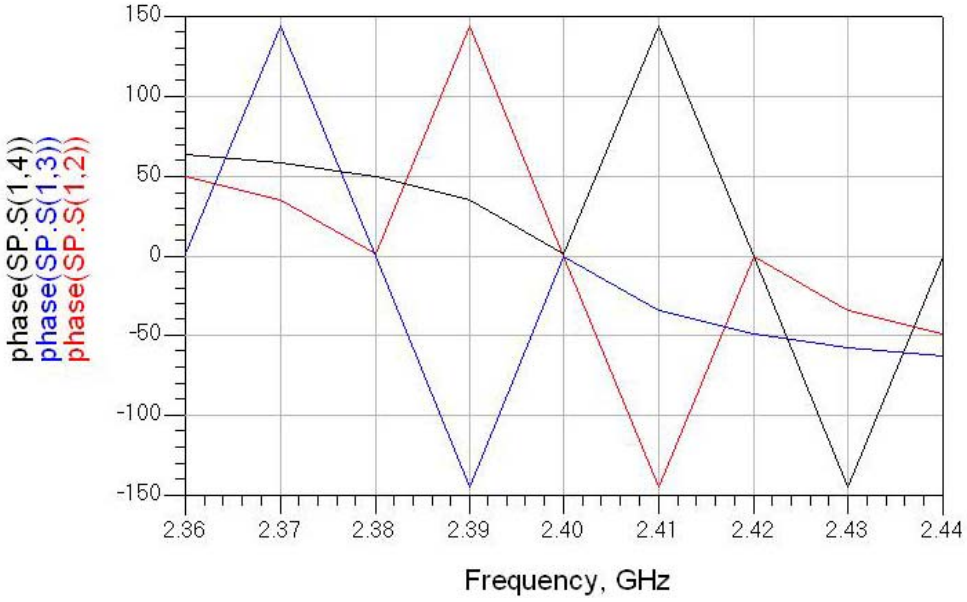

Figure 75. Phase Plots of S-Parameters for the FDMC Using Couplers.

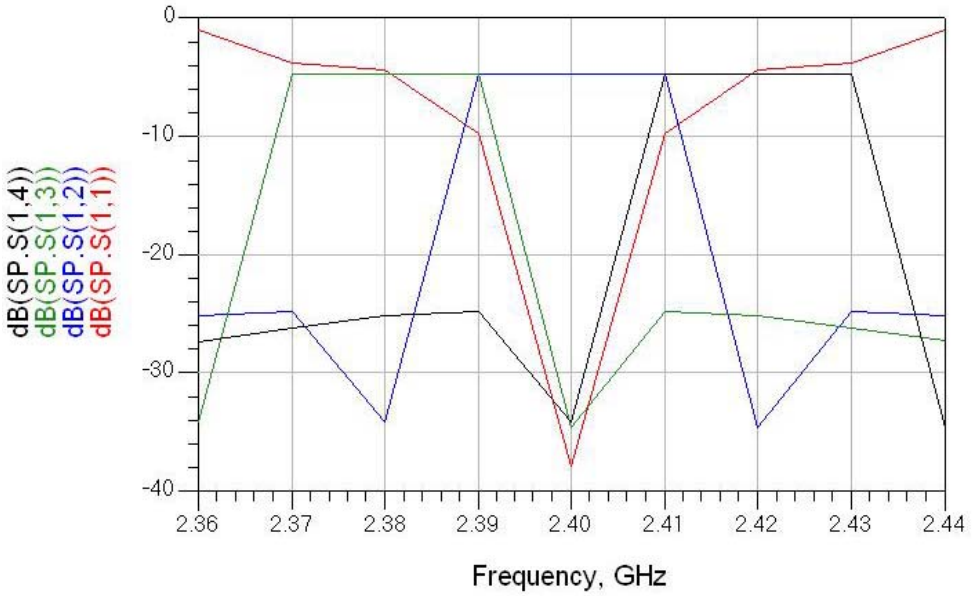

Figure 76. Amplitude Plots of S-Parameters at Port 1 for the FDMC Using Couplers.

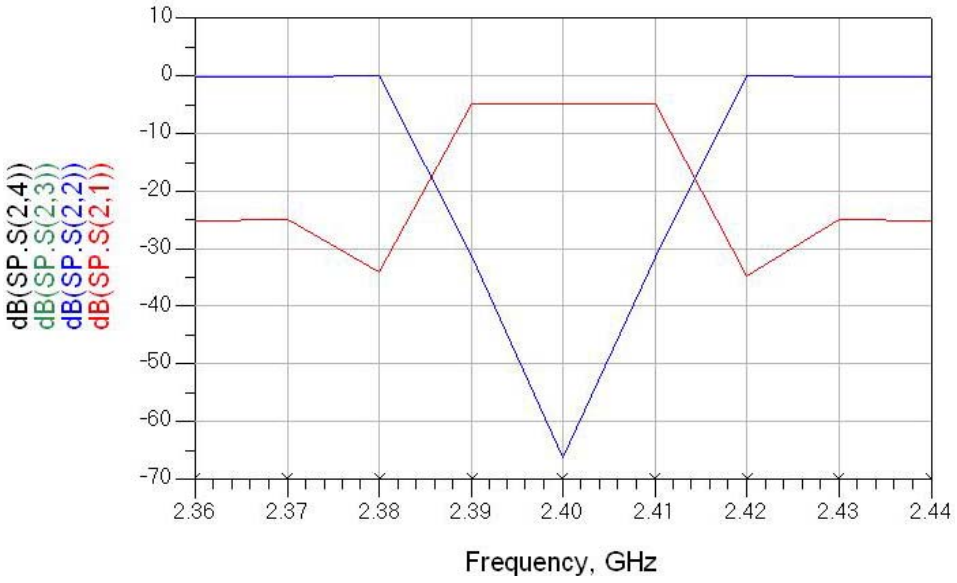

Figure 77. Amplitude Plots of S-Parameters at Port 2 for the FDMC Using Couplers.

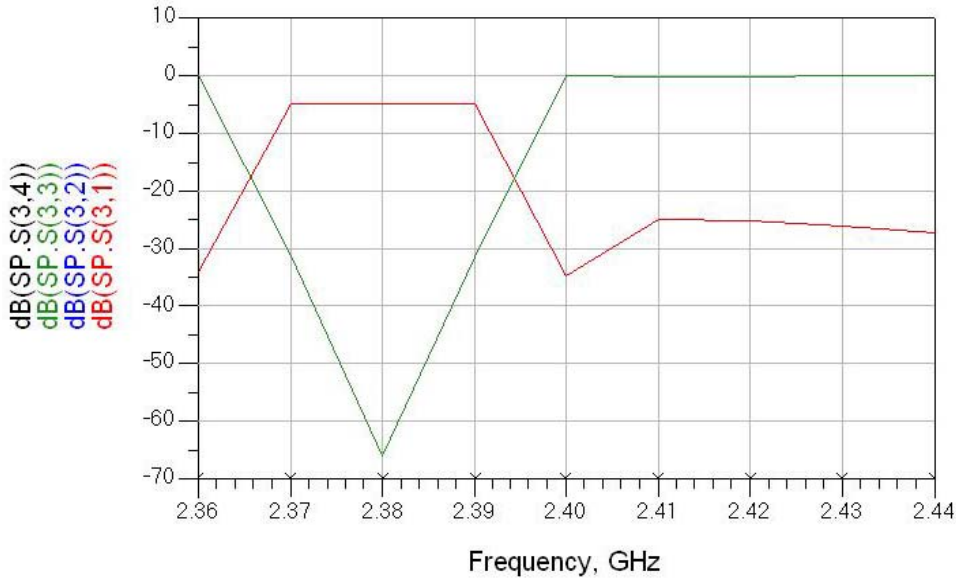

Figure 78. Amplitude Plots of S-Parameters at Port 3 for the FDMC Using Couplers.

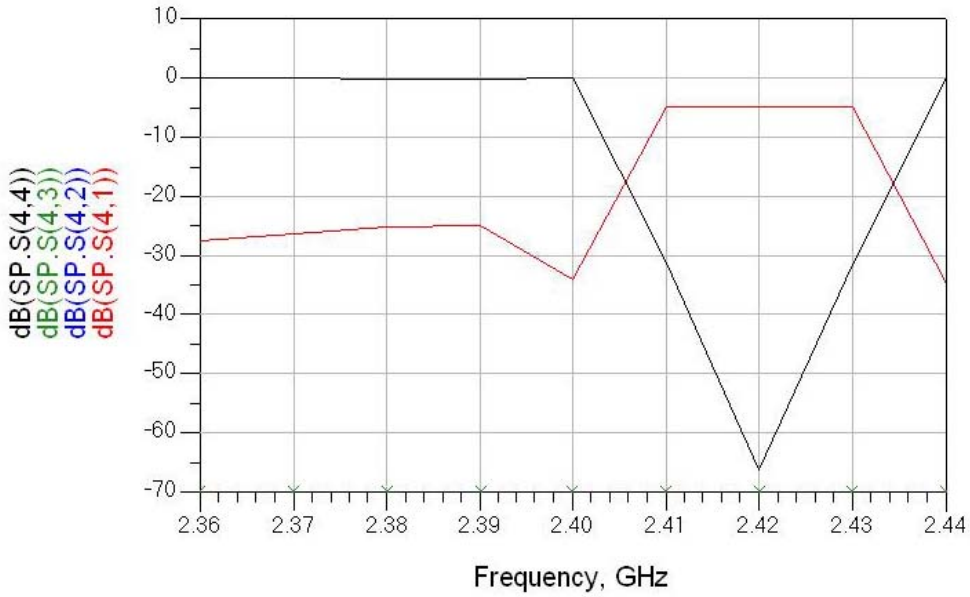

Figure 79. Amplitude Plots of S-Parameters at Port 4 for the FDMC Using Couplers.

D. CONCLUSION

In this chapter, an analysis of the basic single frequency LCC, different types of BPFs and design of the FDMC was presented. The performance of two different designs of the FDMC, one that uses circulators and another that uses couplers, was examined and simulated using five types of BPFs. Further analysis on the S-parameters for the demultiplexer of the FDMC was also conducted and yielded results favoring the design using couplers. Recognizing the strength and weaknesses of each design of the FDMC, we will use both designs in the building of the WLCC model and will further evaluate them in Chapter III.

III. WIDEBAND LEAKAGE CANCELLATION CIRCUIT

A. INTRODUCTION

Following the analysis of the essential building blocks of a WLCC in Chapter II, we document the actual design of the WLCC model in this chapter. Initially, two models of the WLCC were built using idealized component parameters. One used the FDMC employing circulators and the other used the FDMC employing couplers. Elliptic filters were selected for both designs due to their favorable filter output response.

Later in this chapter, the WLCC model using the FDMC with couplers is selected for the final design. This selection was based on its superior performance in matching the phase of the leakage signal. The final design of the WLCC is further evaluated using non-ideal component parameters.

B. DESIGN OF WLCC

1. WLCC Using Circulators

The ADS model of the WLCC design using circulators with ideal component settings is shown in Figure 80. Simulation results are recorded in Table 6 and displayed in Figures 81 to 84.

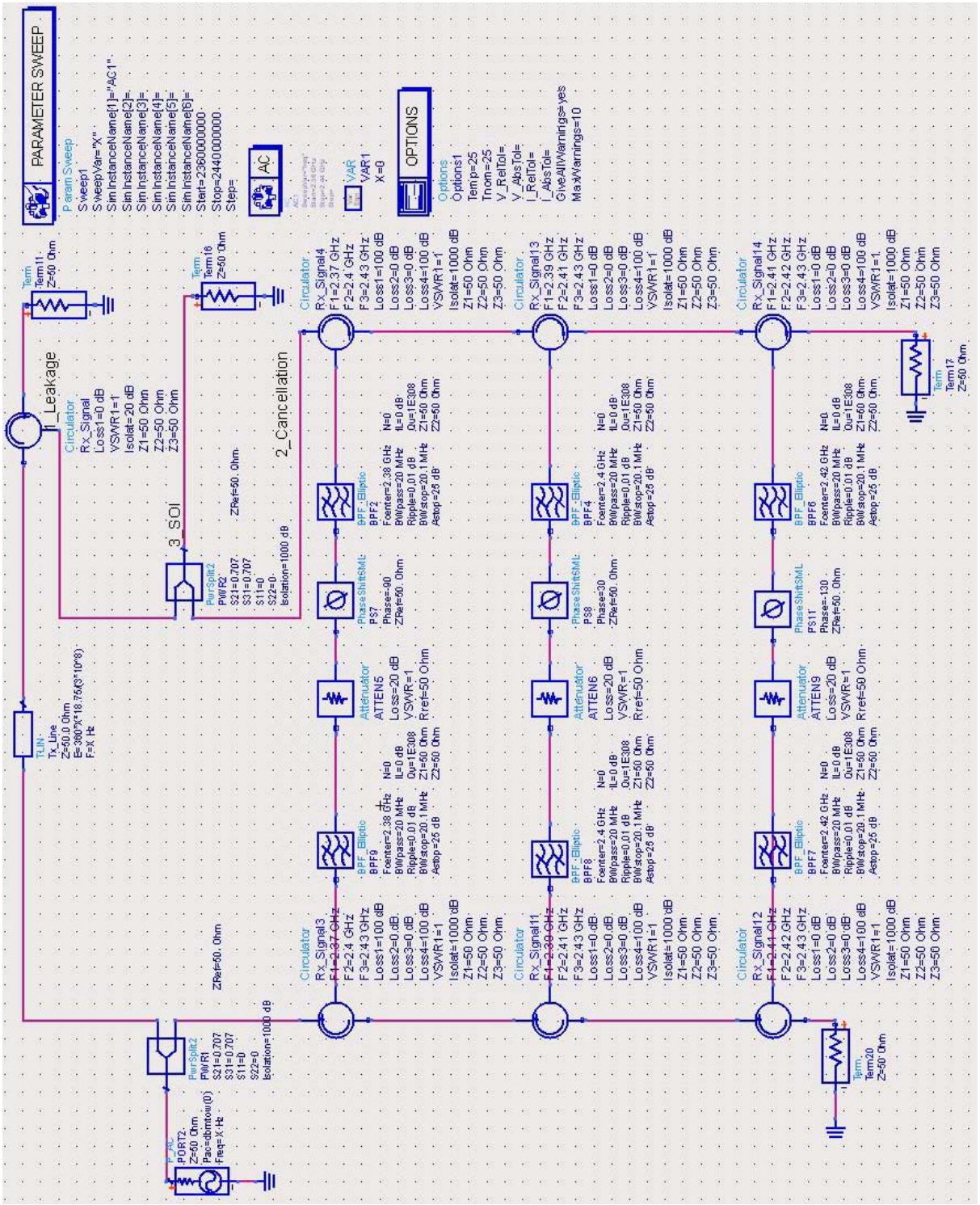

Figure 80. ADS Model of WLCC with FDMC using Circulators with Ideal Component Parameter Settings.

Table 6. Summary of Measurements for WLCC using FDMC with Circulators with

Ideal Component Parameter Settings.

freq	var("1_Leakage")	var("2_Cancellation")	var("3_SOI")
2.38000 GHz	-33.01161 / 90.00000	-33.01161 / -90.04624	-97.88575 / 179.96220
2.38025 GHz	-33.01161 / 84.37500	-33.01191 / -96.54755	-71.88606 / 173.79201
2.38050 GHz	-33.01161 / 78.75000	-33.01269 / -103.05601	-66.05211 / 167.62041
2.38075 GHz	-33.01161 / 73.12500	-33.01393 / -109.57900	-62.54736 / 161.44890
2.38100 GHz	-33.01161 / 67.50000	-33.01556 / -116.12413	-60.00480 / 155.27673
freq	var("1_Leakage")	var("2_Cancellation")	var("3_SOI")
2.40000 GHz	-33.01161 / 0.00029	-33.01496 / 179.99701	-104.21251 / 8.43934
2.40025 GHz	-33.01161 / -5.62500	-33.01671 / 171.27658	-61.36596 / 82.20458
2.40050 GHz	-33.01161 / -11.25000	-33.01921 / 162.62079	-55.44524 / 75.21705
2.40075 GHz	-33.01161 / -16.87500	-33.02244 / 154.01830	-52.01275 / 68.12308
2.40100 GHz	-33.01161 / -22.50000	-33.02632 / 145.45784	-49.59465 / 61.01903
freq	var("1_Leakage")	var("2_Cancellation")	var("3_SOI")
2.42000 GHz	-33.01161 / -90.00000	-33.01627 / 90.14616	-87.70346 / -168.04543
2.42025 GHz	-33.01161 / -95.62500	-33.02224 / 82.75945	-67.01669 / -8.91787
2.42050 GHz	-33.01161 / -101.25000	-33.03423 / 75.44221	-60.79860 / -15.48609
2.42075 GHz	-33.01161 / -106.87500	-33.05231 / 68.18325	-57.31829 / -22.45341
2.42100 GHz	-33.01161 / -112.50000	-33.07659 / 60.97147	-54.90786 / -29.51661

The graphical plots of the measurements in Table 6 are shown in Figures 81 to 84. The plot shown in Figure 81 illustrates successful leakage cancellation at 2.38 GHz, 2.4 GHz and 2.42 GHz. However, the design did not demonstrate cancellation across the entire band of interest of 2.37 GHz to 2.43 GHz.

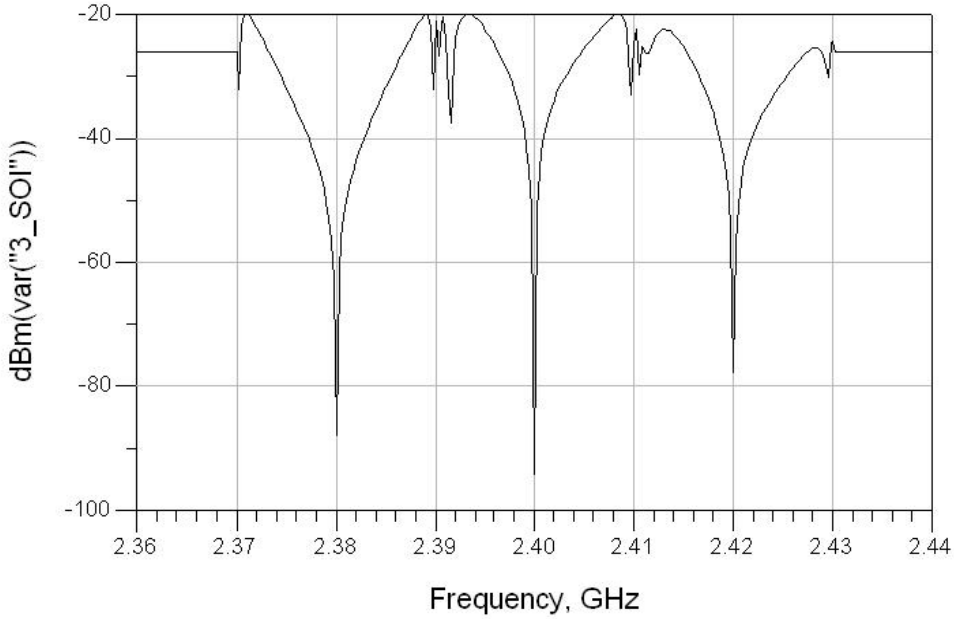

Figure 81. Amplitude Plot of SOI in WLCC.

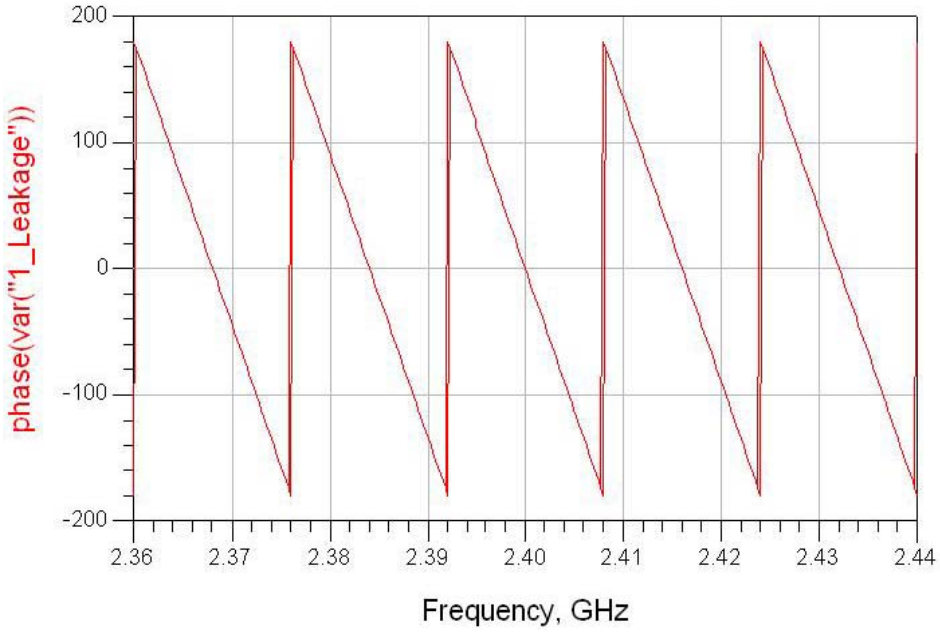

Figure 82. Phase Plot of Leakage in WLCC.

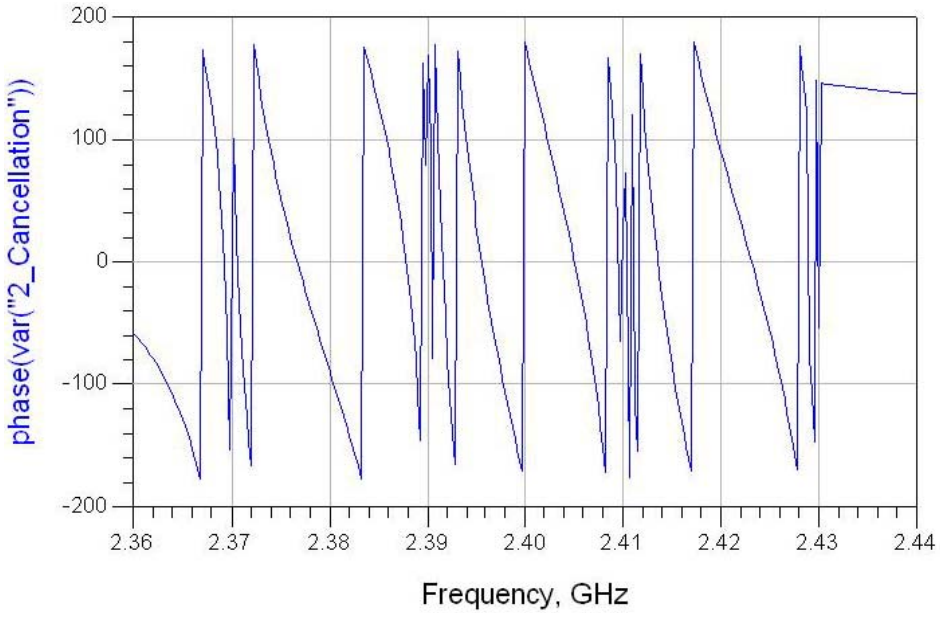

Figure 83. Phase Plot of Cancellation in WLCC.

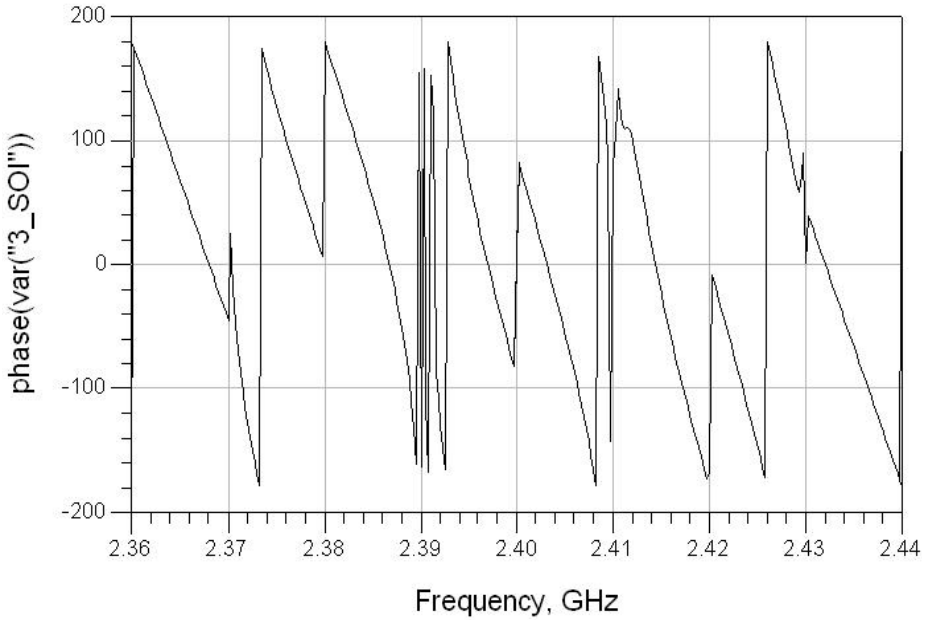

Figure 84. Phase Plot of SOI in WLCC.

Analysis of the phase plots shown in Figures 82 to 84 reveal non-linear curves and cycling of the phase angle of the cancellation signal. This response makes it difficult to match the phase of the leakage signal.

2. WLCC Using Couplers

The ADS model of the WLCC design using couplers with ideal component settings is shown in Figure 85. Simulation results are recorded in Table 7 and displayed in Figures 86 to 89.

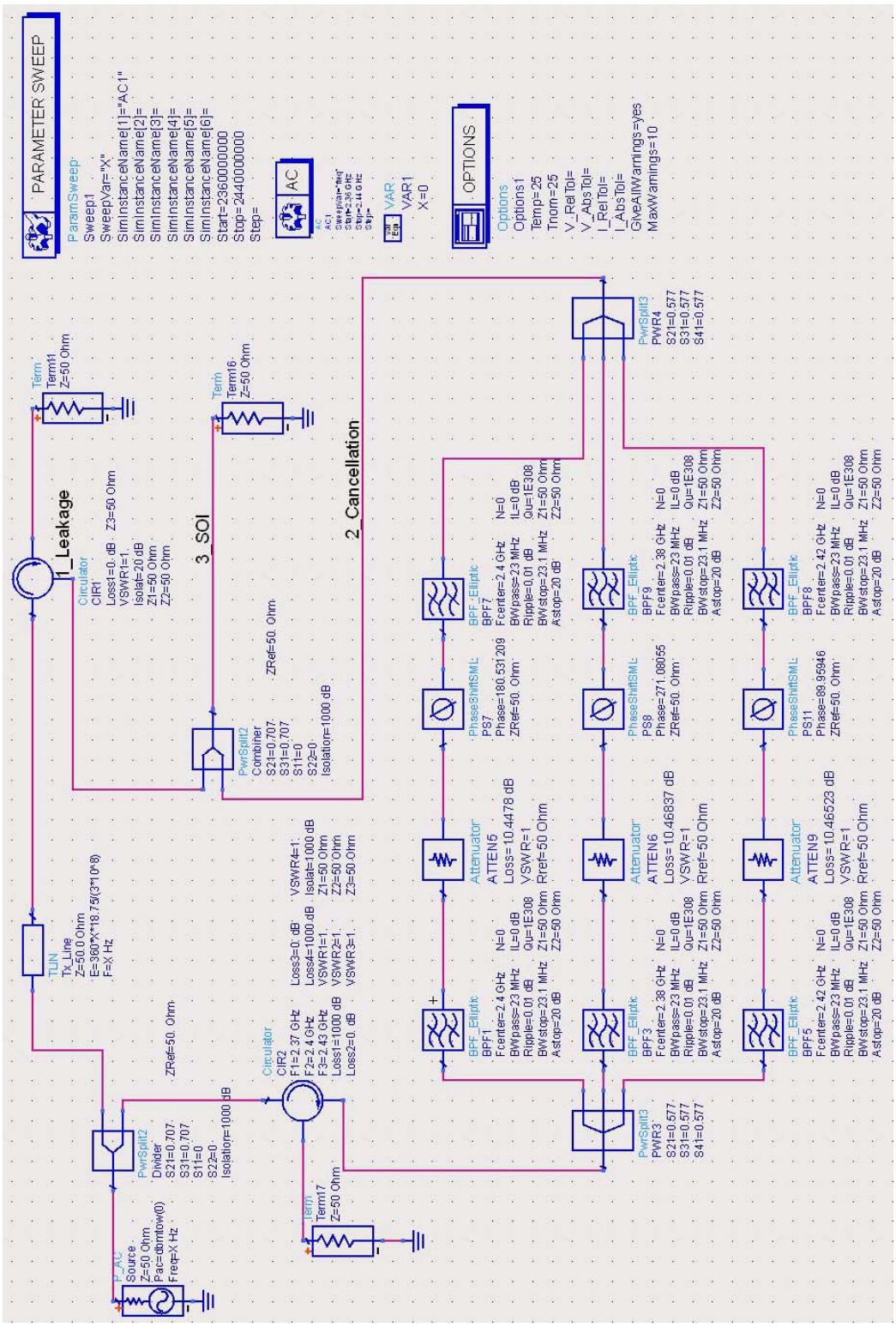

Figure 85. ADS Model of WLCC with FDMC using Couplers with Ideal Component Settings.

Table 7. Summary of Measurements for WLCC using FDMC with Couplers with Ideal Component Parameter Settings.

freq	var("1_Leakage")	var("2_Cancellation")	var("3_SOI")
2.38000 GHz	-33.01161 / 90.00000	-33.01312 / -90.00283	-110.90628 / 105.88079
2.38025 GHz	-33.01161 / 84.37500	-33.00756 / -94.72503	-72.09532 / -6.87636
2.38050 GHz	-33.01161 / 78.75000	-33.00253 / -99.45004	-66.07140 / -12.25687
2.38075 GHz	-33.01161 / 73.12500	-32.99799 / -104.18237	-62.57128 / -17.43953
2.38100 GHz	-33.01161 / 67.50000	-32.99391 / -108.92662	-60.11202 / -22.58418
freq	var("1_Leakage")	var("2_Cancellation")	var("3_SOI")
2.40000 GHz	-33.01161 / 0.00029	-33.01186 / -179.99974	-127.00526 / 1.00186
2.40025 GHz	-33.01161 / -5.62500	-33.01235 / 175.29133	-71.94500 / -94.86430
2.40050 GHz	-33.01161 / -11.25000	-33.01351 / 170.57771	-65.94866 / -99.94266
2.40075 GHz	-33.01161 / -16.87500	-33.01533 / 165.85454	-62.46623 / -104.99522
2.40100 GHz	-33.01161 / -22.50000	-33.01774 / 161.11687	-60.02299 / -110.05096
freq	var("1_Leakage")	var("2_Cancellation")	var("3_SOI")
2.42000 GHz	-33.01161 / -90.00000	-33.01303 / 90.00356	-111.17540 / -110.83872
2.42025 GHz	-33.01161 / -95.62500	-33.01937 / 85.27767	-72.06517 / 178.06977
2.42050 GHz	-33.01161 / -101.25000	-33.02623 / 80.54575	-66.09592 / 172.72056
2.42075 GHz	-33.01161 / -106.87500	-33.03359 / 75.80335	-62.62741 / 167.56260
2.42100 GHz	-33.01161 / -112.50000	-33.04144 / 71.04594	-60.19399 / 162.44828

The graphical plots of the measurements in Table 7 are shown in Figures 86 to 89. In Figure 86, successful leakage cancellation at 2.38 GHz, 2.4 GHz and 2.42 GHz is evident. In comparison to the previous results, depicted in Figure 81, this design is able to sustain a lower cancellation level over a much wider bandwidth.

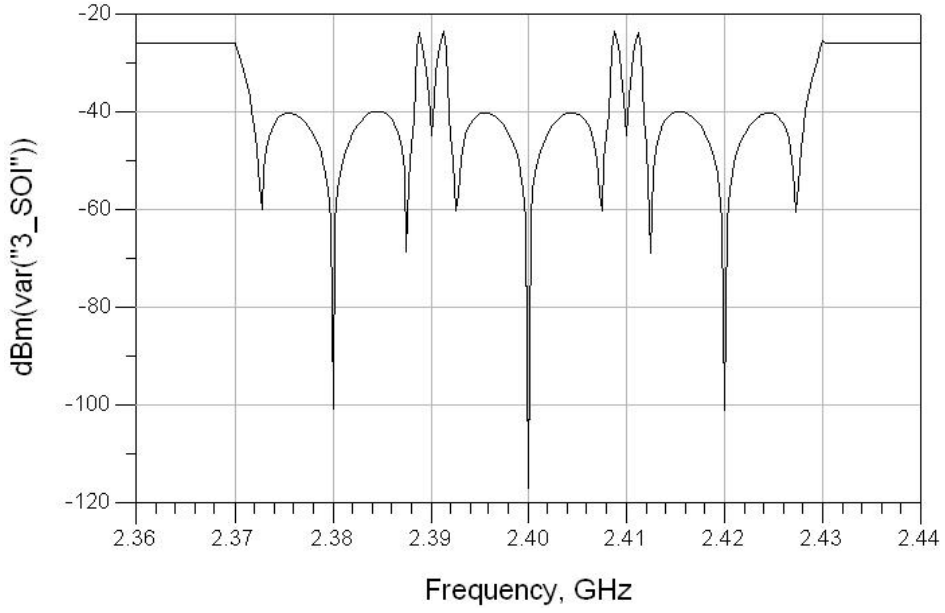

Figure 86. Amplitude Plot of SOI in WLCC.

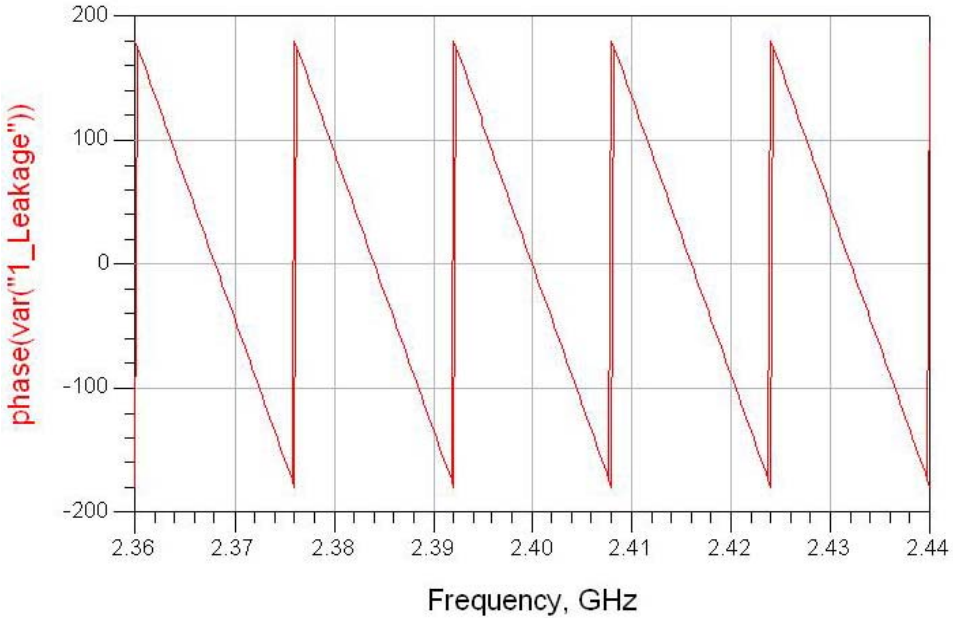

Figure 87. Phase Plot of Leakage in WLCC.

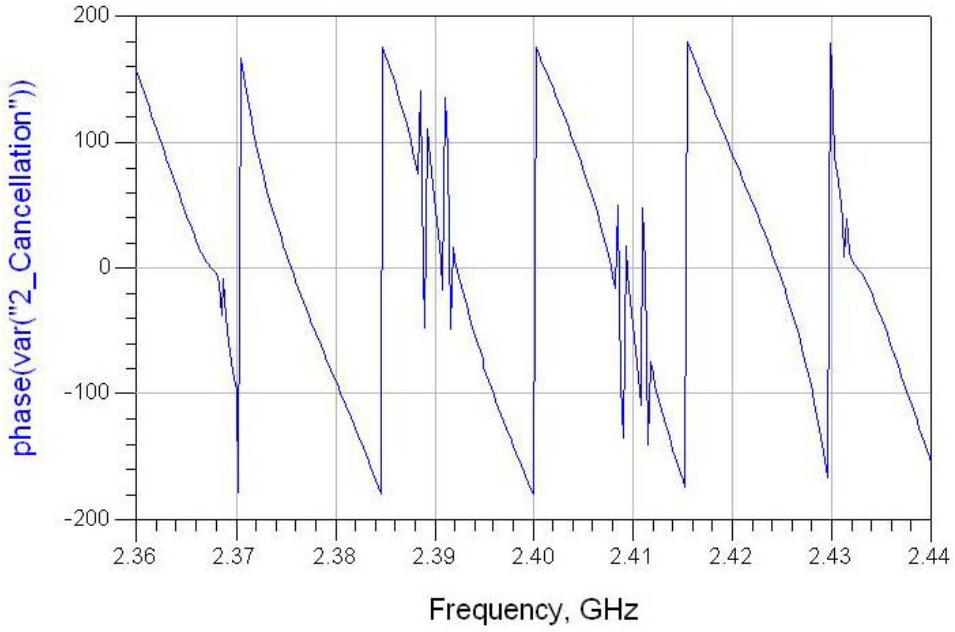

Figure 88. Phase Plot of Cancellation in WLCC.

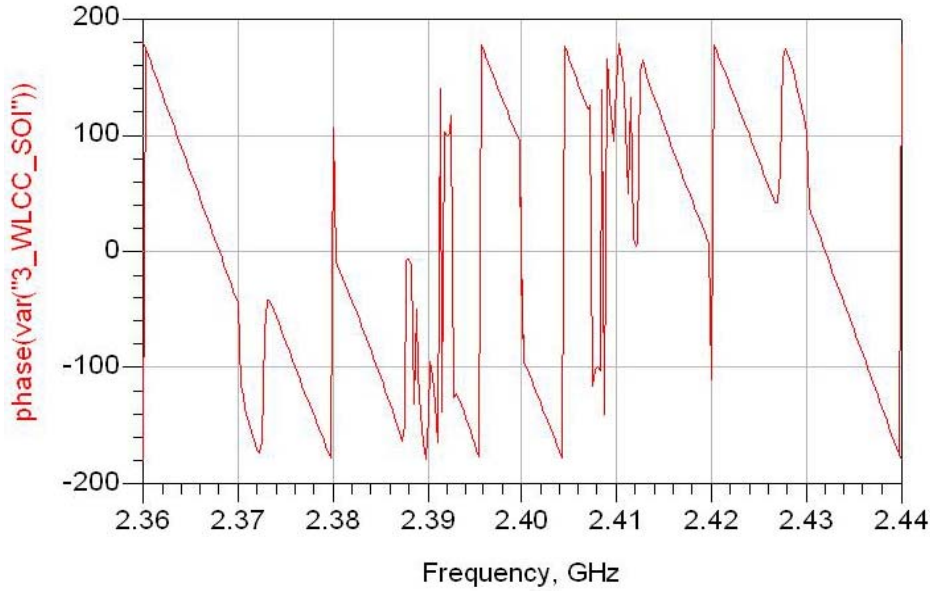

Figure 89. Phase Plot of SOI in WLCC.

An analysis of the phase plots shown in Figures 75 to 77 reveal the ability of this design to match the phase of the leakage signal, resulting in the desired wideband cancellation. These simulation results have shown the superiority of the design using couplers over the design using circulators. Therefore, the couplers design was chosen to be the preferred WLCC design.

C. EVALUATION OF FINAL WLCC DESIGN

1. Evaluation Approach

The analysis of both WLCC designs in Section B.1 and B.2 of this chapter yielded results that favored the selection of the WLCC using the FDMC with couplers as the final design. A comparison of amplitude plots of SOI for both designs with ideal devices is given in Figure 90.

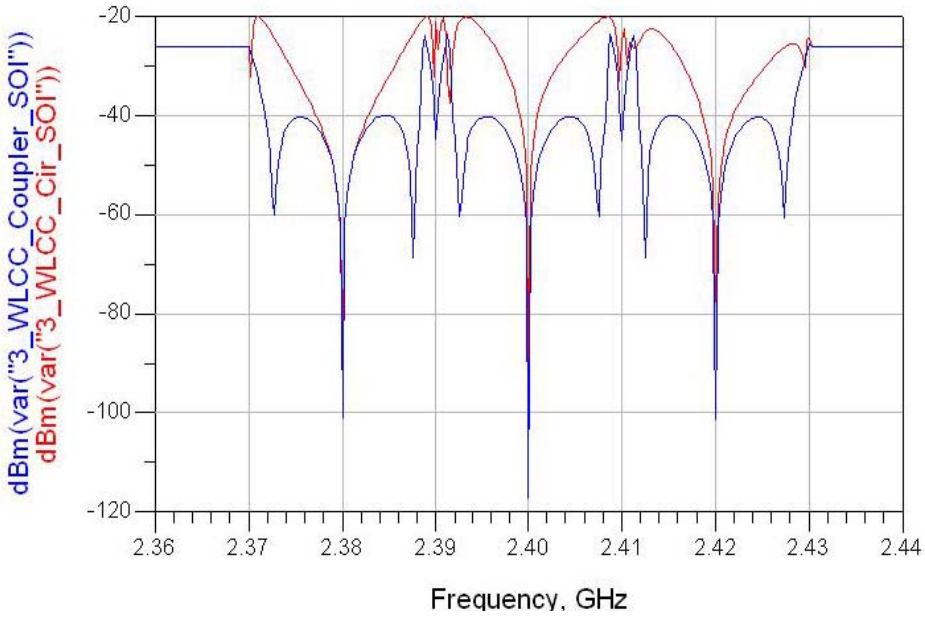

Figure 90. Comparison of Amplitude Plots for both WLCC Designs with Ideal Devices.

A two-pronged approach was adopted to evaluate the effectiveness of the WLCC. The first prong of the approach was to benchmark the performance of the final WLCC design against that of a single frequency LCC using all idealized component parameters. This was followed by another round of benchmarking using all non-idealized component parameters. This approach allows better understanding of the performance of an ideal WLCC and sets a baseline for comparison when actual components were used. The second prong of the evaluation approach was to factor in possible mismatches of the simulated antenna load, hence, providing insight into the robustness of the WLCC design.

The non-ideal component parameter settings in ADS were based on actual components available in the Microwave Lab of the Electrical and Computer Engineering (ECE) Department at NPS, as well as measurements conducted and documented in previous theses using similar components. The technical specifications as well as the assumptions of parameter settings in ADS are tabulated in Table 8.

The ADS models of both the single frequency LCC with ideal and non-ideal component parameter settings and the WLCC with non-ideal component settings are illustrated in Figures 91 to 93, respectively.

Table 8. Actual Component Parameters (After Table 2 from [7] and Table 4 of [11]).

Component	Manufacturer and Model	Technical Specifications	Assumption of Parameter Settings in ADS
Source	Vaunix Technology LSG–402 Signal Generator	Output power 10 to -40 dBm 100 kHz frequency resolution 55 dB output power control 0.5 dB output power resolution -80 dBc non-harmonic spurious	P_AC:No Changes, as per ideal settings. Z=50 Ohm Pac=dbmtow(0) Freq=2.36 GHz to 2.44 GHz in 250 kHz steps
3 dB Power Splitter	Pasternack PE2014	Frequency range 2-4 GHz Minimum isolation 20 dB VSWR 1.30 Maximum insertion loss 30 dB SMA female power divider 2 output ports	PwrSplit2: S21=0.707 S31=0.707 S11=1.1 S22=1.1 Isolation=20 dB
Circulator	DITOM D3C2040	Frequency range 2-4 GHz Impedance 50 Ω Isolation 20 dB Insertion loss 0.4-0.5 dB VSWR 1.25-1.30 AVG power 20 W Peak power 30 W	Circulator: F1=2 GHz F2=3 GHz F3=4 GHz Loss1=20 dB Loss2=0.4 dB Loss3=0.4 dB Loss4=20 dB VSWR1=1.3 VSWR2=1.3 VSWR3=1.3 VSWR4=1.3 Isolation=20 dB Z1=50 Ohm Z2=50 Ohm Z3=50 Ohm

Table 8 [Continued]. Actual Component Parameters (After Table 2 from [7] and Table 4 of [11]).

Component	Manufacturer and Model	Technical Specifications	Assumption of Parameter Settings in ADS
Phase Shifter	SAGE LABORATORIES INC. Model 6708	Frequency range DC-8 GHz Phase shift, min 72 °/GHz Insertion phase @ min phase setting 170 °/GHz Number of turns, min 30 VSWRmax 1.60 Insertion loss, max 0.7 dB AVG power 1000 W Peak power 0.45 W Time delay @ min phase setting 3.1 nsec	PhaseShiftSML: No Changes as per Ideal settings except minimum increment step of 10 degrees. Zref=50 Ohm
Digital Attenuator	TELEMAKUS LCC TEA4000-7	Frequency range 50 MHz to 4 GHz Attenuation 0-31.75 dB in 0.25 dB steps Interface USB 2.0 Current 150 mA @ 5 V High linearity +59 dBm IP3 P1dB +30 dBm SMA connector	Attenuator: No Changes as per Ideal settings except minimum increment step of 0.25 dB Rref=50 Ohm

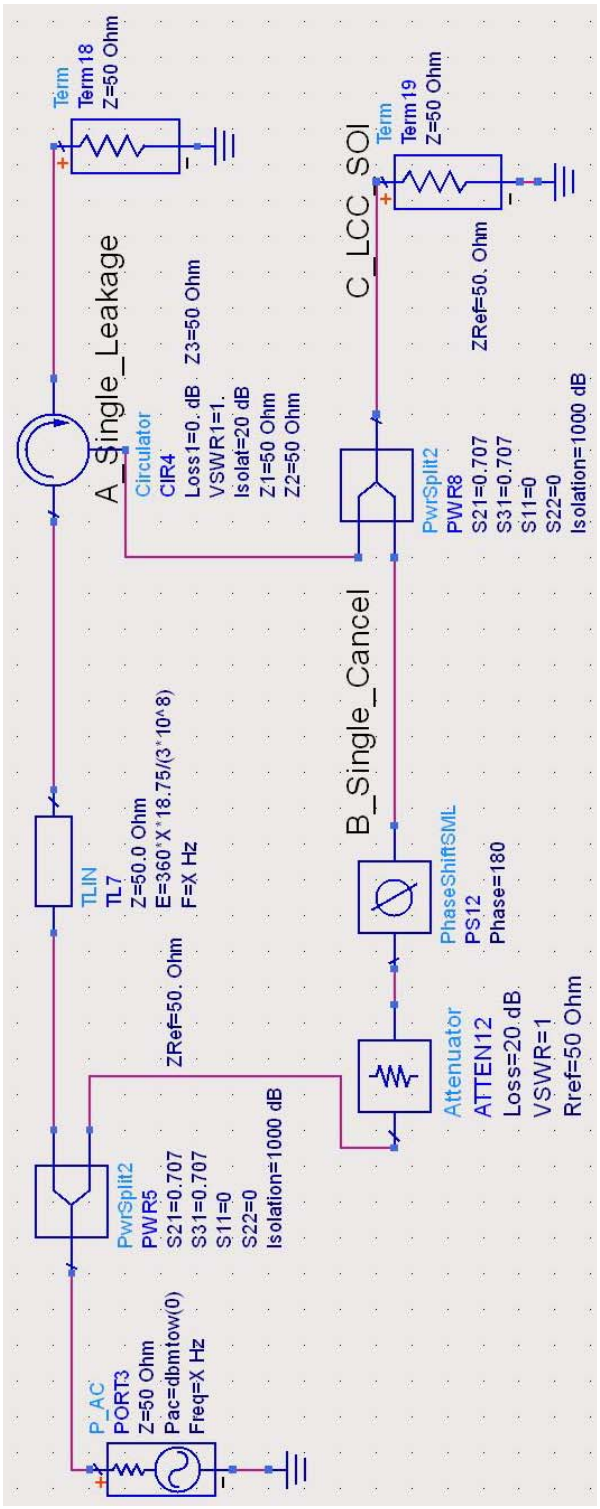

Figure 91. ADS Model of Single Frequency LCC with Ideal Component Parameter Settings.

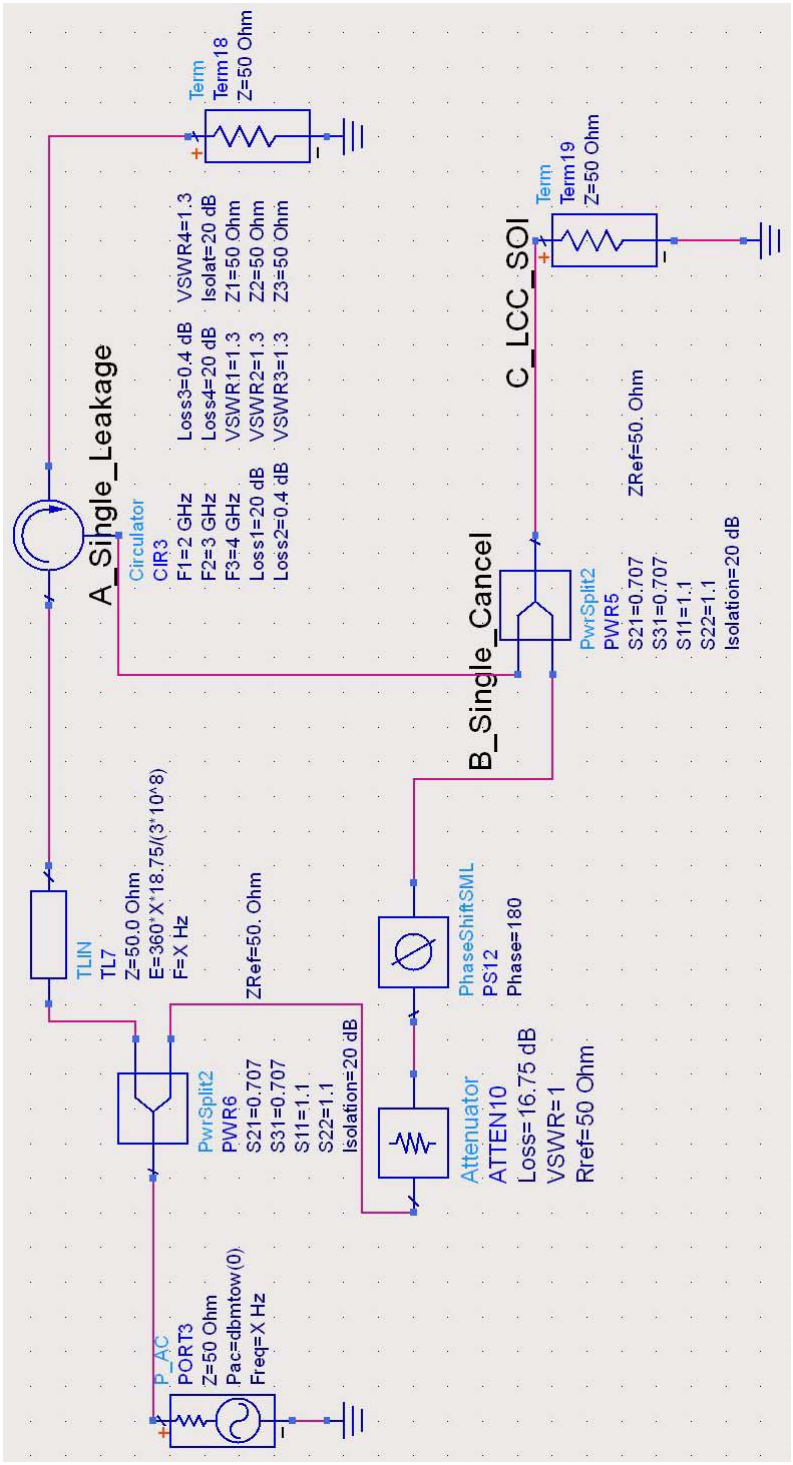

Figure 92. ADS Model of Single Frequency LCC with Non-Ideal Component Parameter Settings.

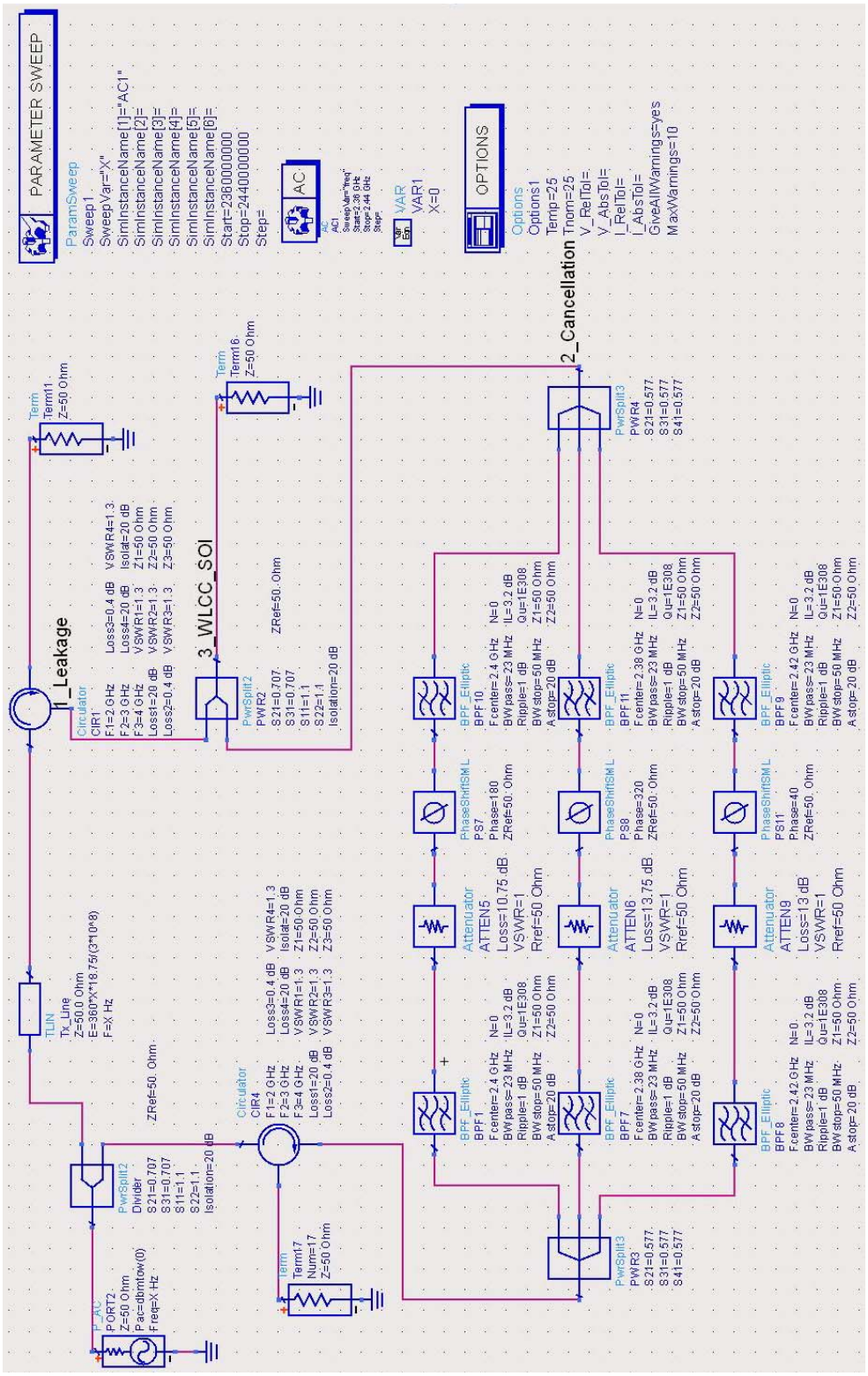

Figure 93. ADS Model of WLCC with Non-Ideal Parameter Settings.

2. Performance Benchmarking Against Single Frequency LCC With Ideal Component Parameter Settings

The measurements for both the WLCC and LCC, in dB / Degrees as well as dBm, are tabulated in Tables 9 to 12. The measurements in dB / Degrees help in determining the amount of attenuation and phase shift required in the WLCC and LCC. The measurements in dBm provide insight into the performance of the WLCC and LCC with reference of the arbitrarily set input source power of 0 dBm.

Table 9. Measurements at WLCC with Ideal Component Parameter Settings in dB / Degrees.

freq	var("1_Leakage")	var("2_Cancellation")	var("3_WLCC_SOI")
2.38000 GHz	-33.01161 / 90.00000	-33.01312 / -90.00283	-110.90628 / 105.88079
2.38025 GHz	-33.01161 / 84.37500	-33.00756 / -94.72503	-72.09532 / -6.87636
2.38050 GHz	-33.01161 / 78.75000	-33.00253 / -99.45004	-66.07140 / -12.25687
2.38075 GHz	-33.01161 / 73.12500	-32.99799 / -104.18237	-62.57128 / -17.43953
2.38100 GHz	-33.01161 / 67.50000	-32.99391 / -108.92662	-60.11202 / -22.58418
freq	var("1_Leakage")	var("2_Cancellation")	var("3_WLCC_SOI")
2.40000 GHz	-33.01161 / 0.00029	-33.01186 / -179.99974	-127.00526 / 1.00186
2.40025 GHz	-33.01161 / -5.62500	-33.01235 / 175.29133	-71.94500 / -94.86430
2.40050 GHz	-33.01161 / -11.25000	-33.01351 / 170.57771	-65.94866 / -99.94266
2.40075 GHz	-33.01161 / -16.87500	-33.01533 / 165.85454	-62.46623 / -104.99522
2.40100 GHz	-33.01161 / -22.50000	-33.01774 / 161.11687	-60.02299 / -110.05096
freq	var("1_Leakage")	var("2_Cancellation")	var("3_WLCC_SOI")
2.42000 GHz	-33.01161 / -90.00000	-33.01303 / 90.00356	-111.17540 / -110.83872
2.42025 GHz	-33.01161 / -95.62500	-33.01937 / 85.27767	-72.06517 / 178.06977
2.42050 GHz	-33.01161 / -101.25000	-33.02623 / 80.54575	-66.09592 / 172.72056
2.42075 GHz	-33.01161 / -106.87500	-33.03359 / 75.80335	-62.62741 / 167.56260
2.42100 GHz	-33.01161 / -112.50000	-33.04144 / 71.04594	-60.19399 / 162.44828

Table 10. Measurements at WLCC with Ideal Component Parameter Settings in dBm.

freq	dbm(var("1_Leakage"))	dbm(var("2_Cancellation"))	dbm(var("3_WLCC_SOI"))
2.38000 GHz	-23.01161	-23.01312	-100.90628
2.38025 GHz	-23.01161	-23.00756	-62.09532
2.38050 GHz	-23.01161	-23.00253	-56.07140
2.38075 GHz	-23.01161	-22.99799	-52.57128
2.38100 GHz	-23.01161	-22.99391	-50.11202
freq	dbm(var("1_Leakage"))	dbm(var("2_Cancellation"))	dbm(var("3_WLCC_SOI"))
2.40000 GHz	-23.01161	-23.01186	-117.00526
2.40025 GHz	-23.01161	-23.01235	-61.94500
2.40050 GHz	-23.01161	-23.01351	-55.94866
2.40075 GHz	-23.01161	-23.01533	-52.46623
2.40100 GHz	-23.01161	-23.01774	-50.02299
freq	dbm(var("1_Leakage"))	dbm(var("2_Cancellation"))	dbm(var("3_WLCC_SOI"))
2.42000 GHz	-23.01161	-23.01303	-101.17540
2.42025 GHz	-23.01161	-23.01937	-62.06517
2.42050 GHz	-23.01161	-23.02623	-56.09592
2.42075 GHz	-23.01161	-23.03359	-52.62741
2.42100 GHz	-23.01161	-23.04144	-50.19399

Table 11. Measurements at LCC with Ideal Component Parameter Settings in dB / Degrees.

freq	A_Single_Leakage	B_Single_Cancel	C_LCC_SOI
2.38000 GHz	-33.01161 / 90.00000	-33.01161 / 180.00000	-33.01292 / 135.00000
2.38025 GHz	-33.01161 / 84.37500	-33.01161 / 180.00000	-33.46094 / 132.18750
2.38050 GHz	-33.01161 / 78.75000	-33.01161 / 180.00000	-33.95545 / 129.37500
2.38075 GHz	-33.01161 / 73.12500	-33.01161 / 180.00000	-34.50208 / 126.56250
2.38100 GHz	-33.01161 / 67.50000	-33.01161 / 180.00000	-35.10784 / 123.75000
freq	A_Single_Leakage	B_Single_Cancel	C_LCC_SOI
2.40000 GHz	-33.01161 / 0.00029	-33.01161 / 180.00000	-142.04381 / 90.00029
2.40025 GHz	-33.01161 / -5.62500	-33.01161 / 180.00000	-56.18671 / -92.81250
2.40050 GHz	-33.01161 / -11.25000	-33.01161 / 180.00000	-50.17658 / -95.62500
2.40075 GHz	-33.01161 / -16.87500	-33.01161 / 180.00000	-46.67222 / -98.43750
2.40100 GHz	-33.01161 / -22.50000	-33.01161 / 180.00000	-44.19791 / -101.25000
freq	A_Single_Leakage	B_Single_Cancel	C_LCC_SOI
2.42000 GHz	-33.01161 / -90.00000	-33.01161 / 180.00000	-33.01292 / -135.00000
2.42025 GHz	-33.01161 / -95.62500	-33.01161 / 180.00000	-32.60683 / -137.81250
2.42050 GHz	-33.01161 / -101.25000	-33.01161 / 180.00000	-32.23892 / -140.62500
2.42075 GHz	-33.01161 / -106.87500	-33.01161 / 180.00000	-31.90607 / -143.43750
2.42100 GHz	-33.01161 / -112.50000	-33.01161 / 180.00000	-31.60570 / -146.25000

Table 12. Measurements at LCC with Ideal Component Parameter Settings in dBm.

freq	dbm(A_Single_Leakage)	dbm(B_Single_Cancel)	dbm(C_LCC_SOI)
2.38000 GHz	-23.01161	-23.01161	-23.01292
2.38025 GHz	-23.01161	-23.01161	-23.46094
2.38050 GHz	-23.01161	-23.01161	-23.95545
2.38075 GHz	-23.01161	-23.01161	-24.50208
2.38100 GHz	-23.01161	-23.01161	-25.10784
freq	dbm(A_Single_Leakage)	dbm(B_Single_Cancel)	dbm(C_LCC_SOI)
2.40000 GHz	-23.01161	-23.01161	-132.04381
2.40025 GHz	-23.01161	-23.01161	-46.18671
2.40050 GHz	-23.01161	-23.01161	-40.17658
2.40075 GHz	-23.01161	-23.01161	-36.67222
2.40100 GHz	-23.01161	-23.01161	-34.19791
freq	dbm(A_Single_Leakage)	dbm(B_Single_Cancel)	dbm(C_LCC_SOI)
2.42000 GHz	-23.01161	-23.01161	-23.01292
2.42025 GHz	-23.01161	-23.01161	-22.60683
2.42050 GHz	-23.01161	-23.01161	-22.23892
2.42075 GHz	-23.01161	-23.01161	-21.90607
2.42100 GHz	-23.01161	-23.01161	-21.60570

The graphical plots of the measurements in Tables 9 to 12 are shown in Figures 94 to 101. The performance of the WLCC by comparing its SOI against that of the LCC, both in dBm and dB, respectively, is illustrated in Figure 93 and 94. The ability of the WLCC to cancel out the leakage at the center frequencies of 2.38 GHz, 2.4 GHz and 2.42 GHz as well as its ability to sustain its cancellation across the entire band of interest from 2.37 GHz to 2.43 GHz was noted. Areas around 2.39 GHz and 2.41 GHz are the transition bands between filters, where the phase becomes more non-linear and difficult to match.

A comparison of the phase plots for the leakage, cancellation and SOI for both the WLCC and LCC are illustrated in Figures 95 to 101.

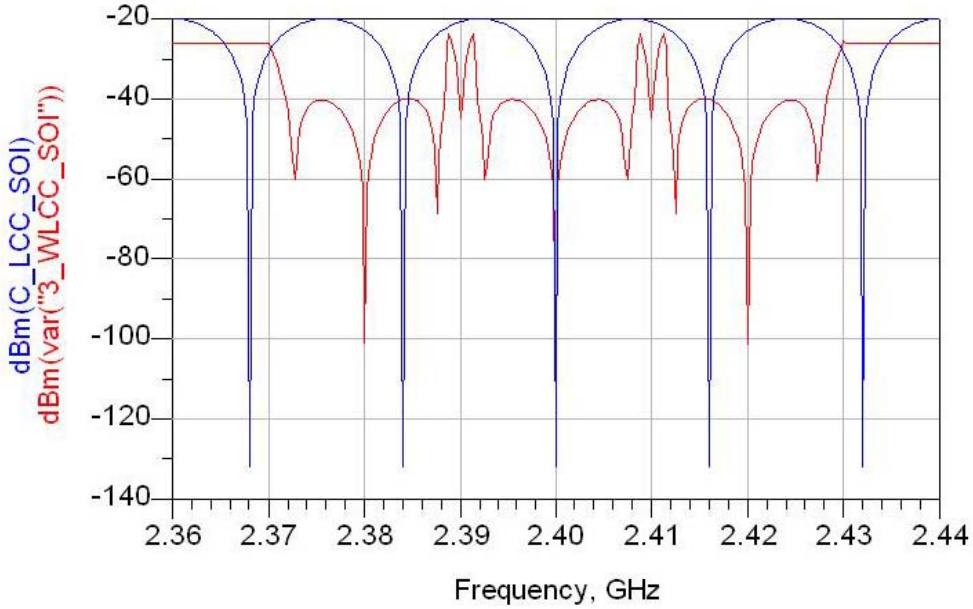

Figure 94. Amplitude Plot of SOI for both WLCC and LCC with Ideal Component Parameter Settings in dBm.

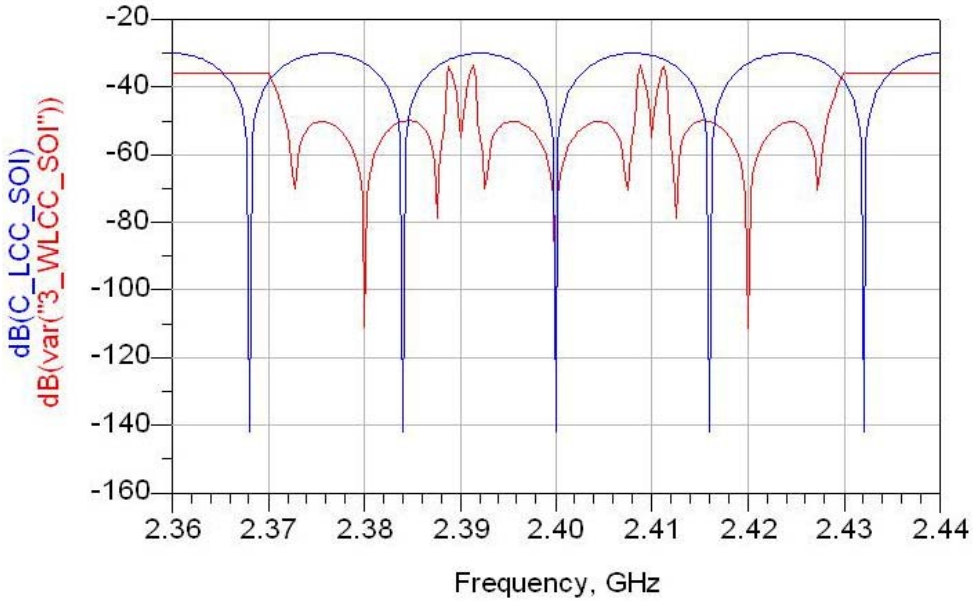

Figure 95. Amplitude Plot of SOI for both WLCC and LCC with Ideal Component Parameter Settings in dB.

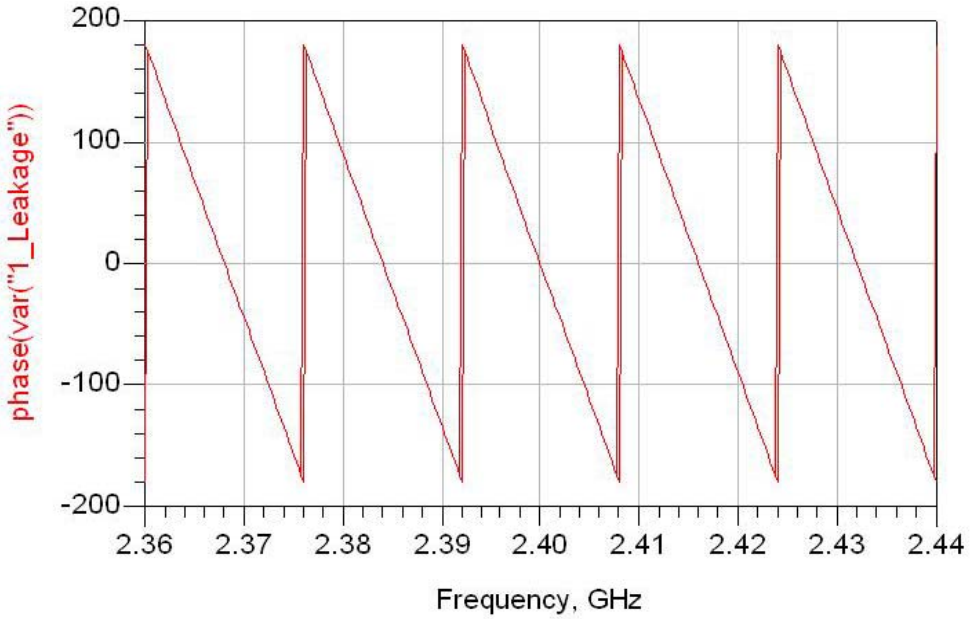

Figure 96. Phase Plot of Leakage in WLCC with Ideal Component Parameter Settings in Degrees.

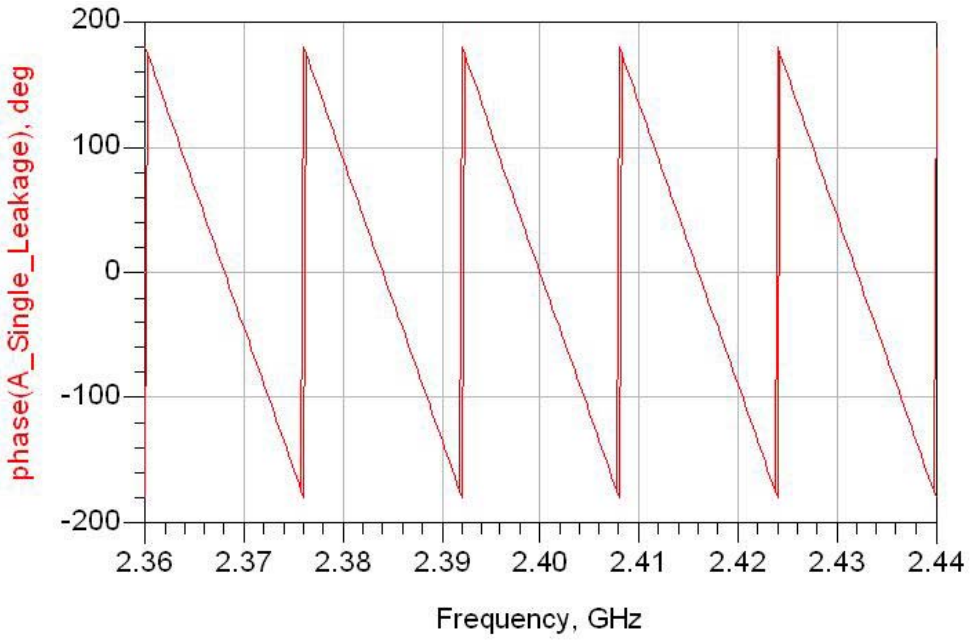

Figure 97. Phase Plot of Leakage in LCC with Ideal Component Parameter Settings in Degrees.

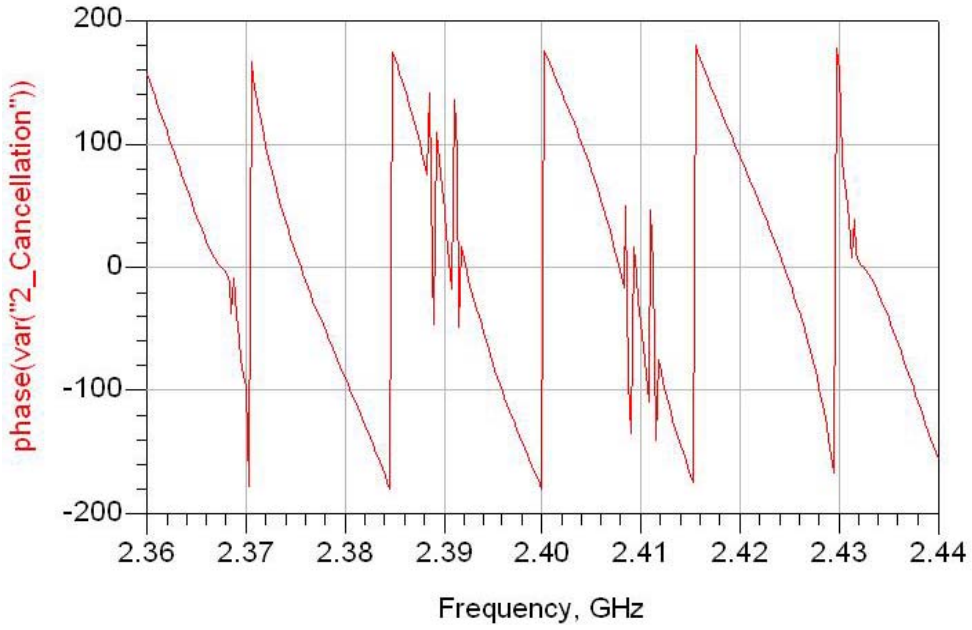

Figure 98. Phase Plot of Cancellation in WLCC with Ideal Component Parameter Settings in Degrees.

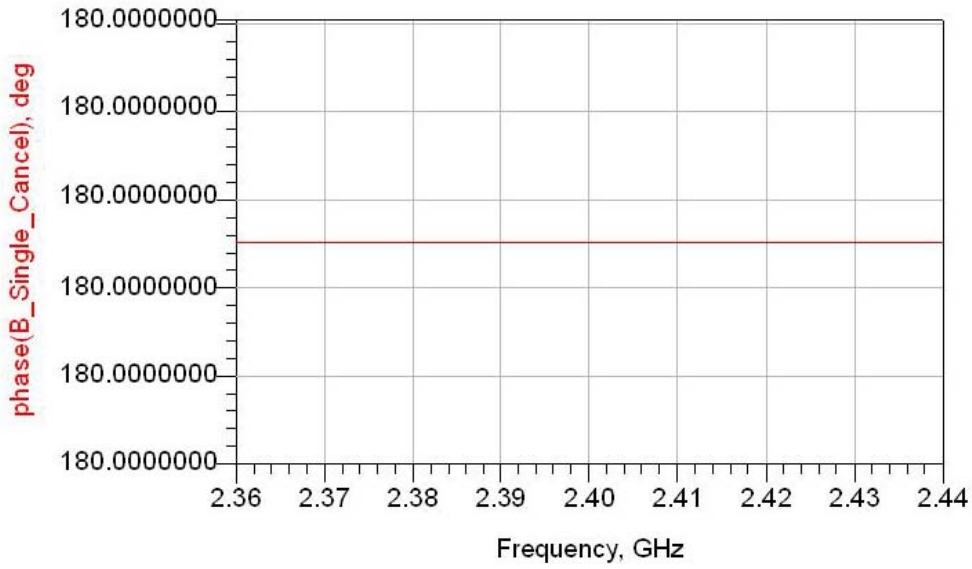

Figure 99. Phase Plot of Cancellation in LCC with Ideal Component Parameter Settings in Degrees.

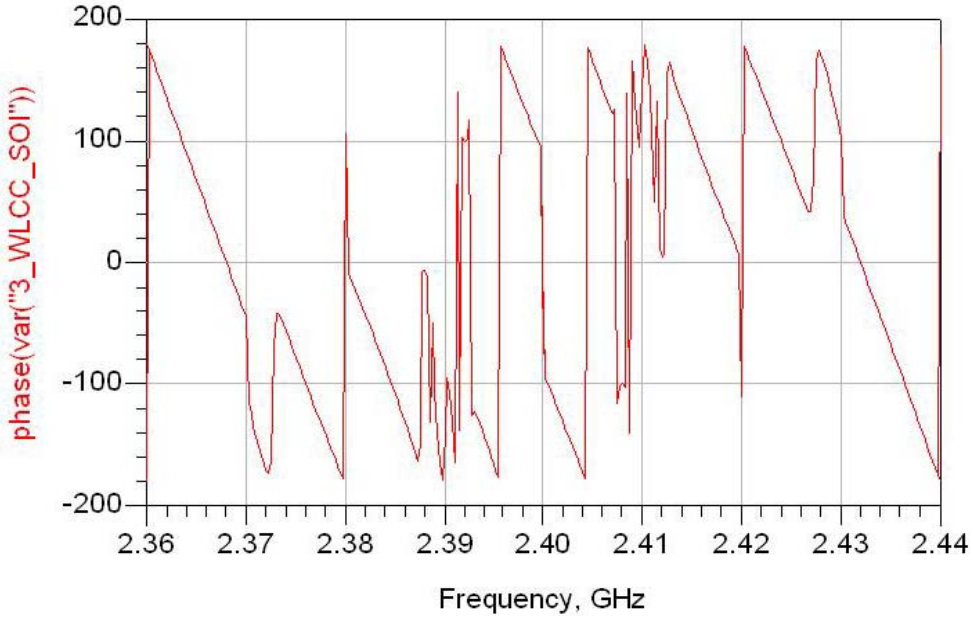

Figure 100. Phase Plot of SOI in WLCC with Ideal Component Parameter Settings in Degrees.

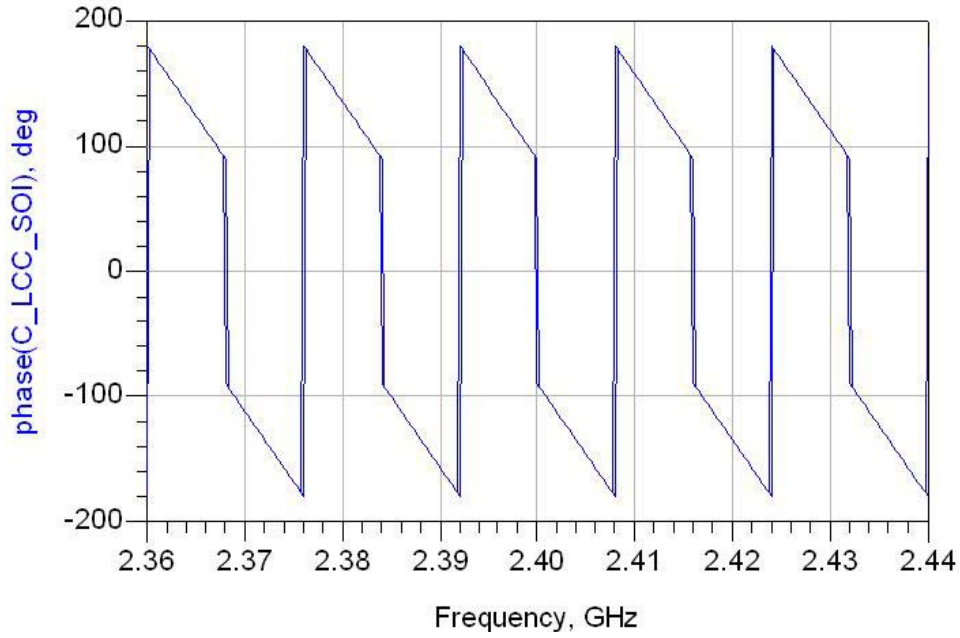

Figure 101. Phase Plot of SOI in LCC with Ideal Component Parameter Settings in Degrees.

3. Performance Benchmarking Against Single Frequency LCC With Non-Ideal Component Parameter Settings

The measurements for both the WLCC and LCC with non-ideal component parameter settings, as illustrated in Figure 80 and Table 7, in dB / Degrees, as well as dBm, are tabulated in Tables 13 to 16.

Table 13. Measurements at WLCC with Non-Ideal Component Parameter Settings in dB / Degrees.

freq	var("1_Leakage")	var("2_Cancellation")	var("3_WLCC_SOI")
2.38000 GHz	-27.56561 / 89.19203	-28.42759 / -78.95595	-50.65556 / 30.64946
2.38025 GHz	-27.53491 / 85.95419	-28.42309 / -82.69919	-50.88815 / 28.84027
2.38050 GHz	-27.44574 / 82.67483	-28.42701 / -86.43328	-50.91175 / 28.74050
2.38075 GHz	-27.29806 / 79.30964	-28.43980 / -90.15393	-50.65112 / 30.01938
2.38100 GHz	-27.09194 / 75.81071	-28.46167 / -93.85392	-50.04998 / 32.00286
freq	var("1_Leakage")	var("2_Cancellation")	var("3_WLCC_SOI")
2.40000 GHz	-22.76604 / 0.01955	-24.77331 / 179.73857	-46.33263 / 1.10015
2.40025 GHz	-22.85484 / -10.05574	-24.76482 / 176.30012	-45.82787 / -33.76385
2.40050 GHz	-23.10768 / -19.74381	-24.73839 / 172.79341	-44.59021 / -63.04203
2.40075 GHz	-23.48932 / -28.75232	-24.70132 / 169.17037	-43.29000 / -85.95921
2.40100 GHz	-23.95515 / -36.92794	-24.66168 / 165.41568	-42.21560 / -104.12577
freq	var("1_Leakage")	var("2_Cancellation")	var("3_WLCC_SOI")
2.42000 GHz	-27.60168 / -89.13830	-27.68176 / 78.97105	-51.16713 / -7.61792
2.42025 GHz	-27.57390 / -92.38404	-27.69712 / 75.23899	-50.80387 / -12.31517
2.42050 GHz	-27.48763 / -95.67355	-27.71922 / 71.50479	-50.42371 / -18.85045
2.42075 GHz	-27.34291 / -99.05077	-27.74758 / 67.76517	-50.01068 / -27.03753
2.42100 GHz	-27.13987 / -102.56299	-27.78191 / 64.01471	-49.53256 / -36.70369

Table 14. Measurements at WLCC with Non-Ideal Component Parameter Settings in dBm.

freq	dbm(var("1_Leakage"))	dbm(var("2_Cancellation"))	dbm(var("3_WLCC_SOI"))
2.38000 GHz	-17.56561	-18.42759	-40.65556
2.38025 GHz	-17.53491	-18.42309	-40.88815
2.38050 GHz	-17.44574	-18.42701	-40.91175
2.38075 GHz	-17.29806	-18.43980	-40.65112
2.38100 GHz	-17.09194	-18.46167	-40.04998
freq	dbm(var("1_Leakage"))	dbm(var("2_Cancellation"))	dbm(var("3_WLCC_SOI"))
2.40000 GHz	-12.76604	-14.77331	-36.33263
2.40025 GHz	-12.85484	-14.76482	-35.82787
2.40050 GHz	-13.10768	-14.73839	-34.59021
2.40075 GHz	-13.48932	-14.70132	-33.29000
2.40100 GHz	-13.95515	-14.66168	-32.21560
freq	dbm(var("1_Leakage"))	dbm(var("2_Cancellation"))	dbm(var("3_WLCC_SOI"))
2.42000 GHz	-17.60168	-17.68176	-41.16713
2.42025 GHz	-17.57390	-17.69712	-40.80387
2.42050 GHz	-17.48763	-17.71922	-40.42371
2.42075 GHz	-17.34291	-17.74758	-40.01068
2.42100 GHz	-17.13987	-17.78191	-39.53256

Table 15. Measurements at LCC with Non-Ideal Component Parameter Settings in dB / Degrees.

freq	A_Single_Leakage	B_Single_Cancel	C_LCC_SOI
2.38000 GHz	-27.30361 / 94.70747	-23.26001 / 178.13309	-31.25083 / 147.94022
2.38025 GHz	-27.34093 / 91.53873	-23.27504 / 178.31003	-31.48370 / 147.18239
2.38050 GHz	-27.32164 / 88.28105	-23.28730 / 178.48172	-31.71544 / 146.27692
2.38075 GHz	-27.24509 / 84.88988	-23.29712 / 178.64831	-31.95246 / 145.18836
2.38100 GHz	-27.11067 / 81.31770	-23.30469 / 178.80998	-32.20249 / 143.87707
freq	A_Single_Leakage	B_Single_Cancel	C_LCC_SOI
2.40000 GHz	-23.07771 / -0.00003	-23.26562 / 179.99997	-56.32890 / -0.00003
2.40025 GHz	-23.16174 / -10.38414	-23.26793 / -179.99573	-47.89852 / -91.34283
2.40050 GHz	-23.40053 / -20.38143	-23.27420 / -179.97683	-42.20395 / -102.49308
2.40075 GHz	-23.75961 / -29.69838	-23.28281 / -179.93415	-39.11839 / -110.71154
2.40100 GHz	-24.19531 / -38.17809	-23.29199 / -179.86556	-37.15397 / -117.52761
freq	A_Single_Leakage	B_Single_Cancel	C_LCC_SOI
2.42000 GHz	-27.30361 / -94.70747	-23.26001 / -178.13309	-31.25083 / -147.94022
2.42025 GHz	-27.21029 / -97.83053	-23.24182 / -177.95094	-31.01126 / -148.58362
2.42050 GHz	-27.06151 / -100.95157	-23.21994 / -177.76395	-30.75998 / -149.14542
2.42075 GHz	-26.85773 / -104.11631	-23.19372 / -177.57306	-30.49234 / -149.66004
2.42100 GHz	-26.59946 / -107.37421	-23.16235 / -177.38015	-30.20398 / -150.16552

Table 16. Measurements at LCC with Non-Ideal Component Parameter Settings in dBm.

freq	dbm(A_Single_Leakage)	dbm(B_Single_Cancel)	dbm(C_LCC_SOI)
2.38000 GHz	-17.30361	-13.26001	-21.25083
2.38025 GHz	-17.34093	-13.27504	-21.48370
2.38050 GHz	-17.32164	-13.28730	-21.71544
2.38075 GHz	-17.24509	-13.29712	-21.95246
2.38100 GHz	-17.11067	-13.30469	-22.20249
freq	dbm(A_Single_Leakage)	dbm(B_Single_Cancel)	dbm(C_LCC_SOI)
2.40000 GHz	-13.07771	-13.26562	-56.32890
2.40025 GHz	-13.16174	-13.26793	-37.89852
2.40050 GHz	-13.40053	-13.27420	-32.20395
2.40075 GHz	-13.75961	-13.28281	-29.11839
2.40100 GHz	-14.19531	-13.29199	-27.15397
freq	dbm(A_Single_Leakage)	dbm(B_Single_Cancel)	dbm(C_LCC_SOI)
2.42000 GHz	-17.30361	-13.26001	-21.25083
2.42025 GHz	-17.21029	-13.24182	-21.01126
2.42050 GHz	-17.06151	-13.21994	-20.75998
2.42075 GHz	-16.85773	-13.19372	-20.49234
2.42100 GHz	-16.59946	-13.16235	-20.20398

The graphical plots of the measurements in Tables 13 to 16 are shown in Figures 102 to 109. The performance of the WLCC by comparing its SOI against that of the LCC, both in dBm and dB, respectively, is illustrated in Figure 102 and 103. The ability of the WLCC to still cancel out the leakage at center frequencies of 2.38 GHz, 2.4 GHz and 2.42 GHz was noted. While the LCC is still able to cancel out the leakage at its center frequency of 2.4 GHz, the rejection level was less compared to that of the WLCC. Therefore, the overall performance of the WLCC is still better than that of the LCC.

A comparison of the phase plots for the leakage, cancellation and SOI for both the WLCC and LCC are illustrated in Figures 104 to 109.

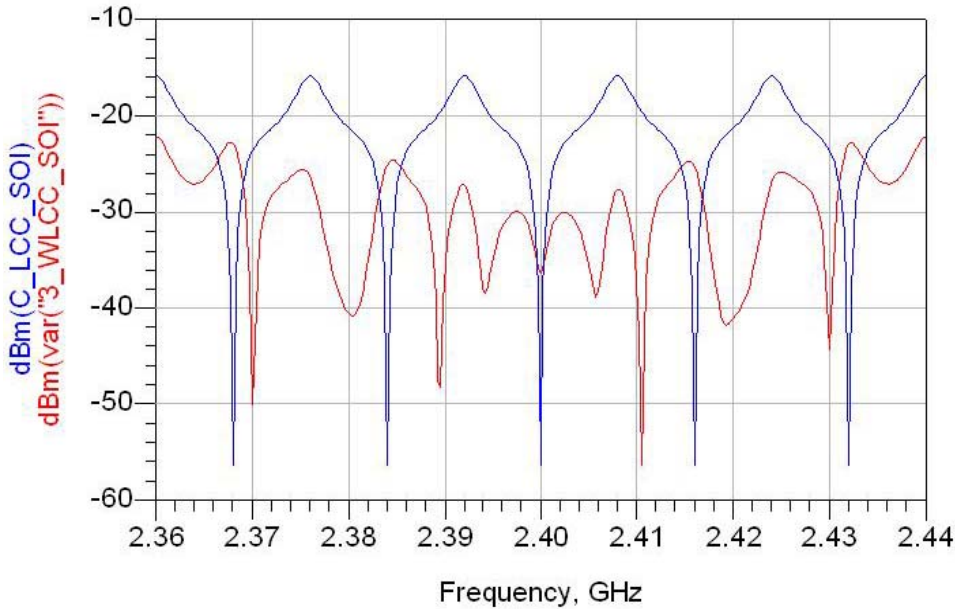

Figure 102. Amplitude Plot of SOI for both WLCC and LCC with Non-Ideal Component Parameter Settings in dBm.

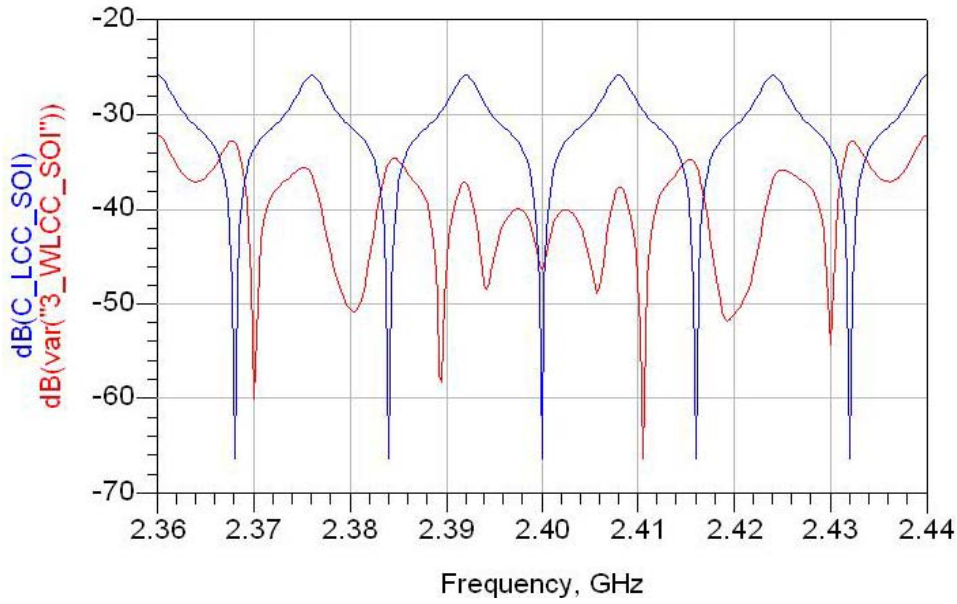

Figure 103. Amplitude Plot of SOI for both WLCC and LCC with Non-Ideal Component Parameter Settings in dB.

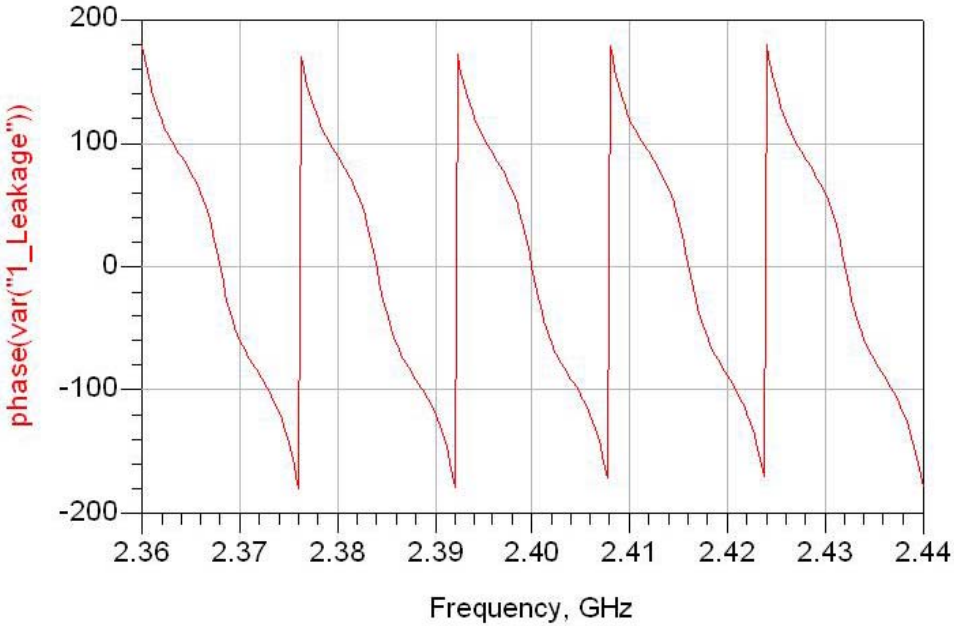

Figure 104. Phase Plot of Leakage in WLCC with Non-Ideal Component Parameter Settings in Degrees.

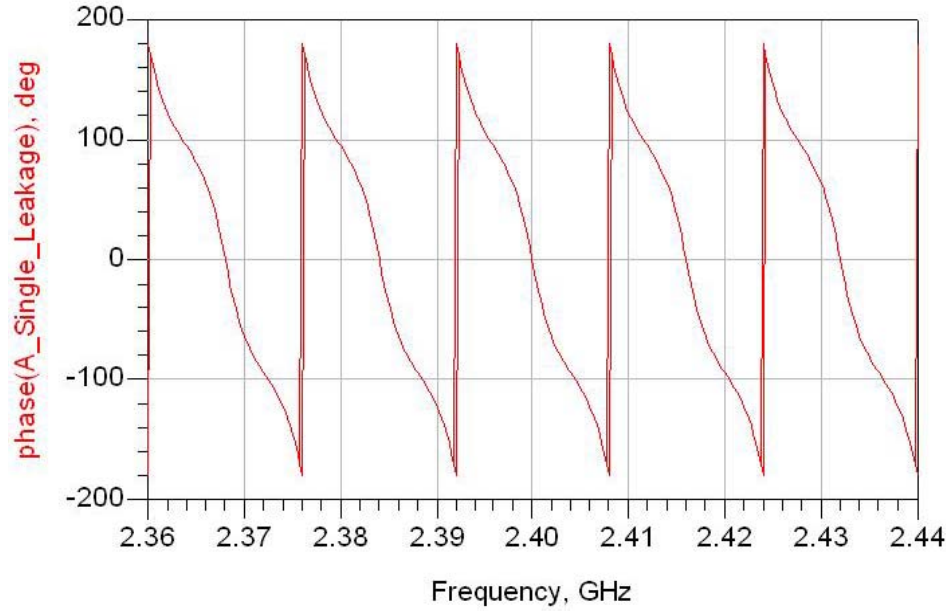

Figure 105. Phase Plot of Leakage in LCC with Non-Ideal Component Parameter Settings in Degrees.

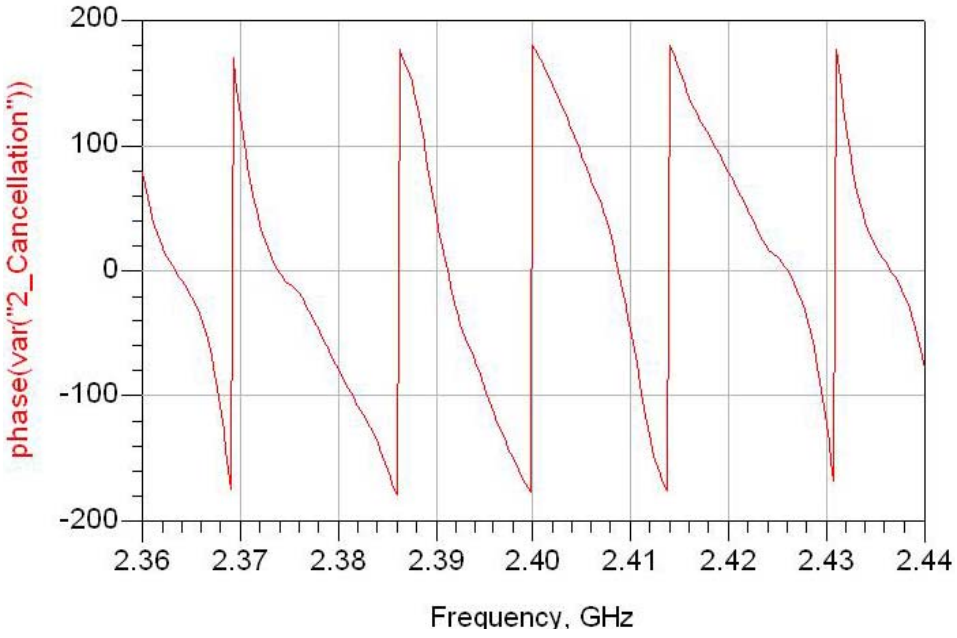

Figure 106. Phase Plot of Cancellation in WLCC with Non-Ideal Component Parameter Settings in Degrees.

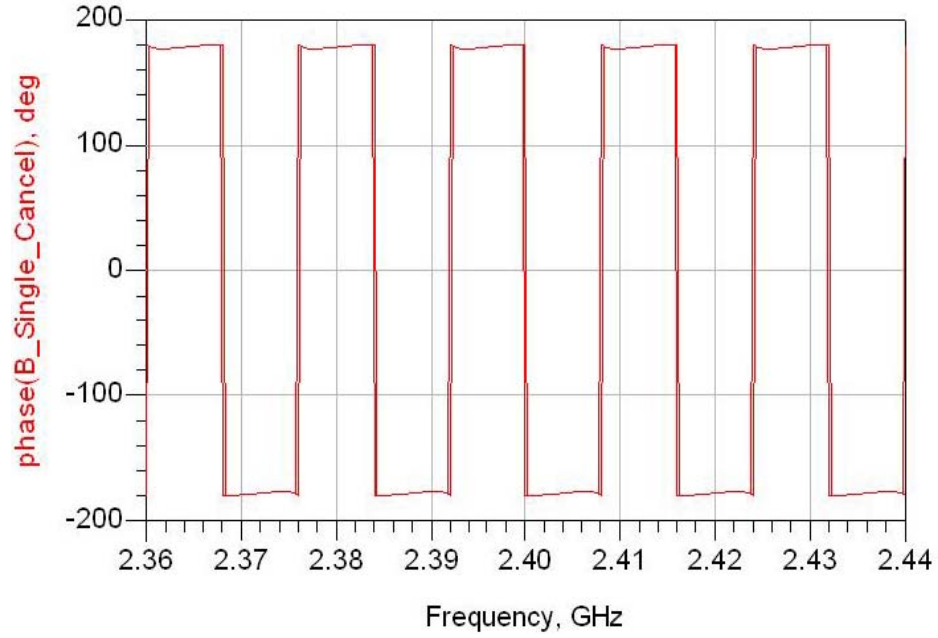

Figure 107. Phase Plot of Cancellation in LCC with Non-Ideal Component Parameter Settings in Degrees.

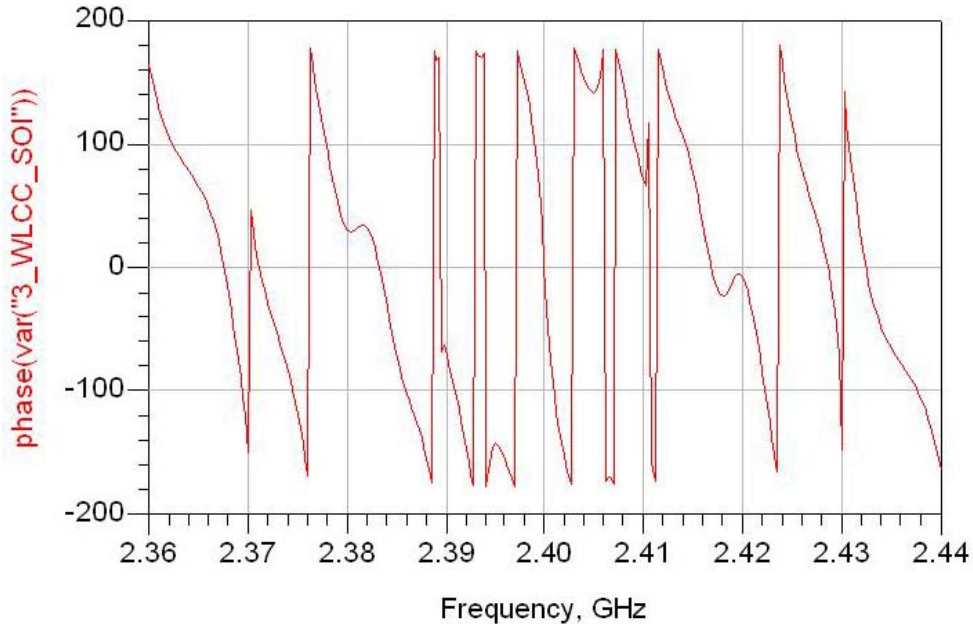

Figure 108. Phase Plot of SOI in WLCC with Non-Ideal Component Parameter Settings in Degrees.

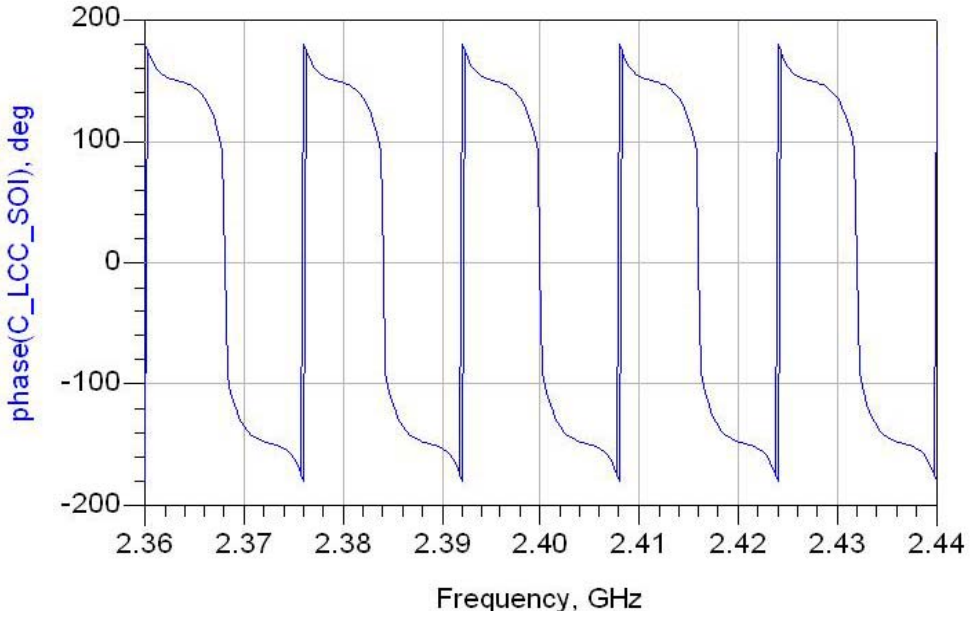

Figure 109. Phase Plot of SOI in LCC with Non-Ideal Component Parameter Settings in Degrees.

4. Performance Analysis With Mismatched Load

The robustness of the WLCC was evaluated by simulating its performance under antenna mismatch conditions where the load of the simulated antenna was stepped from 10 Ω to 100 Ω in steps of 10 Ω. The antenna mismatch can change with received signal angle of arrival or changes in the close-in scattering environment. For the purpose of comparison, amplitude plots of the SOI for both the WLCC and LCC are sorted into two groups. The first group represents the over-loaded condition with loads of 60 Ω, 70 Ω, 80 Ω, 90 Ω and 100 Ω. The second group represents the under-loaded condition with loads of 10 Ω, 20 Ω, 30 Ω and 40 Ω. The overloaded condition is illustrated in Figures 110 to 114 in descending order. The under-loaded condition is illustrated in Figures 115 to 118 in ascending order.

The plots for the over-loaded case, shown in Figures 110 to 114, illustrate the ability of the WLCC to maintain cancellation of leakages at all three center frequiencies of 2.38 GHz, 2.4 GHz and 2.42 GHz. The plots also show better overall attenuation of the leakage signal as compared to the LCC. Therefore, the performance of the WLCC is assessed to be robust for over-loaded situations and better than that of the LCC.

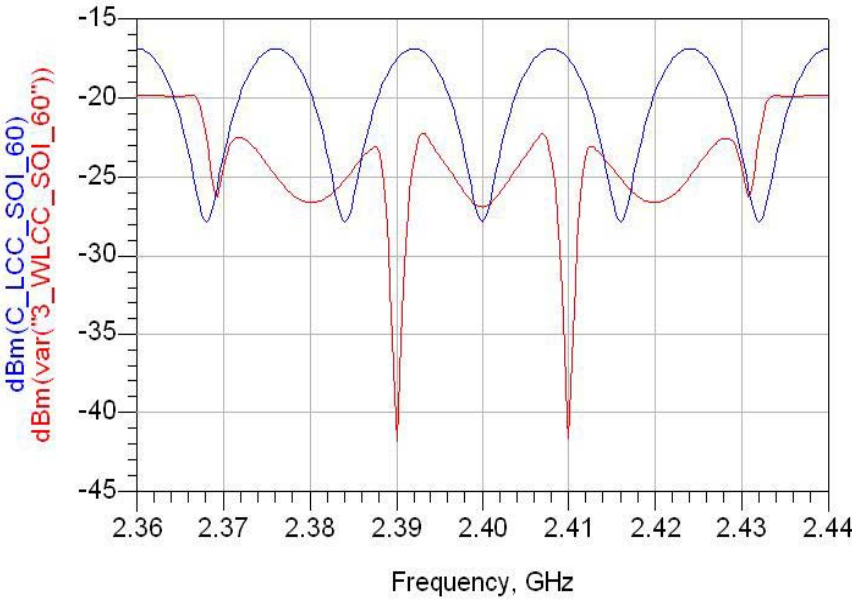

Figure 110. Amplitude Plot of SOI for both WLCC and LCC with Non-Ideal Component Parameter Settings in dBm with 60 Ω Load.

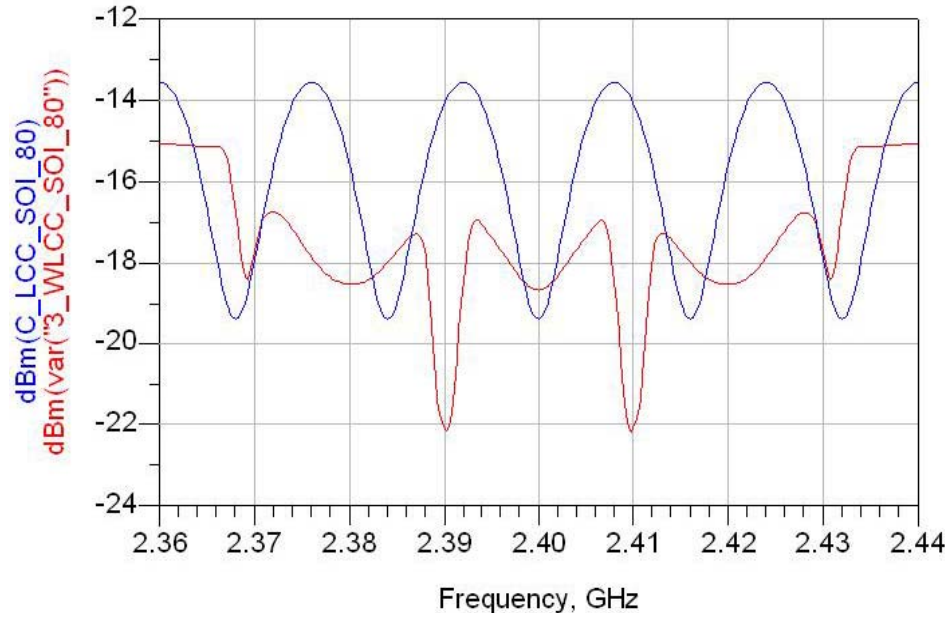

Figure 111. Amplitude Plot of SOI for both WLCC and LCC with Non-Ideal Component Parameter Settings in dBm with 70 Ω Load.

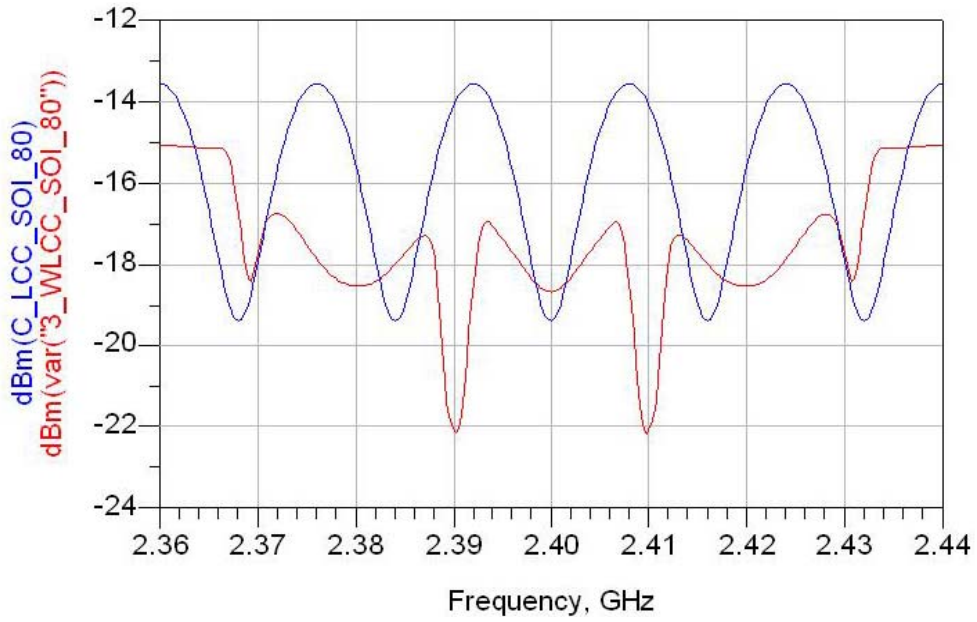

Figure 112. Amplitude Plot of SOI for both WLCC and LCC with Non-Ideal Component Parameter Settings in dBm with 80 Ω Load.

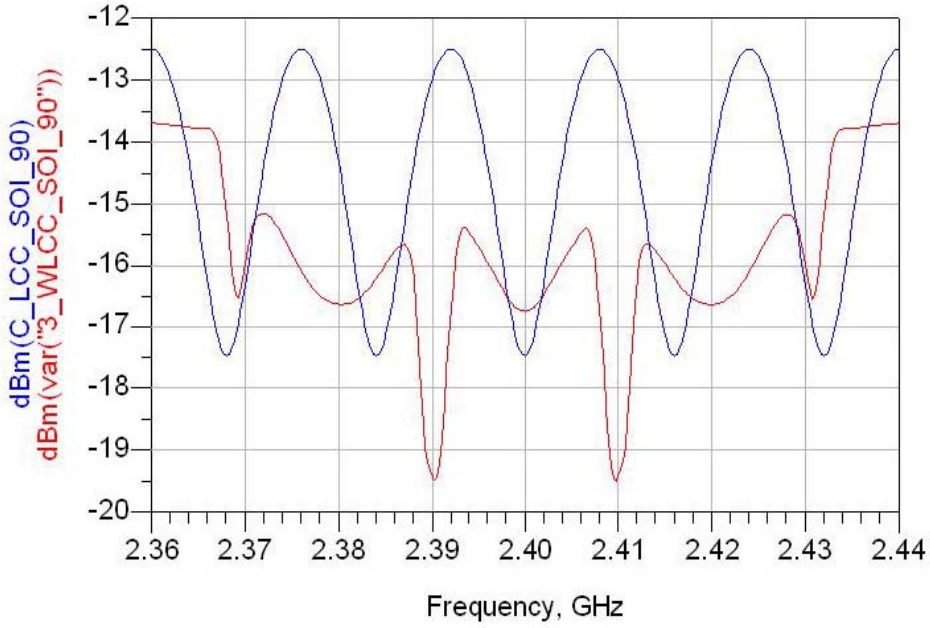

Figure 113. Amplitude Plot of SOI for both WLCC and LCC with Non-Ideal Component Parameter Settings in dBm with 90 Ω Load.

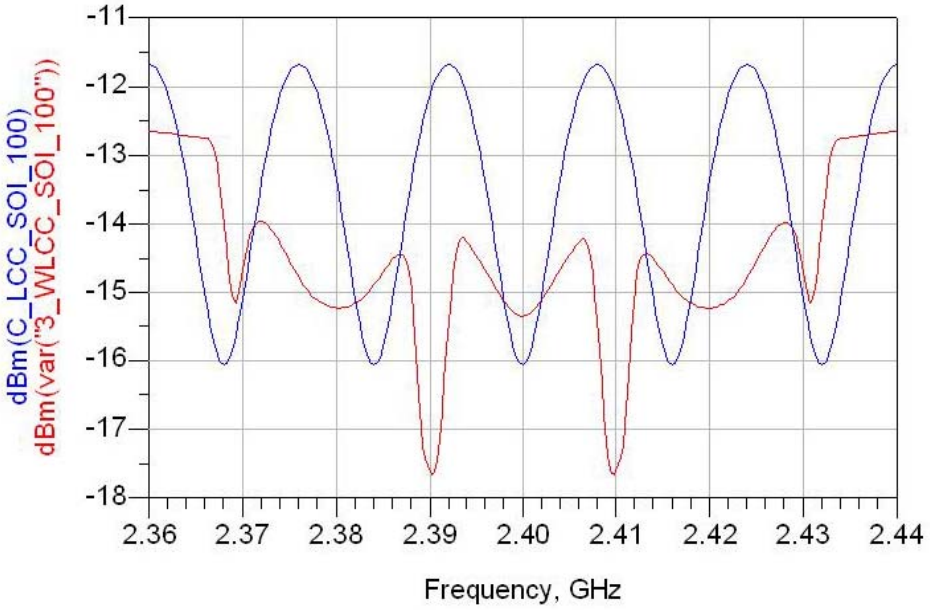

Figure 114. Amplitude Plot of SOI for both WLCC and LCC with Non-Ideal Component Parameter Settings in dBm with 100 Ω Load.

The plots for the under-loaded case, shown in Figures 115 to 118, reveal the inability of the WLCC to perform in the under-loaded condition. This is also true with the LCC. The performance of both the WLCC and the LCC in the under-loaded

condition was equally poor, with the LCC performing only slightly better in terms of overall attenuation.

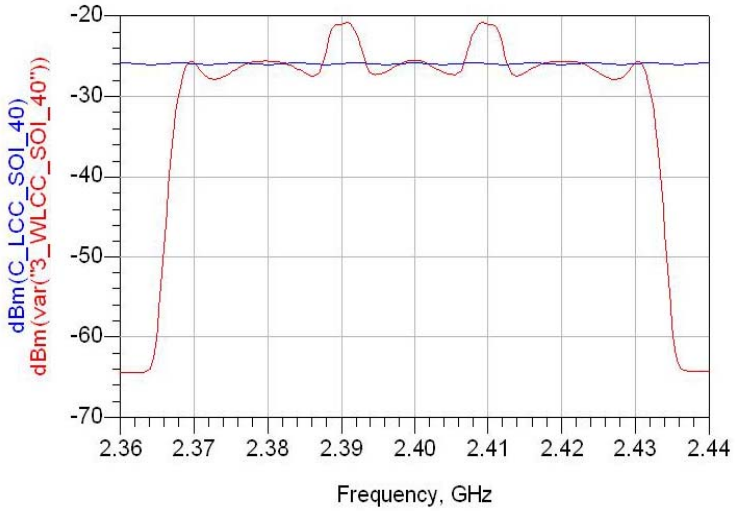

Figure 115. Amplitude Plot of SOI for both WLCC and LCC with Non-Ideal Component Parameter Settings in dBm with 40 Ω Load.

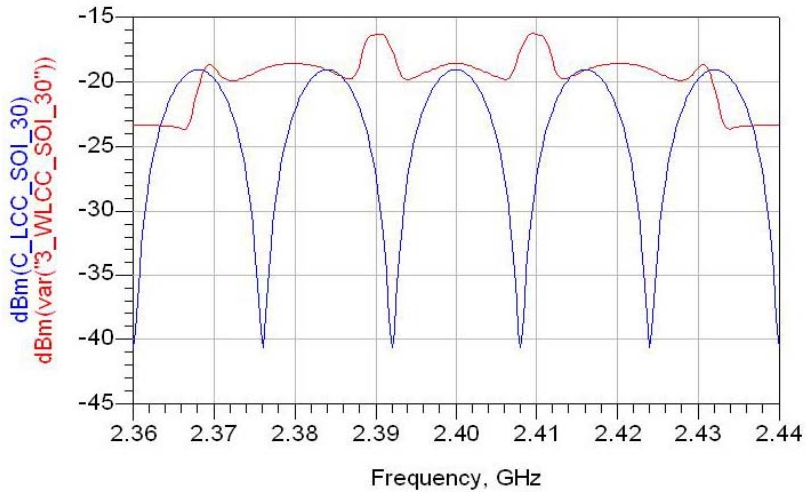

Figure 116. Amplitude Plot of SOI for both WLCC and LCC with Non-Ideal Component Parameter Settings in dBm with 30 Ω Load.

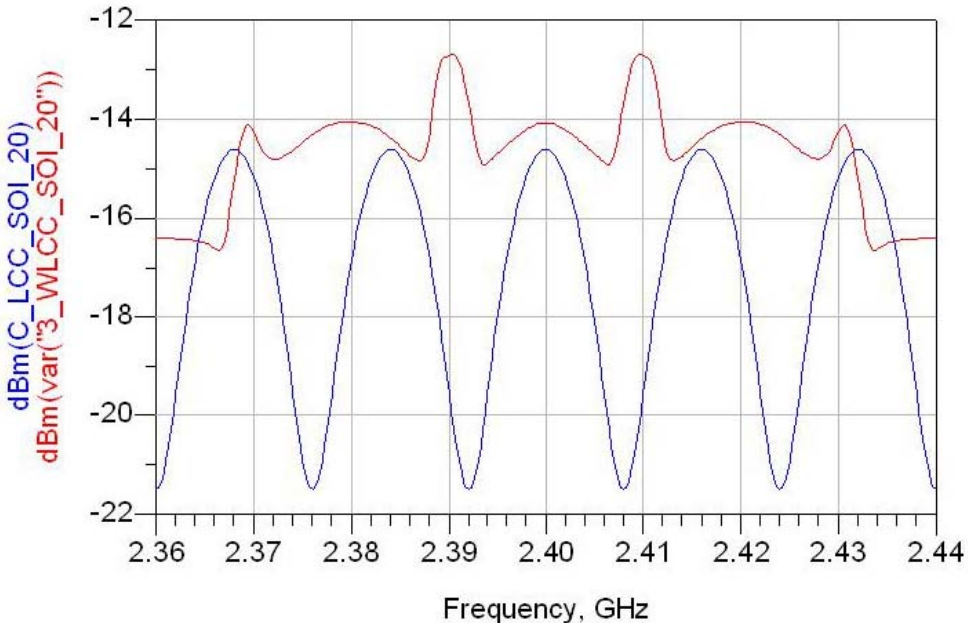

Figure 117. Amplitude Plot of SOI for both WLCC and LCC with Non-Ideal Component Parameter Settings in dBm with 20 Ω Load.

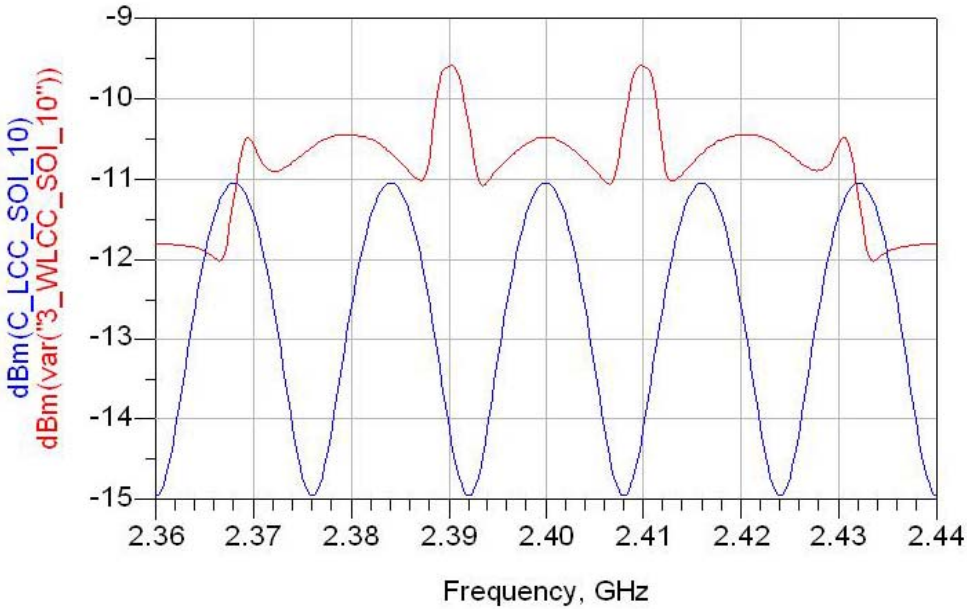

Figure 118. Amplitude Plot of SOI for both WLCC and LCC with Non-Ideal Component Parameter Settings in dBm with 10 Ω Load.

The possibility of the WLCC adapting to mismatched antenna load conditions was also tested by re-tuning the WLCC for 100 Ω and 10 Ω antenna loads. The ADS models of the re-tuned LCC and WLCC are shown in Figures 119 to 122. A comparison of amplitude plots between the case of having the WLCC tuned to 50 Ω matched antenna load, reacting to an 100 Ω and 10 Ω antenna load versus the case where the WLCC is re-tuned to adapt to an 100 Ω and 10 Ω antenna load is illustrated in Figure 123.

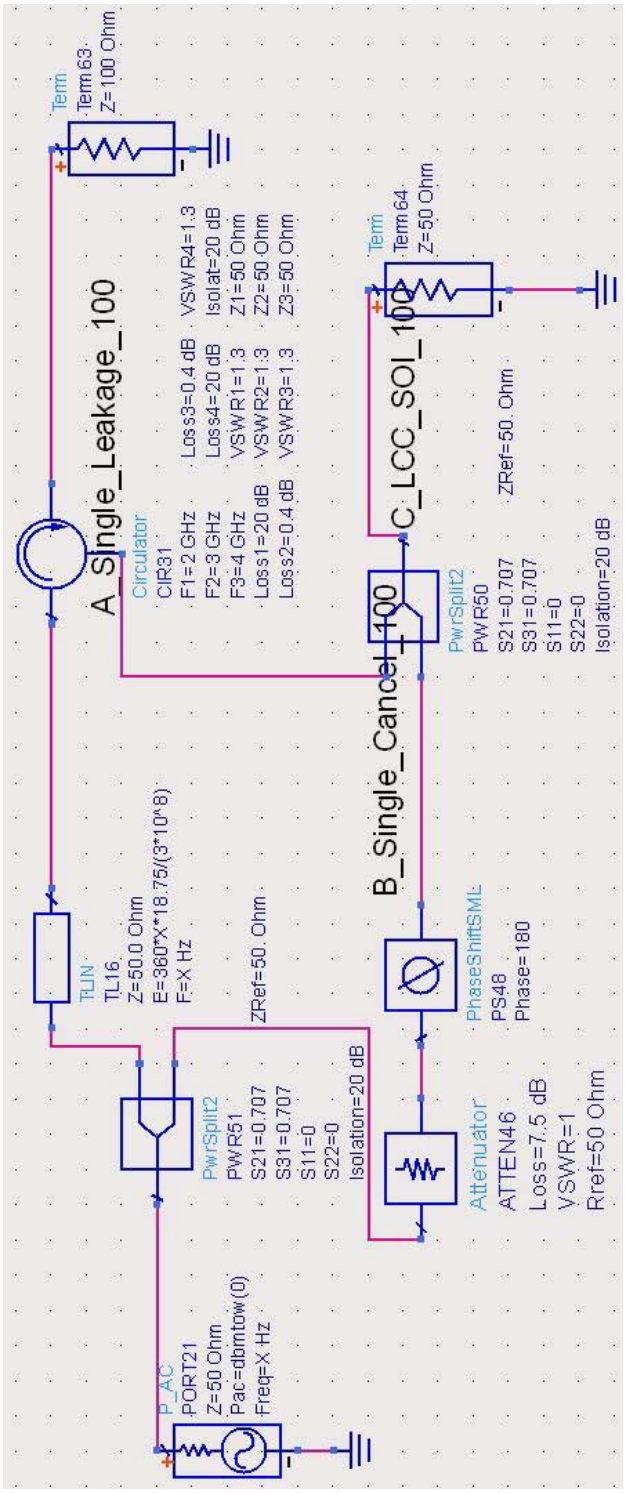

Figure 119. ADS Model of Re-tuned LCC for 100 Ω Antenna Load.

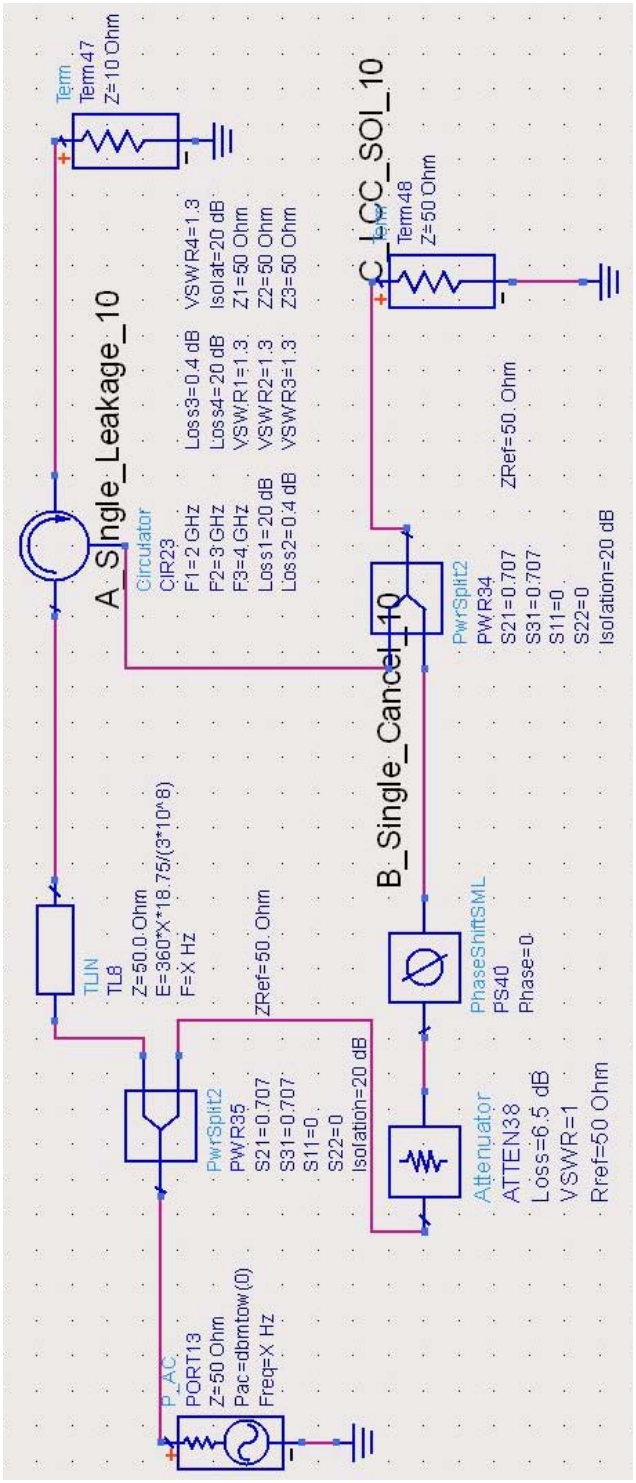

Figure 120. ADS Model of Re-tuned LCC for 10 Ω Antenna Load.

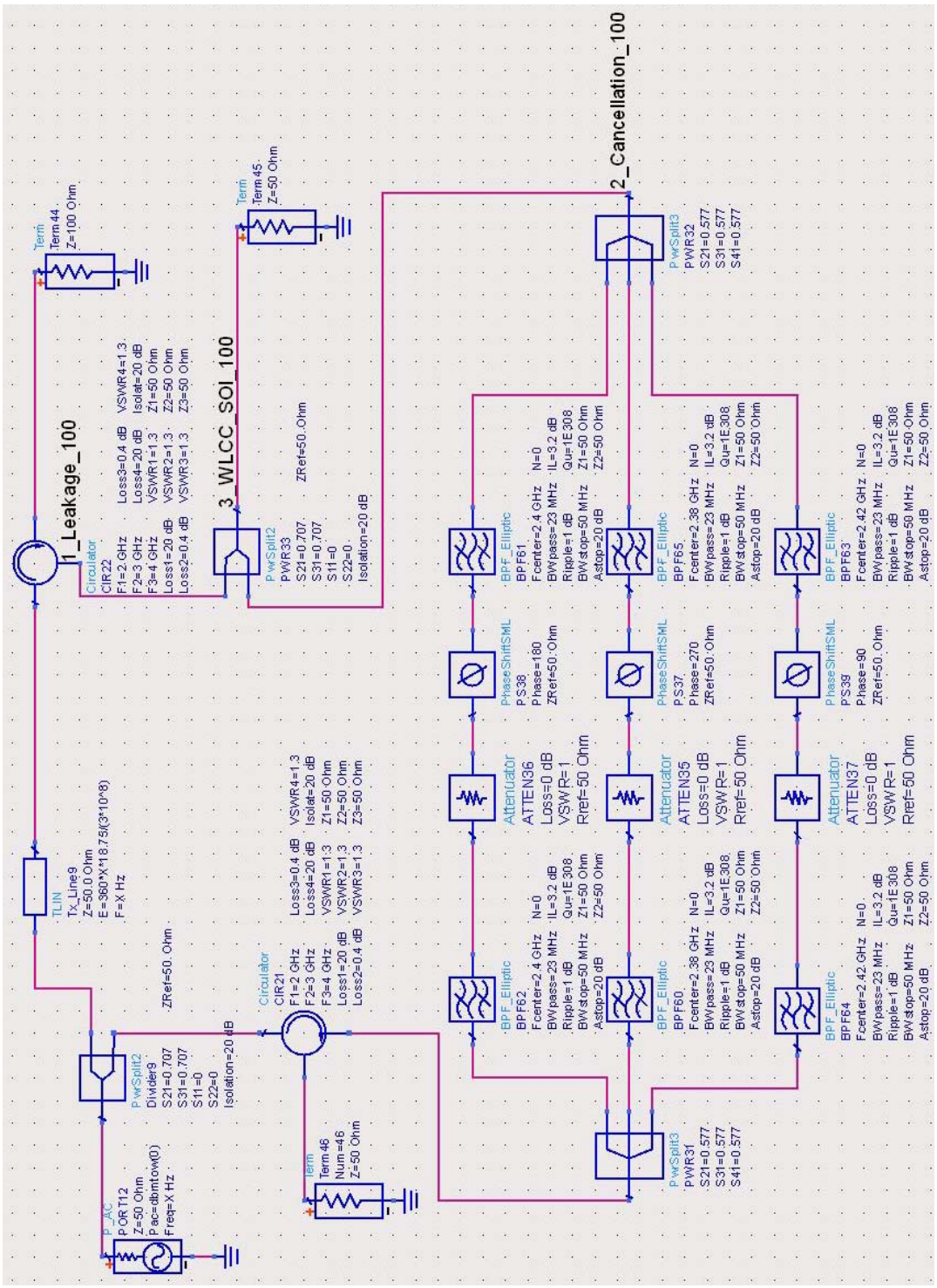

Figure 121. ADS Model of Re-tuned WLCC for 100 Ω Antenna Load.

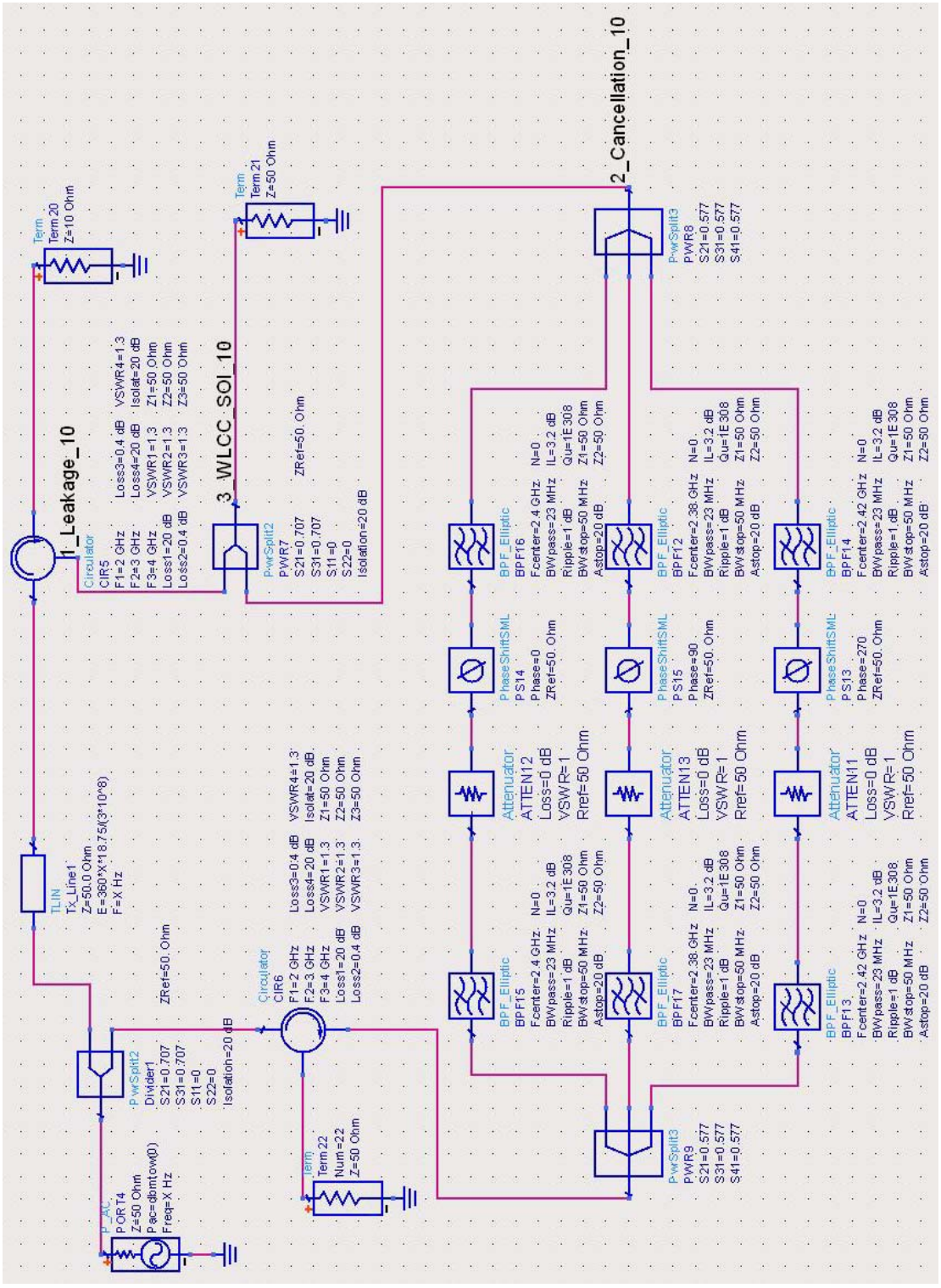

Figure 122. ADS Model of Re-tuned WLCC for 10 Ω Antenna Load.

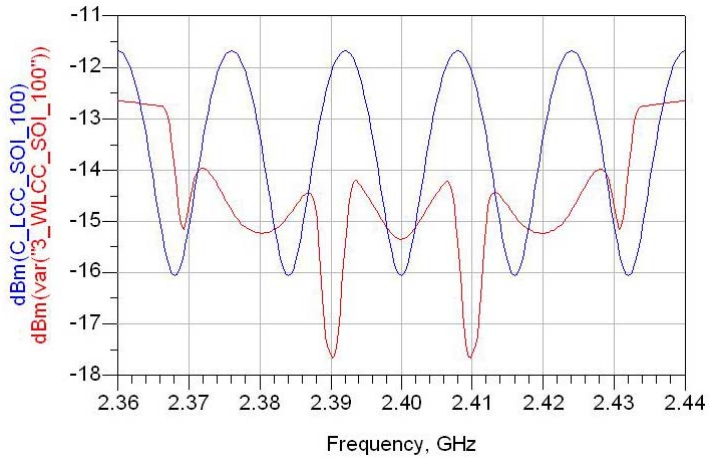

a. 100 Ω Load, tuned to 50 Ω.

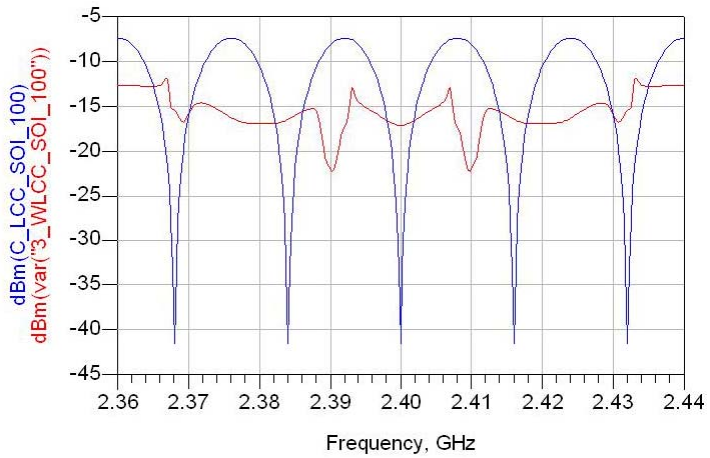

b. 100 Ω Load, re-tuned.

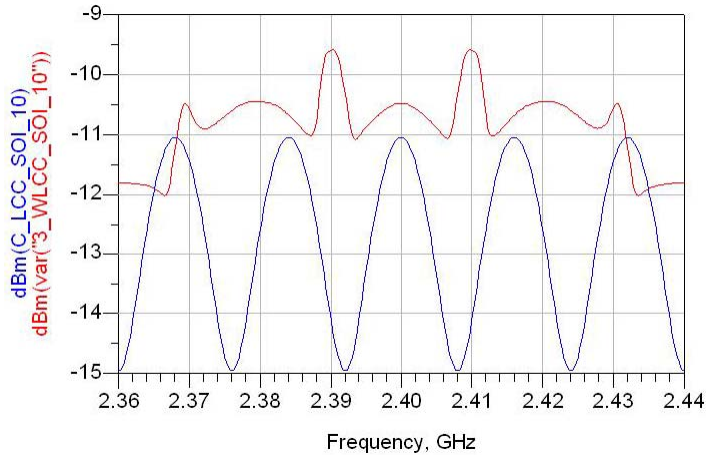

c. 10 Ω Load, tuned to 50 Ω.

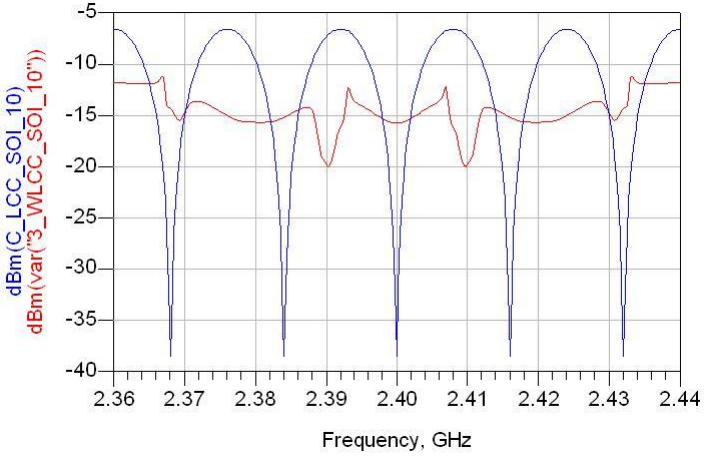

d. 10 Ω Load, re-tuned.

Figure 123. Amplitude Plot of SOI for both WLCC and LCC with Non-Ideal Component Parameter Settings in dBm with 10 Ω Load.

D. CONCLUSION

The WLCC design using a FDMC with couplers displayed better performance compared to the version built using the FDMC with circulators. The key distinctive reason was the non-linearity in phase caused by the bank of circulators and filters. The final WLCC design was also evaluated through a series of simulations using both ideal and non-ideal component parameters. Its effectiveness was highlighted by benchmarking it against the performance of a single frequency LCC model as well as performance against possible mismatches in the simulated antenna load. The possibility of having the WLCC adapt to mismatched antenna conditions was also examined. The results obtained through a series of simulations have shown improvement in bandwidth. The results are summarized in Tables 17 and 18.

Table 17. Comparison of Achieved Attenuation Level for both LCC and WLCC.

	Achieved Attenuation at Channel Center Frequency under Ideal Component Parameter Settings (dB)			**Achieved Attenuation at Channel Center Frequency under Non-Ideal Component Parameter Settings (dB)**		
	Chan 1 f_c=2.38 GHz Δf=20MHz	**Chan 2** f_c=2.4 GHz Δf=20MHz	**Chan 3** f_c=2.42 GHz Δf=20MHz	**Chan 1** f_c=2.38 GHz Δf=20MHz	**Chan 2** f_c=2.4 GHz Δf=20MHz	**Chan 3** f_c=2.42 GHz Δf=20MHz
LCC	NA	-142	NA	NA	-66.3	NA
WLCC	**-110.9**	**-127**	**-111.2**	**-50.7**	**-46.3**	**-51.2**

Table 18. Comparison of Achieved Bandwidth for both LCC and WLCC.

	Achieved Bandwidth under Ideal Component Parameter Settings, Reference to -40dB Attenuation Level (MHz)				**Achieved Bandwidth under Non-Ideal Component Parameter Settings, Reference to -40dB Attenuation Level (MHz)**			
	Chan 1 f_c=2.38 GHz Δf=20MHz	**Chan 2** f_c=2.4 GHz Δf=20MHz	**Chan 3** f_c=2.42 GHz Δf=20MHz	**Overall** f_c=2.4 GHz Δf=60MHz	**Chan 1** f_c=2.38 GHz Δf=20MHz	**Chan 2** f_c=2.4 GHz Δf=20MHz	**Chan 3** f_c=2.42 GHz Δf=20MHz	**Overall** f_c=2.4 GHz Δf=60MHz
LCC	4	4	4	**12**	2	2	2	**6**
WLCC	18	19	18	**55**	10	12	10	**32**

IV. SUMMARY AND CONCLUSIONS

A. SUMMARY

The concept of increasing the bandwidth of a basic single frequency LCC by the use of a FDMC consisting of a bank of narrowband leakage cancelling branches was investigated. First, a conventional narrowband LCC, with ideal components, was simulated in ADS. This served as a baseline for evaluating new approaches for wideband circuits. The use of the ADS electronic-design automation software system allowed the circuits to be designed, tested and evaluated over a wide range of parameters at a very low cost. A design process was developed based on an understanding of various microwave engineering concepts, as well as analysis of components and their impact on circuit response.

A critical component in a WLCC is the FDMC. Several designs were simulated that used circulators, couplers and various types of filter characteristics. In order to make cancellation effective over a wide band, it was necessary to match the phase slopes of the main channel and cancellation branches. Simulation results supported the use of the elliptic filter due to its flat amplitude response in its passband and its very steep roll-off. The phase of elliptic filters is also relatively linear. This was a crucial factor in matching the phase in the leakage signal, thus allowing cancellation over a wide band of frequencies. A comparison of FDMC designs was conducted by evaluating the design that used circulators for splitting of the signal for the processing of a cancellation signal against the design that used couplers for this same purpose. It was found that the FDMC design that uses couplers was more suited for use in the design of a WLCC due to its superiority in phase linearity. An S-parameter simulation was also conducted in ADS to provide a general characterization of the FDMC. The WLCC was successfully evaluated by benchmarking its performance against that of a single frequency LCC. In contrast to the bandwidth-limited single frequency LCC, the WLCC was able to achieve a bandwidth of 55 MHz and 32 MHz, both across a 60 MHz band with typically cancellation of –40 dB, with ideal and non-ideal component parameter settings, respectively. The robustness of the WLCC was also evaluated by a series of simulations

with antenna load mismatch conditions. It was found that retuning the cancellation branches improved the performance when antenna mismatches were present.

The successful findings of this thesis, as summarized in Tables 17 and 18 in Chapter IV, offer potential improvement in FMCW radar and new Wirelessly Networked Distributed Digital Phased Array (WNDDPA) applications.

B. RECOMMENDATIONS

1. Software Design of Essential Components in FDMC

Commercially off the shelf (COTS) variants of the 1 to 3 power splitter and the elliptic BPFs used in the FDMC are probably unavailable for purchase. Therefore, the same low risk and cost effective method used in this thesis should be employ in designing these components. The CST Microwave Studio commercial software could be used to design these components for further evaluation.

2. Further ADS Software Simulations

Critical components in ongoing research on WNDDPA, such as the synchronization circuit, consisting of the Transmit and Receive Modules (TRM) and the Digital Beam Forming Controller (DBFC) circuit, can be modeled in ADS. The potential value-add and flexibility offered by the WLCC could then be assessed further.

Additionally, with the knowledge gained on WLCCs, different synchronization methods could be developed and subsequently tested using ADS.

3. Building a Hardware Prototype

Upon the successful design of the essential FDMC components using CST Microwave Studio and the successful proving of the effectiveness of having a WLCC incorporated into the existing WNDDPA research through ADS simulations, it is necessary to build a prototype of the WLCC to complement the current WNDDPA hardware setup that was built using COTS equipments so as to bring the WNDDPA into the field.

4. Combining WLCC With Digital Cancellation

The performance of the WLCC can be further enhanced by complementing it with a digital cancellation approach [7], where a demodulator is employed to store the residual signal after the analog cancellation by the WLCC.

THIS PAGE INTENTIONALLY LEFT BLANK

LIST OF REFERENCES

[1] Wikimedia. http://upload.wikimedia.org/wikipedia/commons/7/7a/Hawk-radar-hatzerim-1-1.jpg, accessed on 26 Oct 2010.

[2] M. L. Skolnik, *Introduction to Radar Systems*, 2nd ed, McGraw-Hill, pp 83, 750–751, 1980.

[3] DS030_09_08H SCOUT Mk2_LR[1].pdf , www.thalesgroup.com, downloaded on 31 Oct 2010.

[4] P. D. L. Beasley, A. G. Stove, B. J. Reits, B-O. As, "Solving the Problems of a Single Antenna Frequency Modulated CW Radar," *IEEE International Radar Conference*, 1990.

[5] "Microwave Devices & Radar," class notes for EC 4610, Department of Electrical and Computer Engineering, Naval Postgraduate School, pp. 115, Summer 2010.

[6] G. P. Rodrique, "Circulators from 1 to 100 GHz," *Microwave J*. State of the Art Reference, vol.32, pp. 115–132, 1989.

[7] W. H. Cheng, "Cancellation Circuit for Transmit-Receive Isolation," Naval Postgraduate School Master's Thesis, Sept. pp xiv, 11–12, 27, 59, 2010.

[8] D. C. Jenn, Y. C. Tsai, J. H. Ryu, R. Broadston, "Adaptive Phase Synchronization in Distributed Digital Array," *NASA/ ESA Conference on Adaptive Hardware and Systems*, Anaheim, CA, June 2010.

[9] Agilent Technologies. http://edocs.soco.agilent.com/display/ads2009U1/Home, accessed on 6 Oct 2010.

[10] Agilent Technologies. http://edocs.soco.agilent.com/display/ads2009/dbm%28%29+Measurement, accessed on 22 Nov 2010.

[11] P. Djerf and I. Tornazakis, "Development of a Distributed Digital Array Radar (DDAR)," Naval Postgraduate School Master's Thesis, Sept. pp. 39, 2008.

THIS PAGE INTENTIONALLY LEFT BLANK

INITIAL DISTRIBUTION LIST

1. Defense Technical Information Center
   Ft. Belvoir, Virginia

2. Dudley Know Library
   Naval Postgraduate School
   Monterey, California

3. Professor R. Clark Robertson
   Chairman, Department of Electrical & Computer Engineering
   Naval Postgraduate School
   Monterey, California

4. Professor David C. Jenn
   Professor, Department of Electrical & Computer Engineering
   Naval Postgraduate School
   Monterey, California

5. Professor Phillip E. Pace
   Professor, Department of Electrical & Computer Engineering
   Naval Postgraduate School
   Monterey, California

6. Robert D. Broadston
   Staff, Department of Electrical & Computer Engineering
   Naval Postgraduate School
   Monterey, California

7. Professor Tat Soon Yeo
   Director, Temasek Defence Systems Institute (TDSI)
   National University of Singapore
   Singapore

8. Ms Lai Poh Tan
   Senior Manager, Temasek Defence Systems Institute (TDSI)
   National University of Singapore
   Singapore